DEVELOPMENT OF PROTEIN BASED PCBP2 SIRNA NANOCOMPLEX FOR LIVER FIBROSIS THERAPY

A DISSERTATION IN

Pharmaceutical Sciences

and

Chemistry

Presented to the Faculty of the University
of Missouri-Kansas City in partial fulfillment of
the requirements for the degree

DOCTOR OF PHILOSOPHY

by

AKSHAY JAIN

M.S., University of Toledo, 2013

B. Pharmacy, Devi Ahilya University, 2009

Kansas City, Missouri

2018

DEVELOPMENT OF PROTEIN BASED PCBP2 SIRNA NANOCOMPLEX FOR LIVER FIBROSIS THERAPY

Akshay Jain, Candidate for the Doctor of Philosophy Degree

University of Missouri-Kansas City, 2018

ABSTRACT

The objective of this dissertation is to develop a protein-based siRNA nanocomplex for the treatment of alcoholic liver fibrosis. Our laboratory recently discovered that silencing the poly (rC) binding protein 2 (PCBP2) gene in hepatic stellate cells (HSCs) leads to the reversal of the accumulated extracellular matrix. We therefore hypothesize that targeted delivery of the PCBP2 siRNA to HSCs could potentially treat liver fibrosis. Cholesterol and IGF2R (insulin growth factor 2 receptor) specific peptide were used as targeting ligands to deliver the siRNA to HSCs.

In Chapter 1, we briefly introduced the background about RNA interference (RNAi), liver fibrogenesis, markers of liver fibrosis, and the role of PCBP2 in liver fibrogenesis. We also presented the Statement of the Problems and Objectives.

In chapter 2, we reviewed the avidin-biotin technology and its potential applications in nanotechnology, therapy and diagnosis. We also discussed the challenges and biological barriers for siRNA delivery.

In Chapter 3, we rigorously investigated the intracellular barrier which is a rate limiting step for the silencing activity of siRNAs. Using streptavidin as the nanocomplex core, PCBP2 siRNA was delivered to HSC-T6 (hepatic stellate) cells. Intracellular fate of the nanocomplex components and PCBP2 siRNA was monitored. Fluorescent probes were tagged with the siRNA, protamine and streptavidin and analyzed under confocal

microscopy, flow cytometry and fluorescence spectroscopy. We discovered substantial exocytosis and localization of the siRNA in recycling organelles, such as recycling endosomes, endoplasmic reticulum and golgi apparatus. Streptavidin was found to be colocalized with the lysosomes and in some cases along with siRNA potentially leading to the lysosomal degradation. We found that the streptavidin, although, a very efficient delivery carrier has reduced silencing activity at higher incubation time intervals.

In Chapter 4, we compared different variants of avidin such as avidin, neutravidin and streptavidin for *in vitro* activity and cellular uptake over the extended time interval. Addition of polyethylene glycol (PEG) spacer between the biotin and cholesterol ligand was done to improve the biodistribution of the nanocomplex. We tested the live imaging and post euthanized biodistribution of nanocomplexes and found it to be most distributed in liver in comparison to other variants of avidin. In vitro silencing activity and cellular uptake was also significantly higher in case of the neutravidin nanocomplex with negligible lysosomal colocalization and exocytosis.

In Chapter 5, the neutravidin nanocomplex were further improved by using the IGF2R-specific peptide as a targeting ligand for hepatic stellate cells. The siRNA was also annealed to the peptide nucleic acid for attaching the biotin. PNA enhanced the serum stability of the siRNA and helped avoid the endonuclease and chemical reagent mediated degradation during biotin conjugation process. We developed the liver fibrosis model by injecting CCL_4/olive oil intra-peritonealy for 4-5 weeks. We started the neutravidin-PCBP2 siRNA nanocomplex treatment at the beginning of 3rd week of the fibrosis induction to reverse the fibrosis. After the end of dosage regimen, the rats were euthanized and the analysis was performed for the liver fibrosis molecular markers. We

found that the neutravidin PCBP2 siRNA nanocomplex successfully reversed the liver fibrosis by significantly reducing the molecular markers of fibrosis and reduction in the type 1 collagen.

APPROVAL PAGE

The faculty listed below, appointed by the Dean of the School of Graduate Studies, have examined the dissertation titled "Development of Protein Based PCBP2 siRNA Nanocomplex for Liver Fibrosis Therapy", presented by Akshay Jain, candidate for the Doctor of Philosophy Degree, and certify that in their opinion it is worthy of acceptance.

Supervisory Committee

Kun Cheng, Ph.D., Committee Chair

Division of Pharmaceutical Sciences

Chi Lee, Ph.D.,

Division of Pharmaceutical Sciences

Russell B. Melchert, Ph.D.

Division of Pharmacology and Toxicology

Zhonghua Peng, Ph.D.

Department of Chemistry

Xiangping Chu, Ph.D.

Department of Biomedical Sciences

TABLE OF CONTENTS

LIST OF ILLUSTRATIONS

LIST OF TABLES

ACKNOWLEDGEMENTS

I would like to express my deepest and sincere gratitude to my adviser Dr. Kun Cheng for his guidance, support and aspiration during my Ph.D. It was him who believed in me and gave me opportunity to work in his lab. He gave me purpose, motivated me and showed me the path where I could learn and grow further. I am carrying many dreams and responsibilities of my family on my shoulder and Dr. Kun Cheng has given me this opportunity to fulfil them.

I would also like to thank my committee members, Dean (Dr.) Russell B. Melchert, Dr. Chi Lee, Dr. Zhonghua Peng and Dr. Xiangping Chu for their insightful and kind comments which helped me in improving my scientific capabilities and making my project more interesting and successful.

All the professors and staff members at school of pharmacy, department of chemistry, education and graduate studies have a huge impact on me at personal and professional level. I am very grateful to all of them who shared their knowledge and experience with me. Dr. Thomas P Johnston, whom I assisted in teaching and in return he taught me how to be so passionate about something you do and be highly meticulous in your work. I am highly thankful to him for teaching me how to teach and keep the audience engaged while delivering lectures or talks.

I would like to thank my lab colleagues, Dr. Rubi Mahato, Dr. Ravi Shukla, Dr. Zhijin Chen, Dr. Wei Jin, Dr. Hao Liu, Ashutosh Barve, Zhen Zhao, Yuanke Li, Bahaa Mustafa, John Fetse, Pratik Adhikary for their amazing support, teaching, help, insightful suggestions, brainstorming sessions, encouragement and soccer discussions. I was fortunate to have many friends at UMKC, who are my extended family at KC and will

always cherish the moments spent with them for my life time. I would like to thank my family in Toledo, Shantanu Rao, Ritesh Mittal, Anusha Pasumarthi, Pooja Jain.

I would like to pay my sincere most thanks and deepest appreciation to my Mom, Dad, Anshul, Monica and little ones –Vivaan and Vaani. I owe everything to them for their unconditional love and support throughout my life.

My best friend, philosopher, inspiration and my wife, Rajvinder Kaur. This is for us. I cannot thank you enough for your love and support through highs and lows of my life. Keeping me on track and motivating me to be a better version of myself.

Last but not the least the supreme power, almighty, God, for paving the path for me to walk and helping me throughout my journey and teaching me that humility and compassion are the greatest tools to ones' wellbeing and true happiness.

~Dedicated to my late grandparents~

CHAPTER 1

INTRODUCTION

1.1 Overview

RNAi therapeutics have proven to be one of the most potent forms of therapeutic modality for a wide spectrum of fatal diseases. One of the most rigorously investigated type of RNAi based therapeutics is siRNA. After reaching the target cell cytoplasm, single strand of the siRNA (antisense strand) binds to the RNA induced silencing complex (RISC) and inhibits the mRNA that translates the target protein. Efficient delivery of siRNA and sustained silencing activity remains the greatest challenge in its clinical translation. In this proposal, we are targeting liver fibrosis. After chronic liver injury, necrosis/apoptosis of hepatocytes and activation of hepatic stellate cells (HSC-T6) occur. Activation of hepatic stellate cells and apoptosis of hepatocytes results in the excessive collagen I protein secretion which further accumulates in extracellular matrix (space of disse).[1] Due to injury, hepatocytes produce apoptotic bodies that are taken up by the hepatic stellate cells (HSCs) and kuppffer cells. This uptake promotes the HSC activation and T cells, B cells NK cells proliferation, resulting in the upregulation of cytokines like Transforming growth factor beta (TGF β), TNF α, IFN γ, IL 6, platelet derived growth factor (PDGF) etc [2-3]. Activation of HSC-T6 is one of the most critical step of liver fibrosis and type I collagen over expression and accumulation. Fibrous scars are formed with the subsequent progression of hepatic fibrosis that deforms the hepatic architecture and compromises the liver function.[4]

Extracellular matrix is mainly composed for type I collagen protein. Over expression of α-complex protein 2 (αCP2) which is encoded by PCBP2 gene (poly (rC) binding protein 2) is critical for type I collagen accumulation. Silencing (inhibition) of PCBP2 with siRNA can be very effective and has shown promising effects for treatment of liver fibrosis [5]. Efficient targeting of HSC-T6 (rat activated hepatic stellate cells) cells *in-vitro* and *in-vivo* is yet the biggest challenge regardless of the potency of PCBP2 siRNA. Delivery of the drug to the fibrotic liver is also highly challenging as the portal pressure increases with more collagen around the sinusoidal space leading to even lower blood flow to the liver tissue and thus lower chance for the drug carrier to reach target site (HSCs).[5]

Considering the sensitivity of siRNA to ubiquitous RNase, DNase, temperature, harsh pH and organic solvents, it is imperative to keep the formulation of siRNA in clean environment with minimum steps. Self-assembly is nature's process where like attracts like. Avidin-biotin interaction, one of the nature's greatest non-covalent interaction are utilized for many biotech applications. Avidin-like proteins are also one of the most applicable modality in the field of nanotechnology. Avidin (AV)[6] and its other analogues such as Streptavidin (SA)[7] and Neutravidin (NA) due to their strong affinity toward biotin have been extensively utilized for drug delivery. These proteins are functionally analogous but have subtle physical, chemical and molecular differences contributing to their respective special characteristics. Biotinylation of the drug molecule will help it self-assemble to avidin with natural interaction without using any solvent. Avidin and analogous proteins not only act as the backbone for the biotin molecules but also assist in the organ and tissue uptake.

1.2 Statement of Problem

Despite tremendous efforts across the scientific world, there is no potential treatment of liver fibrosis in clinics. Liver tissue penetration of the drug carrier is highly difficult in fibrotic liver due to narrow endothelial fenestration and increased portal to central vein resistance due to collagen accumulation.[8]

Biotinylated PCBP2 siRNA with a disulfide linker and biotinylated targeting ligand (cholesterol or IGF2R peptide) will have high affinity toward avidin like proteins. Using various molar ratios of each components, followed by rapid mixing, it will form uniform nanocomplexes. These nanocomplexes will be further condensed with the help of nucleotide condensing agent, protamine, at various N/P ratios. For targeting the nanocomplexes, it is essential to identify the most unique and highly expressing molecular receptor on hepatic stellate cells. Low density lipoprotein receptors (LDLRs) are present on all the cells especially in liver for the metabolism of the cholesterol.[9-10] Also, IGF2R (insulin growth factor II receptor) is another unique target. HSC-T6, over express LDLRs and IGF2R.[11] We will use the biotinylated cholesterol and biotinylated IGF2R specific peptide, discovered by phage display [11], as targeting ligands to deliver siRNA to HSC-T6 cells. Nanocomplexes upon intravenous (i.v) administration will reach liver and specifically target the LDLRs and IGF2Rs on HSCs. After successful cellular uptake, we expect that nanocomplex will translocate to cytoplasm via escaping endosomes.[12] Protamine will release form nanocomplex and siRNA in particular. Disulfide bond between the biotin and siRNA will be reduced by the cytoplasmic glutathione resulting in the release of free siRNA to perform silencing activity.

1.3 Objectives

The objectives of the dissertation are:

1. To develop, characterize and optimize protein-based PCBP2 siRNA nanocomplexes. We will fabricate the nanocomplex using biotinylated PCBP2 siRNA, streptavidin and biotinylated cholesterol. We will then evaluate the intracellular trafficking and delivery obstacles of the siRNA nanocomplex by confocal microscopy and flow cytometry. We will also monitor the intracellular fate of the multiple components of the nanocomplex and evaluate the exocytosis of the nanocomplex.

2. To compare different avidin protein variants for the efficient delivery of the siRNA to the hepatic stellate cells and fibrotic liver. Cholesterol will be utilized as the targeting ligand in the nanocomplex. We will evaluate the comparative physico-chemical characteristics, particle size, serum stability, silencing activity, cellular uptake, exocytosis, apoptosis, inflammatory cytokine release and *in vivo* biodistribution.

3. To design and develop neutravidin-based siRNA nanocomplex with the help of IGF2R-specific peptide to target hepatic stellate cells. We will noncovalently attach biotin to the siRNA using PNA as a linker. We will optimize the peptide to PCBP2 siRNA ratio and evaluate the morphological characteristics such as particle size and zeta potential. We will also examine the serum stability, cellular uptake of various ratios to determine the best candidate to perform *in vivo* studies.

4. To evaluate the anti-fibrotic activity of the PCBP2 siRNA nanocomplex in Sprague Dawley rats with carbon tetrachloride- induced liver fibrosis. We will treat the fibrotic rats with the PCBP2 siRNA nanocomplex and examine the serum and liver tissues for the

liver fibrosis markers such as ALT, AST, hydroxyproline, Type I, III and IV collagen to evaluate the amelioration of liver fibrosis.

CHAPTER 2

LITERATURE REVIEW

2.1 The Principles and Applications of Avidin-Based Nanoparticles in Drug Delivery and Diagnosis

Avidin-biotin interaction is one of the strongest non-covalent interactions in the nature. Avidin and its analogues have therefore been extensively utilized as probes and affinity matrices for a wide variety of applications in biochemical assays, diagnosis, affinity purification, and drug delivery. Recently, there has been a growing interest in exploring this non-covalent interaction in nanoscale drug delivery systems for pharmaceutical agents, including small molecules, proteins, vaccines, monoclonal antibodies, and nucleic acids. Particularly, the ease of fabrication without losing the chemical and biological properties of the coupled moieties makes the avidin-biotin system a versatile platform for nanotechnology. In addition, avidin-based nanoparticles have been investigated as diagnostic systems for various tumors and surface antigens. In this review, we will highlight the various fabrication principles and biomedical applications of avidin-based nanoparticles in drug delivery and diagnosis. The structures and biochemical properties of avidin, biotin and their respective analogues will also be discussed.

2.1.1 Introduction to the Avidin - Biotin Technology

Nanotechnology holds the greatest potential and promise for biomedical research. Significant progress has been achieved in nanotechnology across a wide spectrum of fields from applied physics to biotechnology to medicine. Naturally occurring interactions are the crux for such innovations and have been explored for various nanoscale applications to achieve uncountable scientific goals.[13] As one of the strongest non-covalent interactions in the nature, the avidin-biotin interaction has been utilized in nanoscale drug delivery systems for pharmaceutical agents, including small molecules,

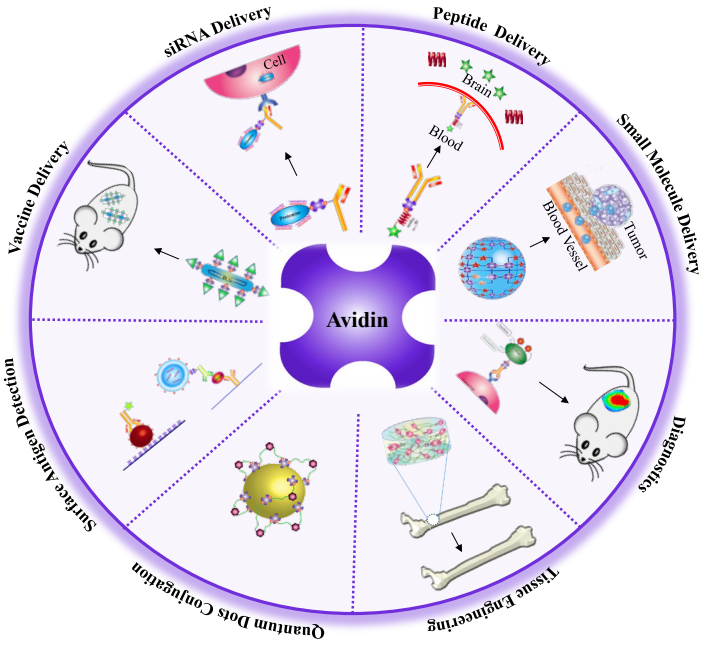

proteins, vaccines, monoclonal antibodies, and nucleic acids (Fig. 1).

Figure 1. Avidin biotin technology and application in nanotechnology, therapeutics and diagnosis.

Avidin is a basic tetrameric glycoprotein composed of four identical subunits, each binds to biotin with high specificity and affinity (K_d ~10^{-15} M).[13] Avidin is originally derived from the eggs of avian species, reptiles and amphibians. Avidin-biotin interaction is considered one of the most specific and stable non-covalent interactions, which is about 10^3 to 10^6 times higher than an antigen-antibody interaction.[14] Several genetically and chemically engineered avidin and its analogues have been studied to improve the functional and structural characteristics of avidins.[15] The biggest advantage of this system is its high affinity interaction, which is robust and stable against manipulation, proteolytic enzymes, temperature, pH, harsh organic reagents, and other denaturing reagents.[16-17] Therefore, the avidin-biotin interaction serves as a great tool in the biomedical and nanotechnological applications. On the other hand, biotin-based conjugates are easy to synthesize and have less impact on the activity of the biomolecules.

Compared to other covalent and non-covalent interactions, the avidin-biotin system provides enormous advantages such as amplification of weak signals, efficient operation and robust stability. Therefore, avidin has been a very versatile modality in the field of biotechnology, especially biochemical assays and affinity purification, over four decades. Tremendous efforts have also been converged to utilize the inherent properties of avidin in biotechnology medicines, and some of them have been evaluated in clinical studies.[18] Recently, the avidin-biotin technology underwent a renaissance in nanoscale drug delivery and diagnostics. Targeting ligands or imaging agents can be easily coupled to nanocarriers via the avidin-biotin linkage. For example, PMA hydrogel capsule functionalized with biotin forms a stable nanocomplex with avidin-coupled antibodies

and improved its cellular uptake in cancer cells.[19] Liposomes modified with biotinylated polyethylene glycol can attract a layer of neutravidin on the surface to resist nonspecific binding to serum proteins, thus leading to prolonged circulation time.[20] Microbubbles coupled with RGD peptide via avidin-biotin linkage were developed for the detection of Hep-2 related tumor angiogenesis.[21] Neutravidin conjugated superparamagnetic iron oxide nanoparticles have also been explored as an imaging agent for rhodopsin degeneration.[22] More recently, avidin-based nanotechnology has found its applications in tissue engineering and cellular regeneration.[23-24] In one such study, an avidin-biotin system was used to improve osteoblast-like cell adhesion to a highly porous calcium phosphate glass scaffold for bone tissue engineering.[24]

2.1.2 Structure and Physical-Chemical Properties of Avidin

Avidin is a basic (pI ~10), highly stable, tetrameric glycoprotein (molecular weight 66-69 kDa) that contains terminal N-acetyl glucosamine and mannose moieties.[25] Each of the four subunits contains 128 amino acids and binds to biotin with high specificity and affinity (K_d ~10^{-15} M).[26] The subunit is composed of eight antiparallel β-strands that form a β-barrel, whose wide end binds to biotin.[27] The avidin-biotin interaction is approximately 10^3 to 10^6 times higher than an antibody-antigen interaction. However, avidin may have a high degree of nonspecific binding *in vivo* due to its basic pI and glycosylation. Rigorous efforts have been made to study the structural properties of avidin using x-ray analysis of its 3D structure to improve its stability and functional properties.[28-29] Investigators have successfully generated several chimeric avidin analogues with better thermal stability and resistance toward proteolytic enzymes. [29-30]

On the other hand, the strong interaction between avidin and biotin may pose a limitation in releasing the tagged biomolecules from the biotin or avidin. Reversibility of the avidin-biotin interaction can be achieved by addition of a highly concentrated biotin solution. Researchers have also developed biotin analogues that have slightly low affinity toward avidin in comparison to biotin. For example, desthiobiotin can be easily released from avidin by addition of a moderately concentrated biotin solution.[31] Another method is to insert a cleavable linker, such as a stimuli-responsive linker, between biomolecules and the biotin or avidin. It is noteworthy to mention that chemical modification of the biomolecules may compromise their activities.[32]

2.1.2 Avidin Analogues

Despite its enormous advantages and wide applicability, avidin has several limitations including non-specific binding and possible immunogenicity. To circumvent these limitations, tremendous efforts have been devoted to discovering and engineering superior variants of avidin by genetic modification or discovering a completely new source, e.g., a different species.[31]

The most widely used analogue of avidin is streptavidin. Derived from *Streptomyces avidinii,* streptavidin is a ~56 kDa non-glycosylated tetrameric protein that binds to four biotins with a K_d of ~10^{-14} M.[33] Homologs of streptavidin have been discovered from other species, including fungus, bacteria, chickens and frogs.[34] Similar to avidin, streptavidin is also resistant to denaturing agents, temperature, pH and proteolytic enzymes. Despite having a tertiary/quaternary structure and amino acid arrangement similar to those of avidin, streptavidin only shows a moderate sequence homology level of ~30% sequence identity and 40% similarity with avidin.[35-36]

Moreover, streptavidin is non-glycosylated and has a slightly acidic pI of ~5-6.[37-38] Due to its different physical-chemical properties, streptavidin shows an *in vivo* tissue distribution and clearance profile very different from those of avidin.[38] Furthermore, streptavidin protects the biotinyl esters from hydrolysis, whereas avidin augments this hydrolysis.[35] A variety of genetically engineered streptavidins such as *Strep*-Tactin have been developed to exploit the outstanding specificity of the genetically encodable peptide *Strep*-tag II. [39] Strep-tag II has been used for protein purification and detection [40] as well as in numerous *in vivo* applications.[41-43]

Neutravidin is another commonly used avidin analogue. It is the deglycosylated derivative of avidin and has a molecular weight of ~60 KDa. In the absence of the carbohydrate moieties, the pI of neutravidin is only slightly acidic (~6.3), which prevents its nonspecific binding to cell surfaces and proteins.[44-45] As a result, neutravidin can be coated on the surface of quantum nanorods to stabilize them and prevent aggregation.[46] In addition, neutravidin has been utilized as a bridge between biotinylated moieties and biotin-coated surfaces for the detection of protein-specific antibodies.[47]

Bradavidin II is a relatively new avidin analogue that was isolated from *Bradyrhizobium japonicum*, a nitrogen-fixing bacteria found in the root nodules of the soybean plant.[48] Bradavidin II shows a moderate amino acid similarity with avidin (38%) and streptavidin (32%), but exhibits the same biotin binding affinity as avidin. Compared to streptavidin, bradavidin II could be a better choice for therapeutic applications because it is less immunogenic. The physical-chemical properties of avidin, neutravidin, streptavidin and bradavidin are summarized in Table 1.

Table 1. Physical-Chemical Properties of Avidin and Derivatives

Properties	Avidin	Neutravidin	Streptavidin
Origin	Chicken egg	Avidin	*Streptomyces avidinii*
Molecular Weight (KDa)	67	60	53
Iso-electric Point	10	6.5	5.5-6.5
Specificity	Low	Highest	High
Biotin Binding site	4	4	4

Most of the avidin analogues have a similar tetrameric structure, which is beneficial to high amplification of a desired signal. On the other hand, the tetrameric assembly may affect the accuracy of binding quantitation due to the uncertainty of the precise binding stoichiometry and possible crosslinking. As a result, avidin analogues, such as hoefavidin and rhizavidin, which have dimeric arrangement are of interest. [49] [50] Their tertiary topologies remain the same as avidin.

Other recombinant or naturally occurring avidin include Tamavidin 2 (*Pleurotus cornucopiae*)[51], Shwanavidin (*Shewanella denitrificans*)[52], Switchavidin (chicken avidin mutant)[53], Zebavidin (Zebrafish)[54].

2.1.3 Biotin and Analogues

Biotin is a vitamin also known as vitamin H, vitamin B7 or co-enzyme R. Biotin is composed of a tetrahydrothiophene ring fused to a ureido (tetrahydroimidizalone) ring. It plays a key role in cell signaling and acts as a cellular growth promoter. Biotin receptor (sodium-dependent multivitamin transporter and high-affinity biotin transporter) is

widely expressed in nearly all living cells. Moreover, its expression in dividing cancer cells is higher than in normal cells, making biotin a potential targeting moiety for cancer therapeutics.[55] Extensive effort has therefore been made to develop biotin-based platforms for tumor targeting and diagnosis.[56]

The functional groups of biotin have been chemically modified to synthesize biotin analogues, such as iminobiotin, ethylbiotin, desthiobiotin, biotin-carbamate, and biotin-carbonate for various applications.[57] Chemical modification of biotin may affect its affinity toward avidin. For example, iminobiotin shows pH-dependent K_d values. Its K_d is 3.5×10^{-11} M at basic pH but lower than 10^{-3} M at acidic pH (3-4).[58]

Apart from biotin, strep-tag (Trp-Ser-His-Pro-Gln-Phe-Glu-Lys) is a peptide that shows high affinity (K_d 2.7×10^{-4} M) to streptavidin.[59] It has been used in a variety of nanotechnology and biotechnology applications [60-61]. Recombinant proteins of interest can be easily fused to strep-tag for protein purification and other applications. Researchers have also discovered other variants of strep-tags, strep-tag I and strep-tag II, with higher affinities. The strep-tag I (Ac-Trp-Ser-His-Pro-Gln-Phe-Glu-Lys) and strep-tag II (Trp-Ser-His-Pro-Gln-Phe-Glu-Lys) peptides bind to streptavidin with a K_d of 37×10^{-6}M and 72×10^{-6}M, respectively.[62]

2.1.4 Applications in Nanoscale Delivery Systems

2.1.4.1 Nucleic Acid Delivery

Nucleic acids, including plasmid DNA, siRNA, miRNA, aptamers, and oligonucleotides have been extensively explored as therapeutic agents for a wide variety of diseases, and some of them have been applied clinically. Their negative charge and poor stability are the two major hurdles that prevent nucleic acids from reaching their full

potential as therapeutics. Although viral vectors are generally effective for nucleic acid delivery, virus-associated safety concerns make non-viral systems better candidates for therapeutic applications. Numerous non-viral platforms, especially nanoscale delivery systems including liposomes, peptide nanocomplex, polymer-based nanoparticles, and inorganic nanoparticles, have been rigorously developed for nucleic acid delivery over the past two decades.

Nano-formulations for the delivery of siRNA face tremendous challenges, including aggregation, short systemic half-life and low cellular uptake [63-65]. Protein-based delivery can efficiently counter such shortcomings. For the delivery of siRNA-like negatively charged molecules, cationic proteins, peptides or polymers are recommended for use. These counter-ions produce a high likelihood of nanocomplex aggregation. In a related study, neutravidin was utilized to deliver siRNA to podocytes by conjugation of a monovalent IgG (mIgG) to neutravidin through a sulfhydryl group (Fig. 2A). Here, instead of the biotinyation of the siRNA, protamine (a cationic protein) was linked to biotin that was coupled to the neutravidin tag on the mIgG. Cationic protamine therefore condenses multiple siRNA molecules and delivers the complex to the target podocytes. Within 30 min of incubation, the IgG with siRNA was detectable in the cytoplasm. This delivery system showed a tremendous reduction (greater than 80%) in the expression of the target protein (p57/Kip2) compared to the control [66].

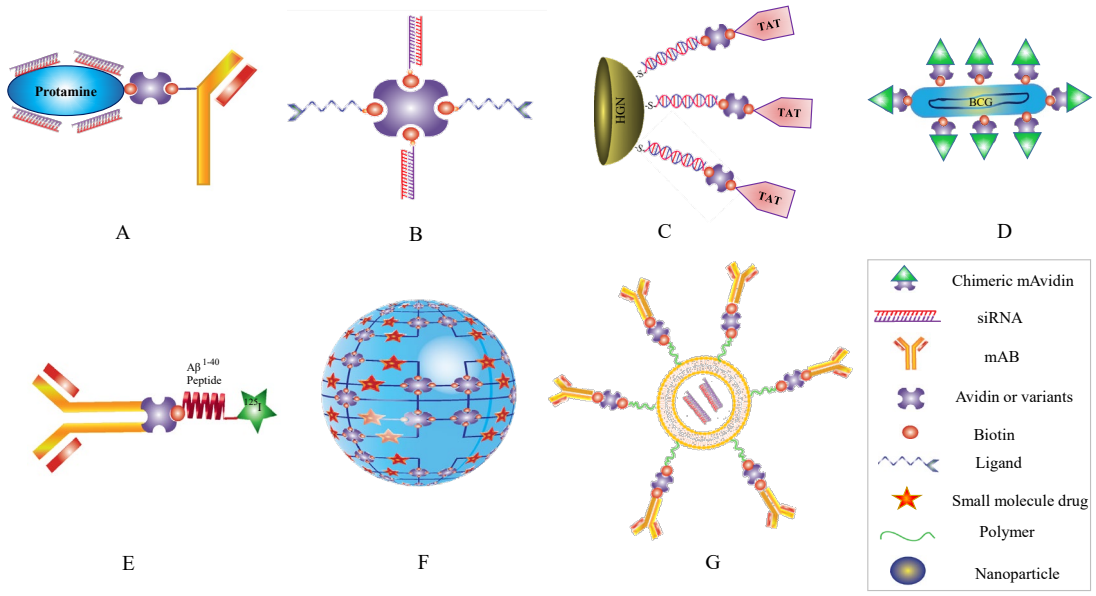

Figure 2. Drug delivery and therapeutic applications of avidin-biotin technology
(A)Biotin modified anti podocyte antibody coupled with biotinylated Protamine with the Neutravidin bridge. Negatively charged siRNA molecules bind to the positively charged protamine. The modified antibody delivers bound siRNA to the target podocyte. (B) Biotinylated siRNA delivery with the help of biotinylated ligand; (C) Plasmonic hollow gold nanoshells (HGN) decorated with siRNA molecules via thiol bond and overcoated with streptavidin to further attach TAT protein. Upon irradiation with biocompatible near infrared (NIR) light (~800 nm), the siRNAs are released from the gold surface (due to carrier surface specific thiol gold bond dissociation); (D) Chimeric mAvidin proteins bound to the Biotinylated BCG for reversible antigens attachment on surface. Antigen coated BCG is then inoculated into the animal to deliver antigens and subsequently induces specific T cell responses; (E) Biotinylated Aβ 1-40 peptide radiopharmaceutical attached with the cTfRMAb-AV fusion protein, TfRMAb delivers this Aβ 1-40 peptide radiopharmaceutical across BBB to the amyloid plaque. (F) Doxorubicin loaded Microhydrogel formed from biotinylated hyaluronic acid, Neutravidin and Doxorubicin-HCL; (G) Liposome surface functionalized with PE-PEG via biotin. The biotinylated antibody-coated on ULVs loaded with siRNA with the help of streptavidin.

In addition to their use as Trojan horses, viral proteins have also been utilized to target nucleic acids to cells. A viral domain that specifically targets a particular cell type is coupled to an avidin moiety via a covalent bond, and the avidin molecule acts as a carrier for the delivery of the nucleic acids. Leisi et al. [67] developed one such delivery system, in which they utilized the VP1u domain of parovirus B19 conjugated to

neutravidin to specifically deliver biotinylated DNA or fluorophores to the targeted erythroid cells that were undergoing differentiation around the proerythroblast stage. For this study, maleimide-activated neutravidin was used because it can attach to 5-6 VP1u in a manner that excludes the four biotin-binding sites. Neutravidin is very versatile and retains its activity after minor chemical modifications. The results demonstrated that this VP1u-neutravidin nanocarrier is highly efficient and has excellent therapeutic and diagnostic applications in a wide variety of blood-associated conditions, including hematological ailments such as thalassemia or leukemia .

Similarly, streptavidin has been employed to deliver siRNA for the treatment of liver fibrosis. The tetravalent structure of avidin makes this protein a very efficient tool for the delivery of biotinylated siRNA by producing stable nanocomplexes. These nanocomplexes have shown rapid uptake silencing of the target gene. As shown in Fig. 2B, the biotinylated siRNA and biotinylated cholesterol anchored to the streptavidin backbone provide efficient silencing of the PCBP2 gene for liver fibrosis treatment [68-69]. Streptavidin-biotin technology has also been utilized for the delivery of Kv1.3 siRNAs in the treatment of autoimmune disorders. Biotinylated polyethylene glycol and cholesterol were functionalized with biotinylated-CD45RO antibodies through the use of streptavidin to provide highly specific targeting and uptake of nanoparticles by Memory T cells, which had the consequence of decreasing the calcium ion influx, thus producing a therapeutic effect [70]. Several other simple and efficient strategies for nucleic acid delivery have recently been reported for the targeted delivery of nucleic acids.

Delivery of siRNA to normal cells is relatively easier compared to the process in stem cells. Biocompatibility is a major concern because incompatibility could otherwise

cause a fatal immunogenic response [71-72]. Synthetic vectors pose various limitations for the transfection of undifferentiated human embryonic stem cells (hESC) with nucleic acids. Huang and coworkers developed a light responsive siRNA delivery system using hollow gold nanoshells (HGN) in which the HIV-derived TAT peptide was utilized to deliver the siRNA into the hESCs under the influence of biocompatible infra-red radiation (~800 nm). The direct conjugation of the TAT peptide to the siRNA resulted in aggregation due to surface charge. As depicted in Fig. 2C, the TAT and siRNA were coupled to different binding sites of the streptavidin molecule, which kept them separated. This structure prevents electrostatic contact, which inhibits particle aggregation [73].

Another novel method of delivering nucleic acids is the avidin-nucleic acid nanoassembly (ANANAS). Here, the nucleic acid acts as a central unit onto which several avidin molecules are nucleated. This assembly forms a toroidal structure, which is further complexed with biotinylated polyethylene glycol [74]. Due to the excellent pharmacokinetic properties of avidin, after *in vivo* administration, fluorescently labeled ANANAS nanoparticles showed substantial subcellular internalization in the mucosal vasculature. This enabled the localization of nanoparticles at the target site, whereas no accumulation was observed in healthy tissues.[74] ANANAS shows tremendously promising characteristics, including easy preparation, no immunogenicity, and excellent pharmacokinetic properties, which make it an outstanding translational therapeutic and diagnostic tool [75-76].

2.1.4.2 Protein and Peptide delivery

Protein and peptide delivery has generated considerable interest in the past two decades on the basis of its potentially important applications in targeted therapy. Therapeutic peptides, enzymes and recombinant proteins are among the highest revenue-generating products among all the pharmaceutical products offered across the globe [77]. However, the macromolecular drugs face substantial delivery challenges including slow or low permeability across biological membranes and low target-specific biodistribution [78]. The greatest hurdle in the delivery of peptides and proteins is their encapsulation. Special consideration must be given to the chemical and physical properties of the biologics before contemplating the nanocarrier. Because proteins are prone to structural distortion that may lead to the loss of biological activity[79], special care is needed in protein modification to minimize the loss of the activity of these molecules.

Due to the minimal modification required by the biotinylation of a protein molecule, avidins have been employed by several researchers as a carrier for peptide delivery, such as cell penetrating peptides (CPP) [80-81] and Tat peptide [82]. The biotinylated peptide sequences are complexed with avidin to reduce the chance of aggregation. Additionally, covalent modifications of peptides may induce conformational changes that can interfere with their ability to be translocated. However, biotinylation acts as a spacer that reduces the constraints on a peptide mandated by the carrier [81]. The four biotin-binding sites on avidin can be exploited for the delivery of different peptide sequences for specific roles such as targeting a ligand, as depicted in Fig. 2B. In one such study, a tumor-targeting peptide (bio-CREKA) and an arginine-rich peptide (Bio-R8) were used simultaneously to deliver the p53 tumor suppressor gene. Here, avidin allowed the use of

the two biotinylated peptides, where the Bio-R8 moiety promoted the internalization of the nanocomplex and bio-CREKA provided for specific binding to the receptors on MCF-7 cells [83].

The internalization of a protein by a target cell involves overcoming a series of barriers. Investigators have developed fusion proteins that include avidin or streptavidin to enhance the uptake of small synthetic molecules mediated by receptors. The presence of the streptavidin in these fusion proteins triggers internalization and thus overcomes the delivery barriers [84]. The avidin modification not only provides a very useful carrier for peptide delivery but substantially promotes the cellular internalization [85]. Several parameters including particle aggregation, size and surface charge play vital roles in cellular internalization. Rational modification of the surfaces of the nanoparticles with avidin showed higher uptake than that of the unmodified nanoparticles. In contrast to the DSPE-PEG nanoparticles, Av-MPG-NPs showed a higher uptake due to their surface charges, which resulted in a smaller size and a higher ligand density. These properties have a combined impact on the internalization kinetics that resulted in the higher internalization of the Av-MPG-NPs [86].

Peptide sequences such as cell-penetrating peptides (CPP) hold considerable potential for the cellular internalization of molecules that are difficult to transfect. However, CPP-based delivery to colorectal cancer (CRC) cell lines or metastatic cancer cells is even more challenging. Streptavidin-like proteins have been used as a model protein carrier for the delivery of several CPP that can promote the internalization of macromolecular drugs, such as DNA or siRNA. Cell-penetrating sequences such as transportan-10 (TP-10) and transportan (TP) have recently been evaluated by Wierzbicki

et al.[87] Biotinylated analogues of TP and TP-10 have demonstrated an endocytosis-independent and highly efficient delivery of siRNA when complexed with streptavidin in HCT116 (metastatic CRC model) and HT29 (early stage CRC model) cell lines and resulted in a high silencing activity of SASH-1 mRNA. [87] It can clearly be inferred that streptavidin provides a substantial advantage for cellular and tissue internalization in addition to its use as a dynamic stoichiometric support (back-bone) for nanocomplexes.

2.1.4.3 Vaccine Delivery

In recent years, vaccine development has generated much interest. Rigorous efforts have been made to reduce the time between the discovery of vaccine candidates and their clinical development. The greatest challenge involves the production of antigens in an appropriate quantity to induce an optimal immune response in the body [88]. Avidin also provides the advantage of varying and adjusting surface chimeric proteins on bacteria to induce a higher immunogenic response toward the vaccine.[89] Furthermore, biotinylation of the bacterial surface proteins has no effect on the phenotypic characteristics of the bacteria or the exogenous properties of the protein, all of which make avidin a very applicable moiety for vaccine development [90]. In addition to all of the other advantages, deglycosylated monovalent avidin substantially reduces the chances that the vaccines will aggregate [90].

The stability of vaccines is the most important aspect of vaccine development. Much effort is being directed toward improving the stability and efficiency of the development of vaccines for a range of conditions, from HIV to dengue. One issue is that the addition of protein molecules that may help to stabilize a vaccine may compromise its activity. Solutions have recently been devised to express an avidin fusion protein along

with the target protein for stable and efficient antigen expression. In one such study, shown in Fig. 2D, *Bacillus Calmette-Guerin (*BCG) bacteria were biotinylated, and the surface of the bacteria was decorated with a monovalent avidin fusion protein.[89] This technique produced BCG vaccines that are more responsive to T cells , and which were reproducible and highly stable for an extended period of time after freeze drying [90]. Another research group developed a technique to employ avidin in the development of a Lassa fever vaccine that undergoes self-assembly. Here, MtbHSP70-avidin proteins were coupled to biotinylated peptides from the Lassa GP1 and GP2 proteins, which are naturally immunogenic. This self-assembling vaccine showed tremendous stability and optimal immunogenicity [91].

The vaccine research and development process also faces the challenge of the extended time required to reach an effective *in vivo* immunogen concentration. Investigators have reported efforts to minimize the long time required for the B cell-specific antigen detection and the slow onset of the immune response. This method involves the sequential staining of biotinylated antigenic gonadotropin-releasing hormone (GnRH)-like peptides with streptavidin or neutravidin. This process increases the ligand avidity, and the 'single epitope multiple staining' principle permits the rapid detection of the B cells after immunization [92].

In addition to binding to the biotinylated antigen, streptavidin is also used as a potent immunostimulant in cases of less immunogenic antigen-based cancer vaccines. Currently, cancer vaccine research utilizes "self" tumor antigens, which are only weakly immunogenic.[93] These antigens are not much different from other cells in the patient's body, hence, the patient becomes tolerant very rapidly. To circumvent such problems,

immunostimulants of bacterial origin, such as streptavidin, have been used. Moreover, streptavidin has also been demonstrated to have a high affinity for surface-bound tumor proteins. The RYDS sequence of streptavidin assists in cell adhesion through the RGD cell adhesion domain . These two qualities have led to the use of streptavidin for the delivery of cancer vaccines. The vaccine-streptavidin combination produced 6 times higher reactivity than the vaccines alone. Streptavidin bound to biotinylated soluble tumor proteins have successfully produced tumor reduction and remission in a 9 L glioma rat model and in canine patients .

Vaccine development requires the vaccine immunogen to be presented at a high density with a uniform orientation through which it can attain ideal epitope spacing and mimic the multivalent epitope of a virus [94-95]. Controlling the orientation and density of the coupled antigen by chemical conjugation poses a tremendous challenge. Additionally, the incorporation of complex antigens onto virus-like particles (VLPs) compromises their assembly and thus the activity. Thrane et al [96]designed a genetically modified HPV16 L1 VLP (Human papilloma virus 16 L1 virus-like particle) to overcome these challenges. The insertion of AviTagTM (Avidin tag) in the L1 coding sequence of HPV16 L1 VLP permits it to be biotinylated specifically. This, in turn, can be utilized to fuse the antigen with monovalent streptavidin without disrupting the assembly of VLPs and their activity .

The use of avidin in recombinant vectors has increased the possibility of delivering various classes of biotinylated antigens. Vectors that target dendritic cells using a single chain antibody (scFv) fused with a streptavidin core is an example of this approach. Dendritic cells play an essential function in the management of antigen-specific immunogenicity. Antigenic vaccines that can specifically target the dendritic cells to

activate the required immunogenic response are being developed and tested clinically [97-98]. However, the optimal immune response was not observed following either *in vivo* or *ex vivo* stimulation. A receptor-targeting approach has been developed to use dendritic cells receptor-specific ligands that can efficiently deliver antigens to the dendritic cells [99]. Investigators have developed a single chain antibody (scFv) fused with a streptavidin core that targets the DEC-205 receptor of dendritic cells. This streptavidin core and biotinylated antigen subsequently form a complex and delivers the antigens to the target dendritic cells [100].

2.1.4.4 Monoclonal Antibody (mAb) Delivery

Avidin-biotin technology has made it possible for a monoclonal antibody to carry a payload to the vital target sites. Avidin-coupling or fusion proteins not only make it easier to formulate the delivery carrier but help to increase the uptake at a target site. Avidin provides a greater advantage in the delivery of drugs via monoclonal antibodies. Avidin-fusion proteins coupled to monoclonal antibodies by genetic engineering have shown excellent target specificity. Molecular Trojan horse and avidin-biotin technologies have been recently exploited to delivery biologics across the blood brain barrier (BBB) via transferrin receptors (TfR). Specifically, TfR-MAb functions as a ferry to transport the biologics into the brain through the BBB TfR [101]. Chemically cross-linking avidin with TfR-MAb is one strategy that has been applied to deliver a peptide across the BBB [102]. Unfortunately, the specificity of monoclonal antibodies is compromised when they are chemically modified. However, an IgG-Avidin fusion protein expressed in Chinese hamster ovary (CHO) cells retained the specificity of the MAb.[103] Similarly, avidin-chimeric-TfR-MAb fusion protein was also expressed and engineered in biotin-depleted

CHO cells [103]. Using the same methodology, the amyloid plaques that accumulate in the brain and result in Alzheimer's disease have also been targeted for imaging and diagnosis using an TfR-MAb-avidin fusion protein.[104] As depicted in Figure 2E, radiolabeled $A\beta^{1-40}$ was attached to the TfR-MAb-avidin fusion protein. This complete conjugate was used to ferry the radio-pharmaceutical across the BBB [104].

Antibodies are also extensively used in radioimmunotherapy, which requires a highly specific interacting molecule for the binding of the effector to the pre-targeting molecule [105]. To achieve a high specificity of the effector for the pre-targeting molecule, avidin-biotin technology has been recently implemented. In contrast, a fusion protein approach using the avidin-biotin system is very effective and produces a superior homogeneity. However, this approach is highly time-consuming and requires extensive efforts and optimization [106]. A pretargeted ^{211}At-radioimmunotherapy developed by Frost et al consists of an avidin-monoclonal antibody that has a high affinity toward radiolabeled and biotinylated poly-L-lysine conjugates. This radioimmunotherapy delivery system is highly efficient, less time-consuming and demonstrates excellent tumor specificity [107]. Compared with conventional radioimmunotherapy, the avidin-conjugated monoclonal antibody produced a higher uptake of radiopharmaceuticals [108].

Patrick Ng et al [109]also developed an avidin-antibody fusion protein (Av-anti-rat TfR IgG3) that is capable of efficient delivery of various molecules into cancer cells. In this approach, the CH3 region of a human lgG3 (rat transferrin receptor-specific) is genetically fused with avidin. Generally, the fusion protein approach requires the chemical conjugation of specific protein components with various applications. This results in decreases in the activities of the respective components, and its development is

very difficult. In contrast, the avidin-Mab construct is a universal construct that eliminates the need to use a specific protein for a particular application. Ng and coworkers [109] demonstrated that the Av-anti-rat TfR IgG3 possesses an ability to deliver various biotinylated molecules and has a strong pro-apoptotic activity against the T cell lymphoma cell line Y3-Ag1.2.3 as well as the rat C58 (NT) D.1.G.OVAR (malignant cancer cells), while a non-recombinant anti-rat TfR IgG3 did not show any activity [109]. They further showed that this recombinant avidin system may induce a high antitumor activity *in vivo* by delivering the biotinylated agents into the cancer cells. [109]

Molecular Trojan horses are also a type of genetically engineered MAb that has recently become the most promising tool for the delivery of macro-molecules across biological membranes such as the BBB. The only caveat of this fusion technology is that the protein cannot be fused with oligonucleotides. However, the avidin-biotin technology enables the targeting of siRNA and peptides *in vivo* in association with fusion protein technology [110]. Merging the Trojan horse technology and the avidin-biotin technology has also allowed a highly specific receptor-mediated means to deliver siRNA using Mab, which have extensive stability *in vivo*. In a similar study, human insulin receptors (HIR) were targeted using HIRMAb that were conjugated with streptavidin (HIRMAb-SA) and subsequently bound to a 3′-biotinyl-siRNA. The delivery of luciferase siRNA with HIR-MAb-SA caused 90% silencing of the luciferase gene. In comparison, avidin, unconjugated streptavidin, or the HIR-MAb alone showed negligible effect [111].

Non-convalent avidin-biotin interactions are very helpful for the surface decoration of nanoparticles with antibodies. The use of avidin-biotin to conjugate the MAbs to the nano-carrier surface helps to retain the MAb's function. Hajdu et al biotinylated

antibodies to CD45RO, a cell surface marker for memory T cells. These biotinylated MAbs were used to functionalize the surfaces of nanoparticles made from pegylated/biotinylated phosphoethanolamine and cholesterol through the use of streptavidin. The resulting CD45RO-functionalized nanoparticles showed highly efficient targeting to memory T cells for potential therapy for autoimmunity (Fig. 2F) [70].

2.1.4.5 Small Molecule Delivery

Nanotechnology has provided many ways to efficiently deliver chemotherapeutic drugs to the site of action. Efficient delivery of small molecules requires high specificity to the target site which can only be achieved by the attachment of receptor-specific ligands [112]. Avidin provides an excellent bridge for diagnostically relevant ligands that target specific receptors [86]. These ligands may or may not be functionally modified with stimulus-responsive cleavable linkage for delivery of these small molecules. Mesoporous silica nanoparticles capped with avidin functionalized with an MMP9 (matrix metalloproteinase 9) specific cleavable linker is one such example [113]. Because MMP9 is over-expressed in the areas of lung tumors that are beginning to metastasize, it allows the controlled release of the drug at the site of metastasis [114]. The mesoporous silica nanoparticles mentioned above are constituted with tunable pores and volume for higher drug loading. The outer surfaces of these mesoporous silica nanoparticles can be functionalized with certain molecules that do not interfere with the pore morphology and integrity. In one such example, the mesoporous silica nanoparticles were tightly capped with avidin molecules, and the pores were blocked by biotin, which prevented the release of the payload (cisplatin) from the core [113]. Thus, the avidin-biotin served as a guard on the surface of the nanoparticles to regulate the release of drug.

The avidin-biotin system has also been widely used as a pretargeting strategy [115-116]. Additionally, biotin and avidin have been reported to target and accumulate, respectively, in tumors [117-120]. These properties make them an excellent choice for a tumor-targeting formulation strategy. High avidin accumulation in the liver after treatment, as well as the properties mentioned above, have been exploited to target hepatic carcinoma. Recently, chitosan nanoparticles modified with biotin and avidin were designed in which the mannose sugar and acetyl glucosamine of avidin were used to target the liver. Moreover, avidin allows the addition of multiple ligands on the surface to achieve highly specific targeting. Bu et al.[121] demonstrated that the avidin bound to the biotin on the surface of the nanoparticles was responsible for the higher liver accumulation of nanoparticles and thus enhanced the anticancer activity [121].

Biotin labeling of the surface of the carrier dramatically increases the possibility of surface functionalization through avidin-modified moieties. This technique has been applied to couple liposomes to the surface of microbubbles. Microbubble-liposome therapeutic carriers for which ultrasound is used to target the therapy toward breast cancer has recently a field of extensive research. Yan et al. proposed this novel form of therapy in which they used avidin for the surface conjugation of paclitaxel-loaded liposomes on the microbubbles. Ultrasound exposure caused the drug payload to be efficiently delivered to the target site [122].

In another approach (Fig. 2G), hyaluronic acid (HA)-based micro hydrogels were prepared by exploiting the avidin-biotin technology.[123] Here, neutravidin-biotin was used to link micro-hydrogel containing doxorubicin to the HA molecule to function as a switch. Avidin-biotin has also been exploited by several researchers for the hydrogel

grafting [124]. These HA-biotin- neutravidin micro-hydrogels show fine porosity in conjunction with micro-beads. Upon addition of excess biotin, the HA microhydrogel-encapsulated drug disassembles to rapidly release additional doxorubicin. In this application, biotin acts as the triggering agent or a switch to release the drug at the target site [125].

We have described the advantage of avidin in the tumor-specific delivery of drug molecules. Delivery across the BBB and other complex biological barriers is even more challenging than metastasized malignant tumor cells. To address this issue, investigators have devised several approaches including the use of apolipoproteins in the design of nanoparticles that mimic natural particles [126]. Low-density lipoprotein receptor-specific apolipoprotein E (Apo-E) target the endothelial cells of the BBB very efficiently. However, chemical conjugation and other modifications of Apo-E reduce its function substantially. Avidin-biotin technology serves as a convenient tool to attach these Apo-E molecules to a drug delivery carrier without compromising their activity. Here, Apo-E was biotinylated and used to functionalize avidin-conjugated solid lipid nanoparticles. The avidin-biotin system is thus useful for the strategic functionalization of nanocarriers for highly efficient delivery of therapeutic small molecule drugs [127].

Stimulus-responsive technology for drug development, controlled release and targeted therapy has been extensively harnessed by research groups across the globe. In this context, the switchable release of avidin from biotin is one of the most simplistic, intriguing and innovative strategies. Imino-biotin is a type of biotin which has avidin-binding properties similar to those of natural biotin.[128] Imino-biotin is coupled to the nano-carrier, where it retains its structure and its noncovalent bond with avidin at

physiological pH. Upon protonation under lower physiological pH conditions, its affinity for avidin is decreased, and it releases the drug attached to it. This switch-release technology using a modified biotin is highly efficient in comparison to the disulfide linkages.

2.1.5 Applications of Nanoscale Avidin Systems in Diagnosis and Biotechnology

2.1.5.1 Surface Antigen Detection

The interaction of avidin with biotin provides an excellent platform for the development of various assay systems. Although antibody-based assay systems are highly specific, chemical conjugation with fluorescent dyes or chemiluminescent compounds may have some impacts on the antibody specificity. Quantum dots have proven to be a highly efficient tool compared to the traditional antibody-fluorescent dye-based assays. Quantum dots provide several advantages such as high signal strength, high photo stability and high quantum yield for the detection of proteins with an enhanced signal amplification [129]. Protein quantification using quantum dots in elemental mass spectrometry (ICP-MS) based immunoassays has also proven to be very effective and efficient. Quantum dots possess outstanding photoluminescent properties, which makes them very important and novel as an antigen-detection system. Quantum dots have a tremendous capacity to improve bioanalytical applications that use bio-labeling and bioimaging methods. To fully exploit the functions of quantum dots, it is necessary to establish strict control for their synthesis and surface modification. The noncovalent interaction between biotin and streptavidin serves as the best tool for the surface modification of the quantum dots and permits the development of selective assay systems without compromising their target-binding specificity.[130] In a similar development, an

immunoassay platform based on streptavidin-conjugated quantum dots, which are used to bind to a biotinylated antibody and can be detected using ICP-MS, has been designed for amplified protein quantitation. This system enables the quantitation of protein in samples with concentrations as low as 50 ng/mL [130]. Neutravidin bioconjugated to highly luminescent quantum dots has also been developed for the detection of the tyrosine kinase B (Trk-B) receptors present on the neurons of the hippocampus. Here, neutravidin was specifically used instead of avidin or streptavidin because the presence of the lysine allows the amide to bind to the carboxylic groups on the quantum dots. The quantum dot-neutravidin bound to the biotinylated anti-TrkB antibody specifically detected the distribution of the TrkB receptors. The quantum dot-neutravidin conjugated to the biotin-TrkB serve as an excellent tool for long-term observations of the trafficking of the fluorescence signals during live imaging of neurons. [131] Quantum dots have also been employed for detecting and tracking enzymes in vivo. As demonstrated in Figure 3, several hydrolase enzymes have been conjugated to quantum dots through the avidin-biotin interaction. It was found that the catalytic activity was retained by the quantum dot-conjugated enzymes compared to the free biotinylated enzymes. The avidin-biotin interaction in this application was critical because it is a robust interaction with a high resistance toward wide range of pH. The avidin–biotin system has ubiquitously been proven to be the best method to functionalize the luminescent quantum dots-enzyme conjugates compared with the traditional approaches. [132]

Non-invasive bio-medical imaging techniques such as magnetic resonance imaging (MRI), single-photon emission computed tomography (SPECT) and positron emission tomography (PET) can evaluate and diagnose the progression of numerous diseases

through the use of surface antigen detection. Among these techniques, MRI is considered to be the technique of choice for imaging soft tissues [133]. Iron oxide nanoparticles are widely utilized as the MRI contrast agent. However, iron oxide nanoparticles need to be stabilized with low-molecular-weight high-affinity dispersants [134] and polymers, such as poly ethylene glycol, to stabilize them against oxidization. In one such study, iron oxide nanoparticles were stabilized with poly-ethylene glycol coated with neutravidin for the immobilization of the biotinylated VCAM-1 (vascular cell adhesion molecule 1) antibodies. VCAM-1 bearing neutravidin-coated nanoparticles showed outstanding affinity and specificity toward the VCAM chimeras. Neutravidin also provides flexibility in varying the ligand density on the nanoparticles, which makes it an excellent agent for the detection of antigens *in-vivo* [135-136].

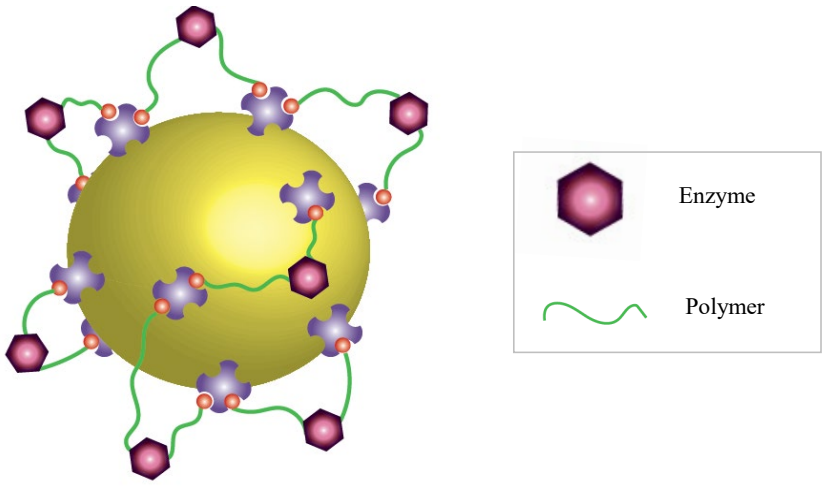

Figure 3. Streptavidin coated Quantum dots modified with biotinylated enzymes. Streptavidin is linked to the carboxylic groups on the surface of the quantum dots. The streptavidin conjugated quantum dots are coupled to biotinylated enzyme via the avidin-biotin interaction for in vivo tracking of the enzyme activity.

Quantification of a specific antigen at extremely low levels and over a wide range is a very important capability in the field of life science [137-138]. For dynamic sensitivity over

a wide range of antigen concentation, immuno-PCR (IPCR) is a system that utilizes antibodies and DNA conjugates. However, this method has several disadvantages, such as challenging preparation, purification, and a low DNA-to-antibody ratio that results in a low sensitivity and high non-specific background signals.[139] To address these issues, as depicted in Fig. 4, modified liposomes with an encapsulated reporter DNA have been designed. The surface of the liposomes is conjugated to a biotin-PEG (polyethylene glycol) phospholipid that acts as a detection agent. Microplate wells on which the target antigen specific antibody is immobilized capture the antigen. A biotin-labeled secondary antibody with a neutravidin bridge binds to the antigen. Biotin-coated liposomes bind to the neutravidin-bridge and anchor the reporter DNA-loaded liposomes. Upon binding to the target antigen, the liposome bursts to release the reporter DNA, which permits the target protein to be quantified using real-time PCR. [139]

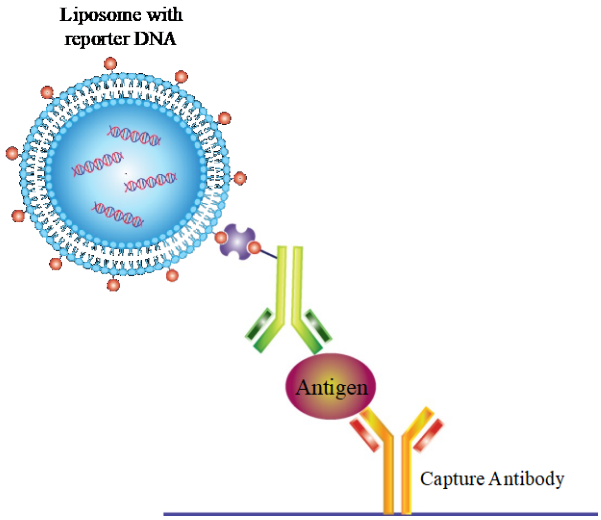

Figure 4. Avidin-biotin based immunoliposomes for antigen detection using PCR. Liposomes encapsulating reporter DNA are conjugated to a biotin-PEG (polyethyleneglycol) phospholipid that acts as a detection agent. A biotin-labeled secondary antibody with a neutravidin bridge binds to the antigen. Biotin-coated liposomes bind to the neutravidin-bridge and anchor the reporter DNA-loaded liposomes. Upon binding to the target antigen, the liposome bursts to release the reporter DNA, which permits the target protein to be quantified using real-time PCR.

The antigenic target is immobilized in the well of a microplate by a capture antibody and the liposome detection reagent is then coupled to another biotin-labeled antibody through a NeutrAvidin bridge. The liposome is ruptured to release the reporter DNA to quantify the protein biomarkers associated with diseases with the help of real-time PCR.[139]

Although sandwich ELISA-based assays are well known and widely applied [140-141], a new assay approach that harnesses the streptavidin-biotin interaction and exhibits a 10-fold higher sensitivity has been recently developed [142]. In addition, this approach reduces the cost by 20-fold in comparison to RT-PCR. In this assay, named NLFOA (nuclease-linked fluorescence oligonucleotide assay), nanoparticles coupled with several streptavidin molecules interacts specifically with the biotinylated TurboNuclease for detection of the HIV-1 p24 antigen. The NLFOA provides a highly sensitive assay system for the clinical diagnosis of HIV or other infectious diseases [142].

2.1.5.2 Imaging and Diagnosis

Imaging technology has been extensively evolved in recent years. Its biggest application is the diagnostics and detection of biological markers for specific diseases, such as cancer. Several radiolabeled antibodies are being extensively studied or are now undergoing clinical trials for the imaging and diagnosis of cancer [143-144]. However, this method poses several disadvantages that prevents its broad clinical application. These include slower tumor diffusion and delayed clearance kinetics that lead to a decrease in the tumor-to-nontumor ratio. To address these shortcomings, the concept of pretargeting has been proposed. For pretargeting, avidin and streptavidin can be conjugated to either monoclonal antibody or radioisotope. The extremely high binding affinity, rapid blood

clearance and high tumor uptake of biotin and avidin make them highly reliable and essentially the best candidate for pretargeting imaging technology.[105] Generally, avidin is used to clear the circulating biotinylated antibodies from the systemic circulation, but for the pretargeting strategy streptavidin or neutravidin are extensively used. Interestingly, it has been found that the fluorescently labeled or radiolabeled streptavidin showed a higher uptake in the tumors compared to the normal tissues than that of the radiolabeled antibody alone [145-147].

For diagnostic purposes, the expression of a specific antigen on a particular cell type can be harnessed and subsequently detected with favorable techniques [148-149]. Similarly, the types of antigens or markers present on cancer cells reveal the degrees of malignancy, invasion, neo-vascularization, and metastasis. Fluorescently tagged antibodies specific for these cell-specific markers are used for efficient detection via imaging or other diagnostic tools. Because avidin is very stable to the chemical modification, it serves as a good candidate for conjugation purposes. Maleimide-activated avidin was utilized to modify a MAb which is specific for the embryonic cancer delta-like protein (Dlk-1). A fluorescent bioluminescent protein (FBP) was designed by the conjugation of biotinylated Cypridina luciferase (CLu) to a far-red derivative of fluorescent indocyanine (Fig. 5). The FBP was subsequently coupled to the Dlk-1-specific MAb to identify the embryonic cancer antigen Dlk-1 via the avidin-biotin interaction [150].

Theranostic modalities that can simultaneously diagnose and treat a condition have driven the development of calcium phosphosilicate nanoparticles (CPNP). CPNP is another type of vehicle that is used for various imaging and therapeutic applications in

biological systems. These particles function by accumulating in the solid tumors via enhanced permeation and retention (EPR) effect. Conjugating these nanoparticles to fluorescent probes has proven to be highly effective. Barth et al[151] utilized avidin to engineer a novel CPNP that was conjugated to biotinylated diferric transferrin (human holotransferrin), biotinylated anti-CD71 antibody (transferrin receptor specific), and biotinylated pentagastrin using an avidin-biotin coupling. These avidin-CPNP-based theranostic materials were shown to specifically target, diagnose and treat breast cancer and other rapidly dividing and transferrin-expressing cells [151].

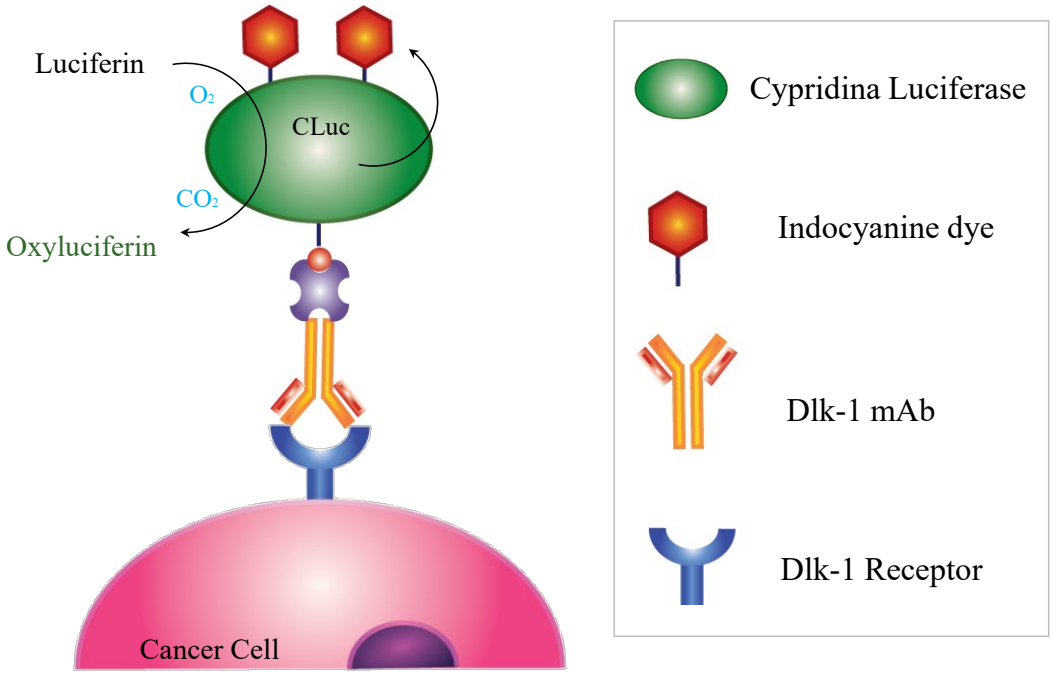

Figure 5. Avidin-based fluorescent bioluminescent protein probe for cancer imaging.
A fluorescent bioluminescent protein (FBP) is designed by the conjugation of biotinylated Cypridina luciferase (CLu) to a far-red derivative of fluorescent indocyanine. These FBP are subsequently coupled to the Dlk-1- specific MAb to identify the embryonic cancer antigen Dlk-1 via the avidin-biotin interaction.

Another widely accepted theranostic application is radioimmunotherapy, which employs streptavidin for the coupling strategy. Direct radionuclide labeling of MAb has been conventionally used for disease control. However, complete eradication is still a challenge because the tumor to normal cell localization ratio is extremely low. Malignant plasma cells are highly radiosensitive, and the management of plasmacytomas and multiple myeloma is possible with the help of radioimmunotherapy combined with streptavidin and biotin technology.[152] Streptavidin-coupled antibodies are highly selective for the tumor tissues or malignant cells. Once the streptavidin-coupled antibodies accumulate at the target site, a biotinylated radioactive small molecule is administered that specifically binds to the streptavidin that has accumulated in the malignant cells or tumor site. Green et al.[153] developed such a streptavidin-biotin pretargeted radioimmunotherapy system that targets the CD38 antigen for the delivery of a radionuclide for the eradication of multiple myeloma. Here, anti-CD38 was conjugated to streptavidin, and ^{90}Yttrium was bound to biotin for pretargetting [152]. The ^{90}Y–DOTA–biotin treatment produced the maximum survival rate in treated mice .

Another diagnostic modality that has received significant interest due to its unique properties and characteristics (Fig. 6) is nanoparticle clusters. However, their structurally and morphologically controlled development is highly challenging. For successful size-controlled construction of nanoparticle clusters, Ryu et al. proposed a method using a DNA-binding zinc finger protein that utilizes the avidin-biotin system. Direct chemical conjugation of metal ions (Zn) to DNA limits their further ability to derivatize the nanoparticle surfaces. To circumvent these challenges, DNA was conjugated to biotinylated zinc finger protein and subsequently incubated with neutravidin-conjugated

nanoparticles. These nanoparticle clusters showed not only the successful development of a size-controlled construct but also increased spin–spin relaxivity three-fold compared to conventional contrast agents such as Feridex [154].

PET scanning is also a highly sensitive and extensively used technique for the quantitative imaging of tumor specific markers. Hypoxic inducible factor 1 (HIF-1) plays a key role in the progression of malignant tumor and radiotherapy resistance. The oxygen-dependent degradation domain (ODD) of HIF-1α has therefore been used for the development of tumor imaging and therapeutic agents. HIF-1-positive tumor cells are one type of the targets that have been most quantitatively diagnosed with the help of noninvasive imaging techniques such as PET.[155] A protein transduction domain (PTD) coupled to the oxygen-dependent degradation domain and to monovalent streptavidin was used to produce the fusion protein PTD-ODD-streptavidin (POS) because of the outstanding *in-vivo* stability of biotin-streptavidin. Streptavidin modification reduces the degradation of POS. The POS conjugated with radioactive ^{123}I-IBB specifically target the HIF-1 exclusive regions in tumors [156]. Another streptavidin fusion protein was developed by the same group to deliver the radiolabeled biotin derivative synthesized as 4-^{18}F-fluorobenzoyl-norbiotinamide (^{18}F-FBB). It was concluded that the areas showing ^{18}F-FBB localization corresponds to the HIF-1α positive areas [157].

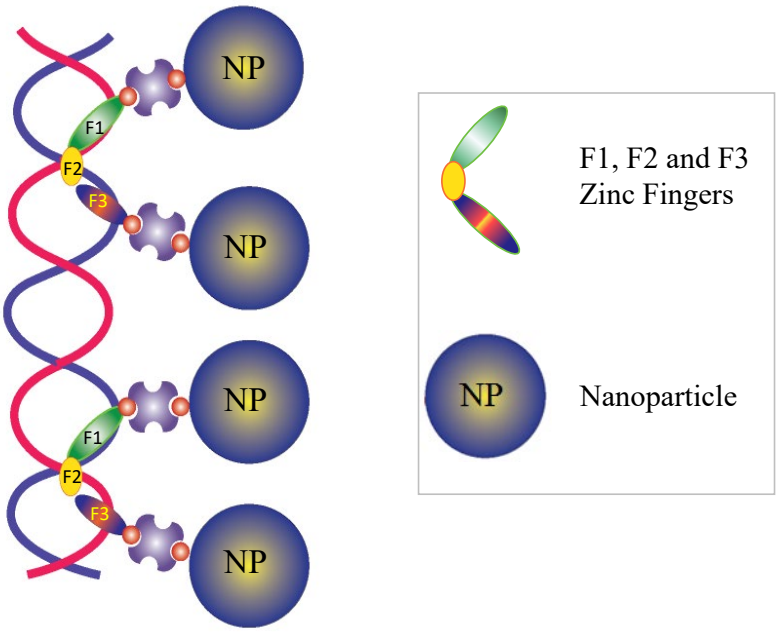

Figure 6. Neutravidin biotin-based nanoparticle clusters for diagnosis and imaging. Biotinylated zinc finger protein is coupled to avidin conjugated nanoparticles. The zinc finger proteins (F1, F2, F3) bind to the DNA template. These zinc fingers and DNA templates are highly sequence specific which helps in the size-controlled construction of NPC for application in diagnosis and imaging.

Streptavidin-based imaging modalities have negligible effect on the pharmacokinetics of their parent drug, which makes them ideal for the application in diagnosis. A streptavidin-based nanoparticle has been developed as a multimodal imaging agent for the fluorescence and nuclear imaging and detection of tumors in a mouse model.[158] Liang et al [158] designed a biotin-binding streptavidin-based nanocomplex that was coupled to a biotinylated anti-Her2 antibody. Tumor targeting was achieved using a biotinylated anti-Her2 (Herceptin antibody), and diagnostic imaging was performed using a biotinylated DOTA-chelator labeled with ^{111}In and a biotinylated Cy5.5 fluorophore. Both radiolabeled and fluorophore-labeled streptavidin nanoparticles

complexes have proved to be very efficient and promising tools for Her2-positive tumor imaging [158].

2.1.5.3 Tissue Engineering

Skin grafts are considered the most common method used for the clinical repair of skin defects.[159] However, contraction of the grafts, rejection due to immunity and graft dysfunction are a few shortcomings of the grafting technique. Tissue engineering is one promising alternative to overcome the deficiencies of the graft techniques This alternative strategy involves the fabrication of a scaffold that mimics the natural extracellular matrix (ECM) of the target [160] Avidin is immobilized on biomaterial surfaces, and the cell membranes are conjugated with biotin. The extraordinary affinity of these two molecules mediates the efficient attachment of the cells to the biomaterials. Natural cellular adhesion occurs by the formation of integrin-mediated bonds between integrin in the cell membrane and adhesion proteins on matrix [161]. Investigators have demonstrated that that avidin-biotin binding system was found to be superior to the integrin-serum protein system with respect to the cell adhesion strength [162]. Recently, the avidin-biotin binding system (ABBS) was used to fabricate PLCL/Pluronic nanofiber matrix for skin care application [163].

Silk biomaterials with attached bioactive molecules are extensively used for drug delivery and tissue engineering. Covalent coupling has a very large negative impact on the bioactivity of the biomolecules due to the amine group reactivity. Non-covalent methods of coupling such as avidin-biotin are therefore recommended. The versatility and simplicity of the avidin-biotin system made it possible to immobilize various moieties, such as growth factors and gelators for tissue regeneration [164].

New bone ingrowth at a bone defect site is also the most important alternative to simple bone replacement, which prevents the possibility of bone rejection by immune system. Investigators have reported the application of avidin and biotin-based systems to attach cells to the surfaces of nonporous 2D and 3D biodegradable scaffolds.

Streptavidin has been used with grafting materials, such as Mylar^{TM} and Teflon-AF^{TM}, for adhesion and proliferation of endothelial cells. In one such study, human umbilical vein endothelial cells (HUVEC) were biotinylated and incubated with streptavidin to immobilize grafting materials. The streptavidin-coupled HUVEC showed significant spreading in comparison to uncoupled HUVEC [165]. In a similar study, ABBS was utilized in the calcium phosphate glass scaffold for bone tissue adhesion. The scaffold immobilized with avidin showed substantially higher cell attachment. ABBS has a major advantage over other scaffolds because it does not inhibit cell proliferation. Scaffold functionalized with ABBS can improve its adhesion with osteoblast-like cells. It was concluded that the ABBS scaffold helps in proliferation after efficient attachment of the osteoblast like cells [24].

In addition to a prominent scaffold for cell adhesion, the biggest prerequisite for tissue engineering is to imitate the local bio-microenvironment and bio-ceramic matrix to provide a 3D support that enables growth of bone tissue [166]. Biologically active molecules, such as protein and peptide, decorated on the surface of these bioceramics can improve bone regeneration [167]. However, there are still a few challenges for tissue engineering: (i) A strong interaction between proteins and the surface of scaffold; (ii) No change in the native structure and biological activity of the proteins; and (iii) Site-directed immobilization. Baeza et al utilized the avidin-biotin technology to address these

challenges in tissue engineering [168]. Another research group developed biotinylated nanofibrous hydrogels for efficient cell adhesion in a 3D matrix of C2 based gelators made from 1, 4-benzyldacarboxamide.[169] As shown in Figure 7, avidin modified cells were used to adhere on the biotinylated gelator-based 3D matrix. This system has shown to produce a universal 3D matrix system where avidin modified cells freely proliferate without any sign of denaturation. Moreover, the density of the cells in the matrix can be manipulated by varying the biotin-gelator amount in the matrix [169].

3D matrices used in tissue regeneration are required to be biodegradable. Repair and regeneration of a bone defect with the help of a biodegradable polymer-based scaffolds are often used along with bone-inducing factors and/or osteogenic cells. In addition to the biocompatibility and appropriate mechanical strength for weight bearing, scaffold for bone regeneration must have interconnected porous structure for tissue in-growth which can support the regeneration [170-172]. BMP-2 and BMP-7 (bone morphogenetic protein) are two main osteo-inductive factors which have the potential to induce differentiation of osteocytes, followed by mineralization and bone regeneration [173-174]. Encapsulation of these growth factors on to polymeric scaffolds using various solvents and electric field for fabrication may result in the loss of biological activity [175]. To overcome such challenges, streptavidin was employed for binding biotin-BMP2 and biotin-SAP (self-assembling peptides). Furthermore, with the help of streptavidin, the degree of BMP2 and biotinylated peptide can be controlled. Intra scaffold retention of BMP2 was also increased by tethering of BMP2 which further prolongs its half-life as well [176].

A group of scientists also focused on the localized 3D differentiation of BM-MSCs (Bone marrow-derived mesenchymal stem cells) by orthogonal matrix-immobilization of BMP-2. A recombinant Glutamine-streptavidin linker peptide, a bio-mimetic scaffold, was genetically engineered.[177] It was covalently coupled to the TG–PEG (Trans-glutamase) hydrogels. Controlled presentation of recombinant rhBMP-2 with streptavidin-coupled PEG hydrogels provides the consequent 3D-localized osteogenic differentiation of BM-MSCs [177].

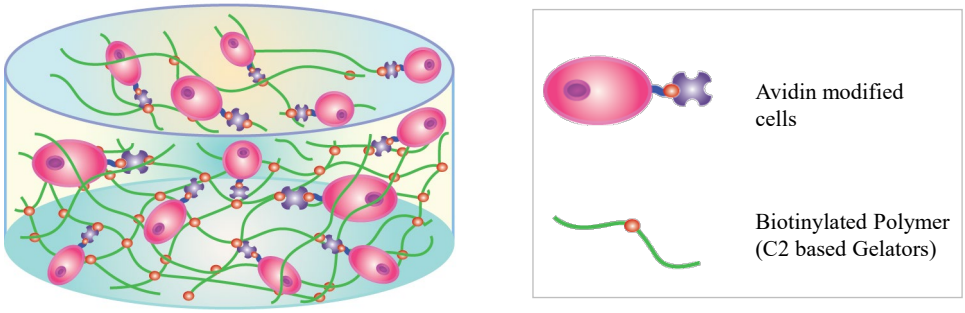

Figure 7: Avidin-biotin-based 3D nanofibrous hydrogels for tissue regeneration. MC3T3 osteoblastic, EAhy926 human endothelial, and SMMC-7721 human hepatoma cells were biotinylated with an EZ Links Sulfo-NHS-LC-LC-Biotin. Using avidin as a bridge, the modified cells were in situ encapsulated in a 3D hydrogel system made of biotinylated and nonbiotinylated 1,4-benzyldicarboxamide (C2) based supramolecular gelator.

2.1.6 Conclusion

As one of the strongest non-covalent interactions in the nature, the avidin-biotin interaction has evolved to become a very versatile platform for a great variety of applications in biotechnology and nanotechnology. At a constant pace, new analogues of avidin are being developed with better efficiency and physical-chemical properties to serve specific purposes. As simplistic this system is in its fundamental principle, avidin-biotin system is as strong and applicable [34]. Extensive use of this system in a wide variety

of fields, such as drug delivery, antigen targeting, diagnostics, and tissue engineering is the proof of its unparalleled advantages.

Noncovalent interactions including hydrogen bonding, hydrophobic interaction, van der Waals interaction, and ionic interaction have also been utilized for nanoscale drug delivery systems. These interactions are stronger when present collectively but are very weak individually. By comparison, the biotin-avidin interaction employs multiple hydrogen and hydrophobic interactions, leading to an extremely high affinity [178]. On the other hand, the use of ionic interactions to load drug may cause problems in the formulation development. For instance, drug molecules with $–NH_2$ may interact with –COOH to form large aggregates [179]. Ionic interaction can also be influenced by pH, which may affect the stability of nanocarriers in acidic tumor microenvironment [121, 180]. Loading of drug to nanoparticles using hydrophobic interaction may result in particle aggregation, which will affect the biodistribution of nanoparticles in the body [181-182]. By contrast, nanocarriers made from the biotin-avidin interaction have a uniform size-distribution and robust stability against enzymes, temperature, pH and harsh organic regents [68, 105].

Tetravalent structure of avidin and its analogues provides a great advantage in the nanoparticle design, development and delivery. It provides a strong backbone for the biotinylated ligand and drug molecules with four biotin binding sites per avidin molecule. This characteristics provides the flexibility in loading drugs and ligands to nanoparticles [183]. Biotin and avidin are also readily available with various functional groups for chemical conjugations. Moreover, the chemical conjugation on biotin or avidin avoids direct modification of the active biomolecule, thus maintaining their activity.

The application of avidin-biotin system is more than just coupling biotinylated molecule to avidin-conjugated moieties. Properties such as high tumor accumulation, immune modulation and easy genetic engineering make them highly advantageous for a variety of applications in nanotechnology. Particularly in the pretargeting field, the avidin-biotin system is a leap ahead of the conventional radiolabeled antibody approach. Despite of multiple advantages of this system in biotechnology, further research is required to understand the immuno-toxicity of the avidin and its variants. In this review, we have compiled the most recent reports that have utilized this system in various fields of nanotechnology.

2.2 RNA Therapies Delivery Challenges and Advances: Conceptualization to Clinical Development

siRNA is considered one of the greatest therapeutic discoveries since past century. It is the most efficient solution for the pathological conditions caused by the over expression and mutation of a gene. siRNAs and other RNAi therapies are being significantly utilized for the treatment of the variety of diseases and regenerative medicine. It is widely pursued in therapeutic development of many fatal disease because of its specificity, targetability and adaptability. RNAi as a whole is a technology that can potentially cure the "undruggable" targets. Despite its therapeutic potential, siRNA are highly unstable if injected as such into the blood stream. It may also lead to some fatal immunogenic responses. For siRNA delivery, a very safe and effective carrier is required which can deliver the siRNA to the target site and maintaining the siRNA's therapeutic integrity without imparting any unwanted immunogenic response. Progress in deeper

understanding of the molecular mechanisms of the diseases and RNAi has improved the preclinical development and performance for wide range of disease targets.

2.2.1 Materials and Modifications for the RNA-based Therapeutics

RNAi therapeutics and especially siRNA delivery systems comprise of non-viral and viral vectors. Adeno-virus vectors have been rationally engineered to deliver the RNAi therapeutics to the target site. [184] However, due to high degree of immunogenic response due to viral vectors, non-viral vector materials are primarily utilized for the nucleic acid delivery. These non-viral materials are proteins, peptides, polymers, lipids etc. siRNAs are encapsulated in these materials to form nanoparticles which not only deliver the siRNA to target site but protects it from the degradation. Cationic charge is critical for the development of the nanoparticle for the siRNA delivery as negative charge of the nucleic acid hinders its cellular uptake.[185] Cationic lipids are also one of the most studied categories which are utilize to condense the siRNA with electrostatic interaction to form nanoparticles. Such cationic polymers or lipids have amine functionality (one or many). At physiological pH it gets protonated and imparts a positive charge to condense the nucleic acid. These nanoparticles further create charge imbalance that leads to the endosome rupture and release of siRNA in the cytoplasm. Commercially, many products are available for such applications such as DOTMA[186], DOTAP[187], Polyamido amines[188], polyethyleneimine [189], poly-L-Lysine [190], protamine etc. Cationic lipids in particular (DOTMA, DOTAP) are positively charged at acidic pH, ionization helps in the condensation of siRNA, self-assembly and subsequently releasing siRNA from endosome after internalization into the target cells. Biodegradable polymers such as polyethylene glycol and Poly (β-amino esters) have also been widely used for siRNA delivery. [191]

These cationic lipids have no significant toxicity in comparison to the cationic polymers that are more immunotoxic due to their cationic nature at physiological pH.[192]

2.2.2 Barriers and Challenges in Delivery of siRNA

Regardless of the delivery system and route of administration, the biggest barrier for siRNA remains to be degradation by nuclease and renal clearance during systemic circulation.[193] Rapid biodistribution to the target site is the greatest requirement for an ideal delivery system which also minimizes the chances of the siRNA clearance and degradation. Extravasation of the siRNA delivery system to the target site also poses a significant challenge. Nanoparticles are developed with optimum size to be able to transit across the blood vasculature.[194] Once reaching the target site, delivery systems must be efficiently taken up by the cells. Targeting ligands and rational modification of the delivery system have been rigorously investigated over the years to make them highly efficacious and enhance the internalization to the target cells via receptor mediated endocytosis. After internalization, the delivery carrier reaches the endosome of the target cell and has to escape the endosome to avoid the lysosomal degradation and exert activity in the cytoplasm.[195] Delivery systems are designed to enhance the endosomal escape and efficiently release the siRNA into the cytoplasm. Scientists have made tremendous efforts over the years to invent such delivery systems that can bypass all the barriers to produce maximum therapeutic efficacy.

Particle size of the siRNA delivery carriers such as nanoparticles is a very crucial factor. Larger particles (>200nm) are generally cleared by the reticuloendothelial system (RES). Enhancement or attachment of polyethylene glycol on the nanoparticle not only

reduces the particle aggregation and size but help in preventing the RES uptake and increase the half-life.[196]

Endothelial vasculature fenestration and extravasation determines the target localization of siRNA delivery system.[197] Capillary fenestration or pore size determined the upper limit of the particle size. Depending on the target organ, capillary pore sizes are different from very small (blood brain barrier) to comparatively big (digestive system). [198-199] siRNA- based systems or naked siRNAs favor hepatic localization over any other organs which makes them great drugs for liver diseases. However, delivery systems are exclusively designed to accumulate in the liver or target tissues to slow down the clearance process and enhance target uptake.[200] Moreover, lipid based systems are preferred to deliver the siRNA to the liver because the lipid metabolism occurs in liver. This enhances the possibility of the siRNA to reach the target site more preferably and efficiently.

Cellular uptake and inter-organelle transit of the siRNA is a rate limiting step. Uptake of the siRNA loaded nanoparticles or delivery carriers occurs via multiple pathways such as clathrin – caveolin dependent or independent pathway, [201-202] Limited understanding of the complex molecular transit of siRNA makes it hard for it to be developed and reach clinics. After being taken up by the cell, therapeutic payload is sorted by the cell to either proceed to the lysosome or matured late endosome. Soon after the reaching late endosome, the carrier releases the siRNA to the cytoplasm.[69] During this process, it has been argued that there are many other alternative pathways that a delivery system may be directed to, which may eventually reduce compromises to the therapeutic

efficacy of the system. Recycling endosomes (Rab5), Golgi apparatus and endoplasmic reticulum are major organelles which participate in such recycling process. [69, 203-204]

2.2.3 Conclusion

Decades of research efforts for the development of the siRNA delivery systems have revealed key mechanisms and great knowledge about the parameters to be considered for an efficient delivery system. Size, chemical, physical, biological and other implications that influence the performance of the siRNA delivery system have been thoroughly investigated. All the barriers including the systemic and intracellular can be overcome by thoughtful design of therapeutic carriers. Immunogenic responses and toxic side effects have halted the clinical translation of siRNA, but scientists across the globe have made astonishing progress in the field to circumvent such shortcomings. Lipid-based nanoparticles and other types of non-immunogenic polymeric or protein-based systems hold promise for the future of the siRNA delivery.

CHAPTER 3

INRACELLULAR FATE AND EXOCYTOSIS OF PCBP2 SIRNA NANOCOMPLEX IN HEPATIC STELLATE CELLS

3.1 Introduction

RNAi (RNA interference) is considered one of the greatest discoveries of the 21st century. Soon after its discovery, it has been regarded as the most promising therapeutic approaches to potentially inhibit the target genes (or mRNA) responsible for several fatal illnesses including many hereditary diseases, cancer and liver fibrosis.[205-207] Absence of effective delivery systems is one of the biggest stumbling blocks in the path of the siRNA's translational success and beholds limitation to its therapeutic promise.[208-209] In order to perform its function in target cell cytoplasm, siRNA has to face multiple physiological and biological challenges.[210-211] Many delivery systems have been developed in the past few decades, such as lipid based, polymer based (cationic peptides/polymers), and many other types of nanoparticles.[212-214]

Previously, we designed a nanocomplex using streptavidin as the delivery carrier for the PCBP2 siRNA.[5, 68] We observed that cellular uptake of these nanocomplexes in hepatic stellate cells (HSCs) is highly dependent on the siRNA condensing agent used for this nanocomplex formulation, protamine, and LDLR (Low Density Lipoprotein)-receptor mediated uptake by cholesterol. Additionally, reduction of the disulfide bond between biotin and siRNA is very critical for the silencing activity of siRNA. Efficient release of the siRNA from multiple components of nanocomplex in cells is necessary to facilitate the assembly of siRNA into RNAi machinery.[215] However, the exact mechanism of disassembly of the nanocomplex and intracellular fate remains elusive. We

were curious to know the fate of the different components of the streptavidin based siRNA nanocomplex inside the hepatic stellate cells. How endosomal escape of siRNA occurs? How siRNA is released form the nanocomplex in cytoplasm? These are the primary questions for the siRNA delivery systems in general. Investigating this area will yield significant and thorough understanding of the fate of the siRNA nanocomplex after internalization.

The importance of delivery in therapeutic applications of siRNA has long been realized, but analysis of the intracellular fate of siRNA delivery systems still remains elusive and requires more insight. Rapid exocytosis of nanocomplexes could be a typical transcytosis mechanism to transfer nanocomplex from one cell to another or recycle the nanocomplex by non-secretory exosomes. Exocytosis of nanoparticles varies with cell types, and there are a number of possible recycling routes for siRNA nanocomplex.[216] Several strategies such as elemental analysis have been utilized to study the intriguing phenomenon of endocytosis and exocytosis of nanoparticles.[217-218] By contrast, fluorescence microscopy and fluorescence tracking are the most accepted methods that can provide both qualitative and quantitative analysis [216].

In this study, we employed flow cytometry and confocal microscopy to examine the intracellular fate of the all the components of the siRNA nanocomplex (siRNA, streptavidin and protamine) in HSC-T6 cells. We labeled each component with different fluorescent probes such as Alexa Fluor 647 and Alexa Fluor 488. siRNA, protamine and streptavidin exhibit divergent cellular distribution.

3.2 Methods

3.2.1 Materials

Streptavidin, Alexa Fluor® 350 succinimidyl esters (NHS esters) and Streptavidin-Alexa Fluor 350 conjugate was purchased were purchased from Thermo Fisher Scientific. Protamine sulfate (salmon X grade) was purchased from Sigma-Aldrich (St. Louis, MO). Cell culture medium, Lipofectamine-2000, PCBP2 siRNA (sense sequence 5′-GUCAGUGUGGCUCUCUUAU-3′), negative control siRNA, and Alexa Fluor 647-siRNA were purchased from Invitrogen (Carlsbad, CA). Sephadex G-15 was obtained from GE healthcare life sciences (Pittsburgh, PA). Biotin–PCBP2 siRNA was purchased from Gene Pharma (Shanghai, China). Alexa Fluor 647 was conjugated to the 5′ end of the siRNA antisense strand, while biotin was conjugated to the 3′ end of the siRNA sense strand. RAB5 antibody (rabbit IgG), goat anti-rabbit IgG (H+L) secondary antibody (Alexa Fluor® 488 conjugate) and BODIPY® FL C_5-Ceramide complexed to BSA were purchased from Thermo Fisher Scientific (Waltham, MA).

3.2.2 Formulation of Streptavidin-Based siRNA Nanocomplex

Nanocomplexes were prepared as previously reported.[68] Briefly, biotin–PCBP2 siRNA with a disulfide cleavable linker at the 3’ end of the sense strand and Alexa Fluor 647 probe in the 5’ end of the antisense strand was mixed with biotin-cholesterol and streptavidin at a molar ratio of 2:2:1 and incubated at room temperature for 10 min followed by condensation with protamine (10/1 = N/P ratio) for another 30 min to form the streptavidin PCBP2 siRNA nanocomplex. Morphology and surface charge (Particle size and zeta potential) were analyzed with the help of Malven Zetasizer Nano ZS. For confocal microscopy and flow cytometry, Alexa Fluor 350-labeled streptavidin and

protamine were used along with the Alexa Fluor 647-labeled siRNA were used to formulate the Nanocomplex.

3.2.3 Cellular Uptake Study

The rat hepatic stellate cell line (HSC-T6) was kindly provided by Dr. Scott L. Friedman (Mount Sinai School of Medicine, New York University). HSC-T6 cells were cultured in DMEM supplemented with 10% FBS, 100 units/mL penicillin–streptomycin at 37 °C in a humidified atmosphere containing 5% CO_2. The cells were seeded in Chambered Cover glasses (Fisher Scientific; Pittsburgh, PA) at a density of 1×10^4 cells/well as reported previously.[5, 205, 219] The streptavidin based siRNA nanocomplex containing 100 nM final siRNA concentration was added to each well along with OptiMEM medium. The hepatic stellate cells (HSC-T6) were incubated with Nanocomplex for various time points. Following the completion of the time point, the cells were stained with 150 nM lysotracker to stain the lysosomes and fixed with 10% formalin buffer. Cells were counter stained with DAPI mounting media and analyzed under a confocal microscope (Leica TCS SP5).

3.2.4 Assessment of Cellular Uptake Using Flow Cytometry

25000 HSC-T6 cells per well of 24-well plates were seeded. The cells were transfected with the streptavidin based siRNA nanocomplex or Lipofectamine-2000 containing Alexa Fluor 647-labeled siRNA for various time periods as mentioned above. The cells were then washed with DPBS, detached, and subjected to fluorescence analysis using a BD FACS II Flow Cytometer (Bectone Dickinson Instruments, Franklin Lakes, NJ).

3.2.5 Exocytosis and Cellular Recycling of the SSCP Nanocomplex

Alexa Fluor 647-labeled siRNA was utilized to prepare the SSCP complex. In this study, the final siRNA concentration was maintained at 50 nM because the major purpose of this study was to monitor the siRNA recycling and exocytosis and excessively labeled siRNA might give false positives.[220] Five thousand HSC-T6 cells per well were seeded in 96 well plates and transfected with the SSCP nanocomplex diluted in OptiMEM. In one group, the medium was collected at 3, 6, 12, and 24 h post-transfection to evaluate exocytosis. In another group, the cells were transfected with the SSCP nanocomplex for 6 h, followed by replacement with fresh medium. The fresh medium was then collected at 1, 3, 6, 18, 21, and 24 h to determine the fluorescence of exocytosed siRNA. Fluorescence of the collected media was measured using a multimode fluorescence detector.

To further investigate the nature of exocytosed siRNA in the medium, we developed a method to determine whether the exocytosed siRNA is still entrapped inside the nanocomplex or simply in a free form. Briefly, the harvested media containing exocytosed siRNA were treated with heparin to release siRNA from the nanocomplex. By comparing the fluorescence intensity before and after the heparin treatment, we can determine the fraction of free siRNA in the exocytosed samples. We incubated the nanocomplex prepared in OptiMEM with various heparin concentrations (10, 20 and 40 μM) to understand the extent of fluorescence quenching by complexation and OptiMEM. After optimizing the concentration and incubation time of heparin, we again performed exocytosis study by treating the HSC-T6 cells as described above and collected medium at various time points after 6 h incubation with the SSCP. Followed by replacement of

fresh medium and subsequent collection of medium at different time points, we incubated collected medium with or without heparin for 30 min to analyze the nature of siRNA exocytosed.

3.2.6 Early Cellular Trafficking of the SSCP Nanocomplex

HSC-T6 cells were transfected with the SSCP nanocomplex containing Alexa Fluor 647-siRNA for 1h. One group of the cells were immediately washed and fixed with 10% formalin, followed by staining with the early endosome marker (Rab5 antibody). For the second group of the cells, the transfection medium was replaced with fresh culture medium and incubated for another 1 h before fixation with 10% formalin and staining with Rab5 antibody. Alexa Fluor® 488 conjugate secondary antibody was added to visualize early endosomes under confocal microscope.

Since Trans-Golgi Network (TGN) plays a vital role in the recycling of nanoparticles, we also stained the Golgi complexes using BODIPY-FL C5 ceramide as per manufacturer's protocol.

3.3 Results

3.3.1 Preparation of the Streptavidin Nanocomplex Containing Alexa Fluor Labeled Components

Nanocomplexes were formulated with the alexa fluor labeled components to monitor intracellular events after cellular uptake in HSC-T6. The Alexa Fluor dyes were selected because of their pH independence and excellent photo-stability.[215] The nanocomplex has demonstrated uniform average size of 230 nm with a PDI smaller than 0.15. Zeta potential of the nanocomplex is approximately 23 mV. Fluorescent-labeled

streptavidin and protamine were used for the SSCP nanocomplex preparation to evaluate cellular uptake and intracellular trafficking.

3.3.2 Streptavidin Nanocomplex Show Efficient Cellular Uptake

Thorough investigation of the intracellular fate of the different components in the nanocomplex will reveal the important mechanisms that influence the efficacy of the system. In our previous study, we hypothesized that the streptavidin nanocomplex, after internalization, escapes from endosome by leveraging the proton sponge pump owing to the multiple arginine present in protamine.[221] After escaping endosome, Nanocomplex releases siRNA in the cytoplasm by reduction of the disulfide linker with the help of cytoplasmic glutathione. The siRNA further forms the RNA-induced silencing complex (RISC) and perform mRNA inhibition or silencing.

Confocal microscopy and flow cytometry were utilized to investigate uptake of the streptavidin nanocomplex. First, HSC-T6 cells were transfected with the SSCP nanocomplex containing Alexa Fluor 647-labeled siRNA for 0.5, 1, 3, 6 and 24 h. As shown in Figure 8A, the SSCP nanocomplex rapidly enters the cells and reaches its highest uptake at 6 h post-transfection. Nearly all the cells were transfected with the SSCP nanocomplex at 6 h. LysoTracker® was used to evaluate lysosome entrapment of the siRNA. LysoTracker® is a highly specific, one-step staining dye for acidic organelles and has been widely employed to track lysosomes.[222] As the merged images illustrated (Figure 8A), only a very small amount of the siRNAs were entrapped in late-endosomes/lysosomes between 0.5 and 6 h post-transfection. Moreover, majority of the siRNAs were localized in the cytoplasm and few translocated into the nucleus at 3 and 6 h post-transfection. However, there was a significant decrease in cellular uptake at 24 h

post-transfection where siRNAs were mainly located in the cytoplasm as clustered aggregates at the perinuclear space localized with lysosomes.

Using the same method, we studied cellular uptake of the siRNA using Lipofectamine-2000 (Figure 8B). The resulting confocal images indicate that there was a continuous increase in cellular uptake up to 24 h post-transfection, and only a small fraction of them were entrapped in lysosomes. Compared to Lipofectamine-2000, the SSCP nanocomplex exhibits a faster and more uniform uptake of siRNA in HSC-T6 cells.

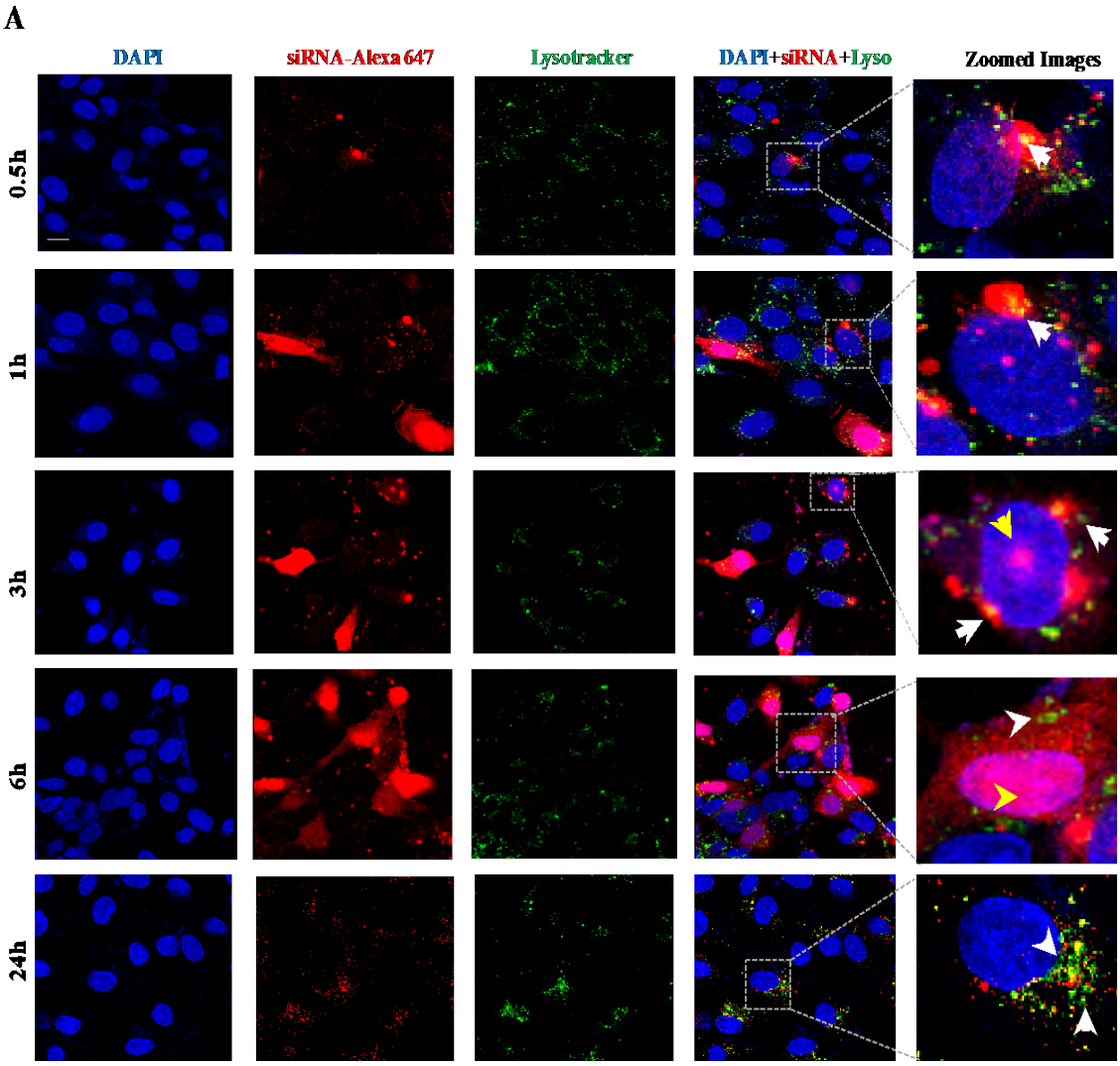
A
DAPI
siRNA-Alexa 647
Lysotracker
DAPI+siRNA+Lyso
Zoomed Images
0.5h
1h
3h
6h
24h

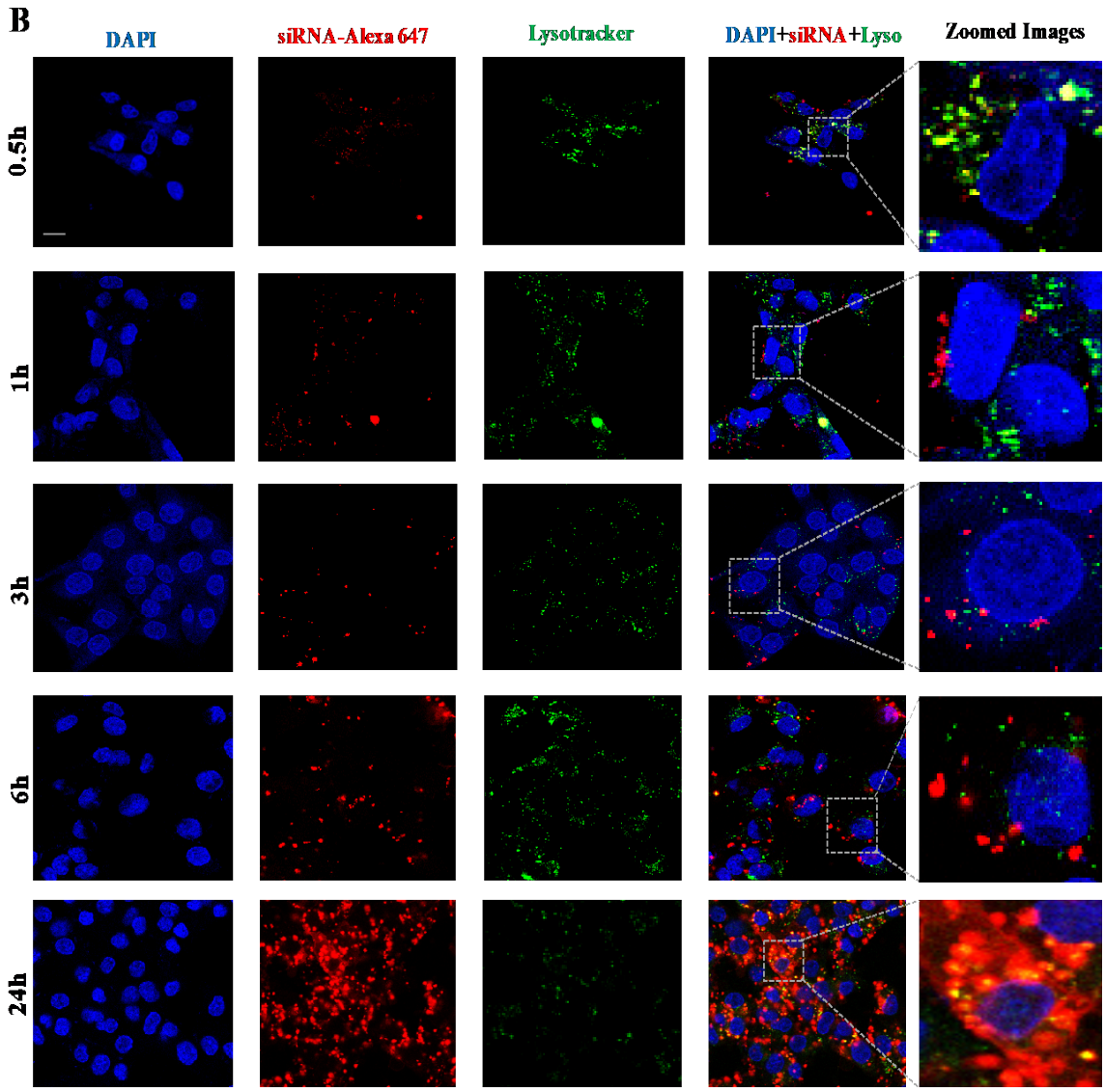

Figure 8. Cellular uptake of the PCBP2 siRNA in HSC-T6 cells by Nanocomplex. The Alexa Fluor 647 labeled siRNA is encapsulated in the SSCP nanocomplex (A) or Lipofectamine-2000 (B). The siRNA is incubated with HSC-T6 cells for 0.5, 1, 3, 6, and 24 h, followed by fixation and confocal imaging. DAPI = Nucleus, Alexa-647 =PCBP2 siRNA and Lysotracker = endosomes and lysosomes. Scale bar = 20 μm

We validated the cellular uptake of the PCBP2 siRNA with streptavidin nanocomplex and Lipofectamine-2000 in HSC-T6 cells using flow cytometry. As shown in Figure 9, nearly all cells were transfected with the streptavidin nanocomplex at 3 and 6 h post-transfection, indicating rapid cellular uptake of the streptavidin nanocomplex. In contrast, the Lipofectamine-2000 had lower transfection efficiency at early time-points but it escalated dramatically at 24 h post-transfection as compared to streptavidin nanocomplex (Figure 9). The fluorescence intensity results at 3 and 6 h post-transfection (Figure 9C) indicate that the streptavidin nanocomplex is able to deliver more siRNAs into the cells at early time points compared to Lipofectamine-2000. However, the fluorescence intensity in streptavidin nanocomplex treated cells decreases at 24 h post-transfection. These results are in congruence with confocal microscopy results (Figures 8A&B) where a decrease in fluorescence intensity was observed at 24 h post-transfection.

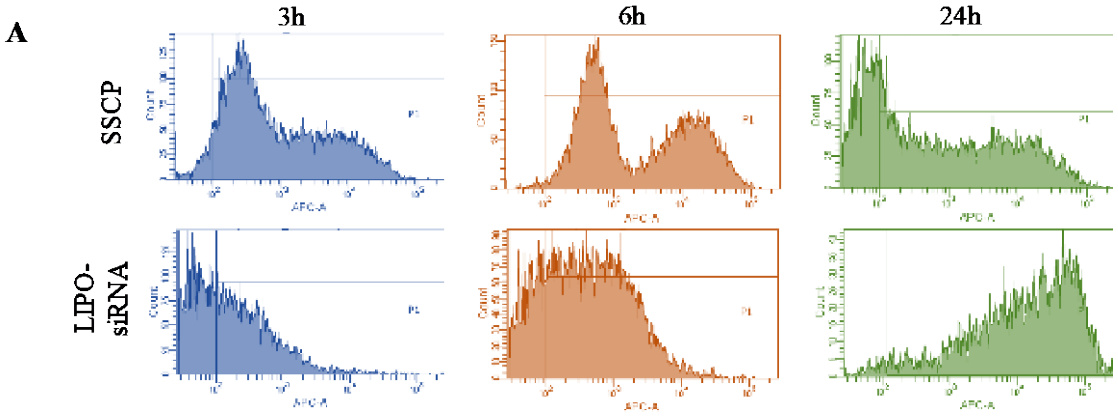

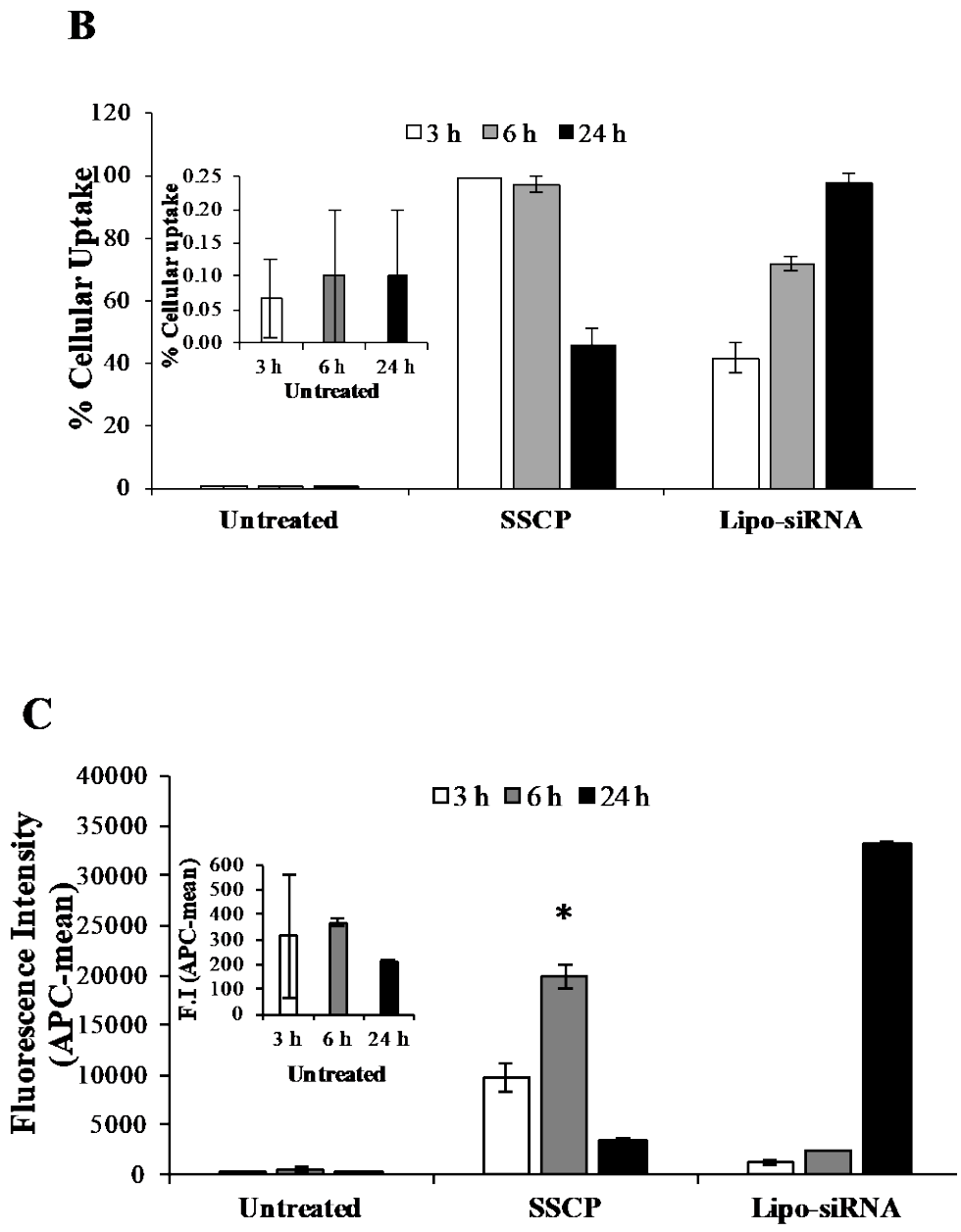

Figure 9. Cellular uptake of siRNA with SSCP nanocomplex and lipofectamine. Alexa Fluor 647 labeled PCBP2 siRNA was incubated with HSC-T6 cells for 3, 6, and 12h, followed by flow cytometry analysis. (A) Histogram of flow cytometry. Percent of cellular uptake (B) and relative fluorescence intensity (C) are presented as the mean ± SD (n=3).

3.3.3 Subcellular Distribution of Multiple Components of Nanocomplex

Confocal microscopy was used to further investigate distribution of different components (streptavidin, siRNA, and protamine) of the streptavidin nanocomplex in HSC-T6 cells. HSC-T6 cells were transfected with the streptavidin nanocomplex containing Alexa Fluor 647-labeled siRNA (far-red) and Alexa Fluor 350-labeled protamine (blue) for 1, 3, 6 and 24 h. As Figure 10A illustrates, a small percentage of the siRNAs in the cytoplasm are co-localized with protamine (indicated with yellow arrows) at early time points, while majority of the siRNA are co-localized with protamine in lysosomes at 24 h post-transfection (indicated with white arrows). We observed that fraction of the siRNA can be delivered into the nucleus without protamine co-localization (Figure 10A). This result indicates that protamine only acts as cell penetrating peptide in the uptake process. It dissociates from the streptavidin nanocomplex inside the cells and slowly translocate to perinuclear space and other parts in the cytoplasm while some of the siRNAs transit into the nucleus.

We next evaluated subcellular trafficking of streptavidin in HSC-T6 cells. Alexa Fluor 350-labeled streptavidin (blue) was used in the streptavidin nanocomplex along with Alexa Fluor 647-labeled siRNA (red). As shown in Figure 10B, streptavidin is localized with siRNA in the cell cytoplasm at all the time points. However, streptavidin shows variable co-localization with lysosomes. Streptavidin distributes in the cytoplasm at early (1 and 3 h) time points with negligible co-localization with lysosomes, but co-localization increases (indicated with yellow arrows) at 6 and 24 h post-transfection. The merged images of streptavidin and siRNA (Figure 10B) illustrate that majority of siRNAs are in the cytoplasm and few of the siRNAs are co-localized with streptavidin inside

lysosomes, suggesting incomplete release of SSCP from endosomes at extended time points or reuptake of nanocomplex by lysosomes (indicated by yellow arrows).

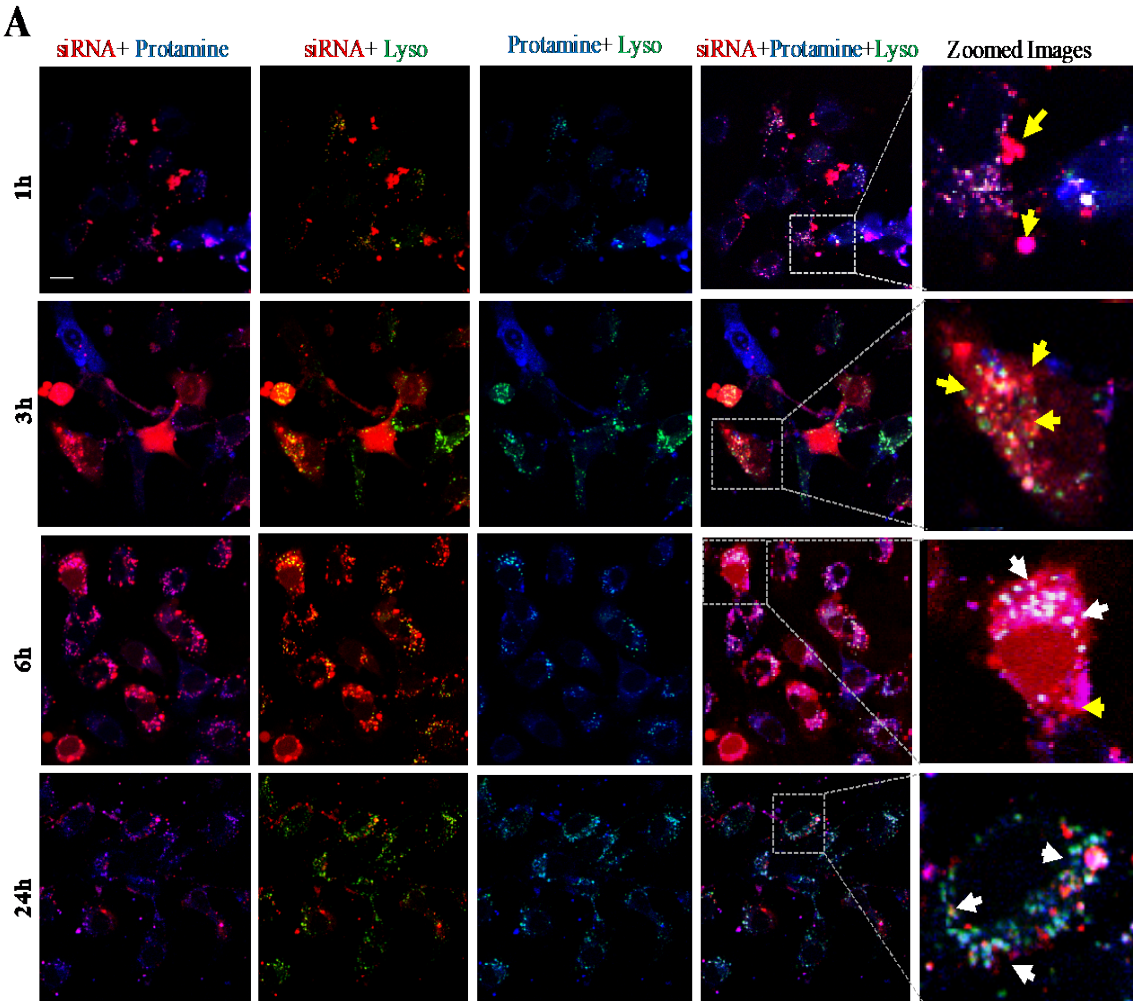

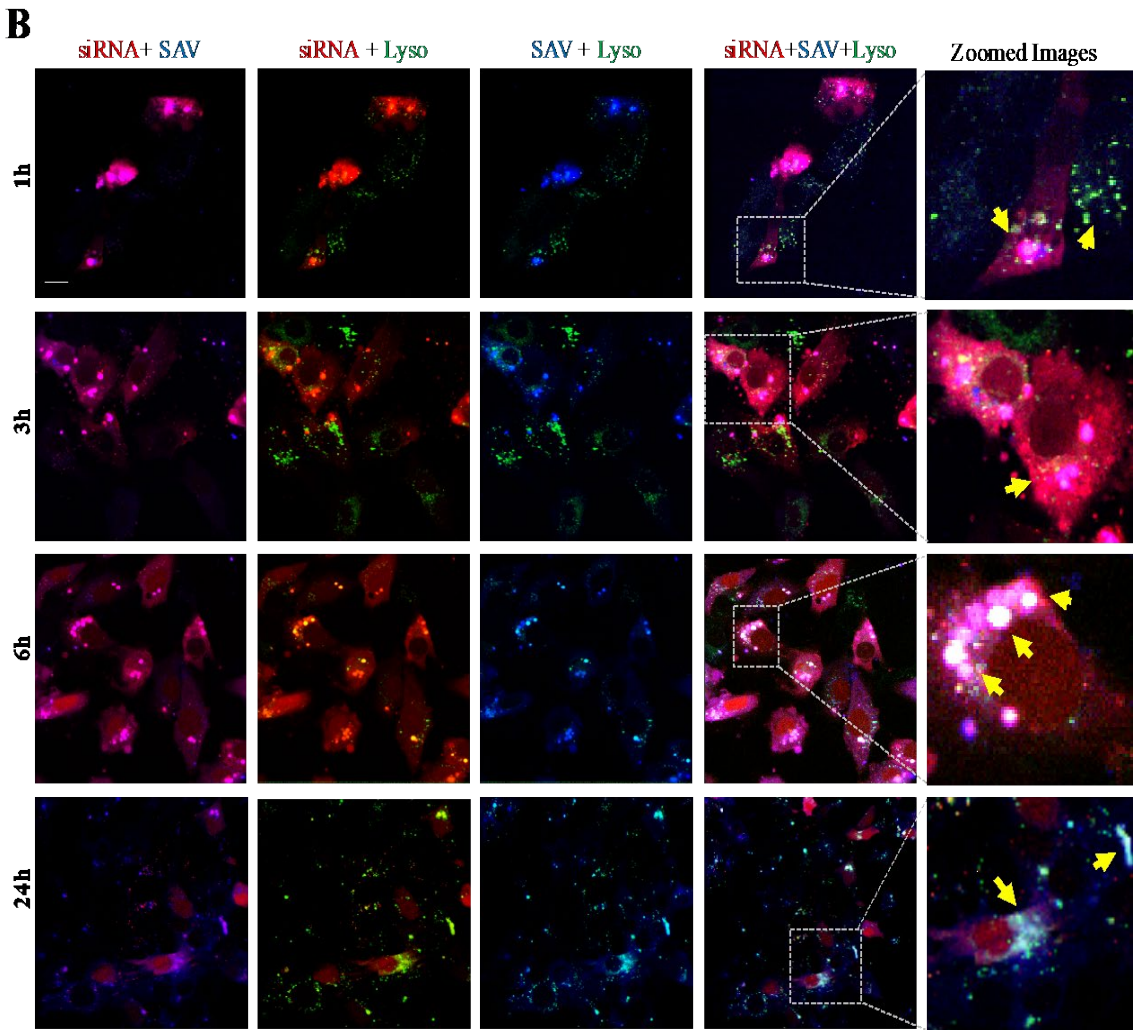

Figure 10. Co-localization of siRNA with protamine (A) and streptavidin (B). The siRNA nanocomplex was incubated with HSC-T6 cells for 1, 3, 6 and 24h, followed by fixation and confocal imaging. White color shows the co-localization of siRNA (red), lysosome (green) and protamine or streptavidin (blue). [Lyso: lysosome]. Scale bar = 20 μm.

3.3.4 Exocytosis and Cellular Recycling of the SSCP Nanocomplex

Confocal microscopy and flow cytometry results (Figures 8-10) suggest that SSCP can rapidly and efficiently deliver siRNA into the HSC-T6 cells at early time points, but cellular uptake of the siRNA is reduced at 24 h post-transfection. We hypothesized that siRNAs inside the cells may be exocytosed or transcytosed by

recycling vesicles. We therefore studied exocytosis of SSCP containing Alexa Fluor 647-labeled siRNA in HSC-T6 cells. As depicted in Figure 11A, fluorescence intensity in the medium constantly decreases till 6 h post-transfection, indicating a rapid uptake of the nanocomplex into the cells where the rate of endocytosis exceeds exocytosis. However, the fluorescence intensity starts increasing after 6 h, suggesting exocytosis of the SSCP nanocomplex dominates the uptake/excytosis kinetics. This is in accordance with the findings in the confocal and flow cytometry studies (Figures 8-10).

To further investigate whether exocytosed siRNAs are still complexed with the carrier, we treated the medium with heparin to dissociate the encapsulated siRNAs. We first studied the fluorescence quench effect of nanocomplex and cell culture medium (OptiMEM) on the fluorescence intensity of the Alexa Fluor 647-labled siRNA. As Figure 11B shows, both the formation of the SSCP nanocomplex and addition of OptiMEM medium reduces fluorescence intensity of the Alexa Fluor 647-labeled siRNA. Incubation of SSCP with 40 μM heparin can dissociate siRNAs from the nanocomplex and therefore reverses the quench effect of the nanocomplex and OptiMEM. Figure 11C also shows that incubation of SSCP with 40 μM heparin for 30 min can completely dissociate siRNAs form the nanocomplex. We therefore used the optimized condition to dissociate siRNAs from the exocytosed samples using heparin. After transfection with the SSCP nanocomplex for 6 h, HSC-T6 cells were washed and incubated with fresh medium. The media were then collected at different time intervals, and the fluorescence intensity was detected after incubation with 40 μM heparin for 30 min (Figure 11D). Without the heparin treatment, the fluorescence intensity in the medium increases with time and reaches the highest value at 18 h post-incubation. The heparin treated samples

exhibit the same trend of fluorescence intensity. However, heparin-treatment significantly increases the fluorescence intensity of all exocytosed samples, indicating that a significant amount of the exocytosed siRNA are complexed with the SSCP nanocomplex. This result suggests a significant amount of intracellular siRNAs are exocytosed, leading to the low concentration of the siRNA in the cells at 24 h post-transfection.

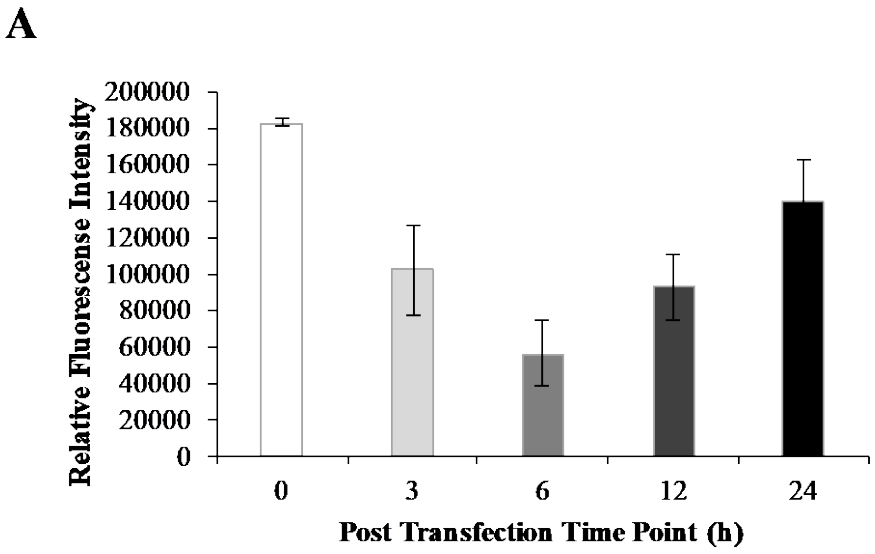

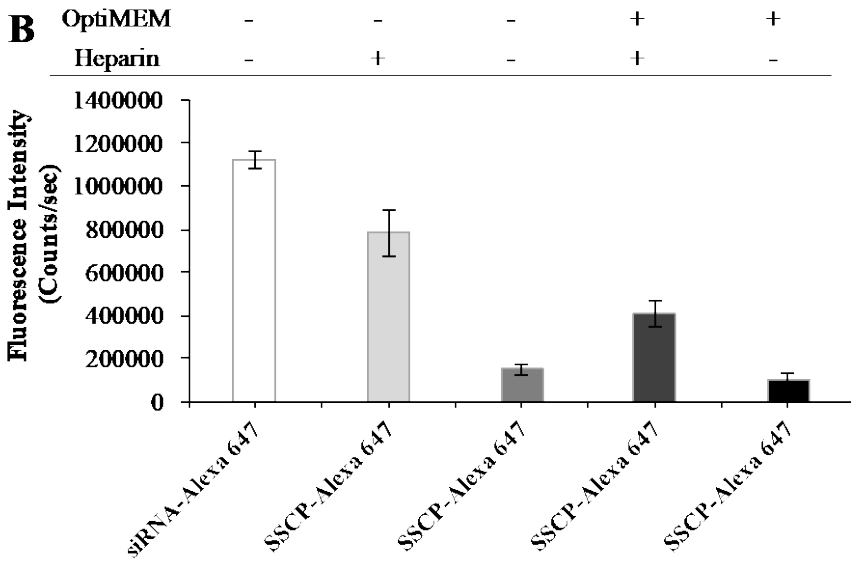
B
OptiMEM - - - + +
Heparin - + - + -
Fluorescence Intensity (Counts/sec)
1400000
1200000
1000000
800000
600000
400000
200000
0
siRNA-Alexa 647
SSCP-Alexa 647
SSCP-Alexa 647
SSCP-Alexa 647
SSCP-Alexa 647

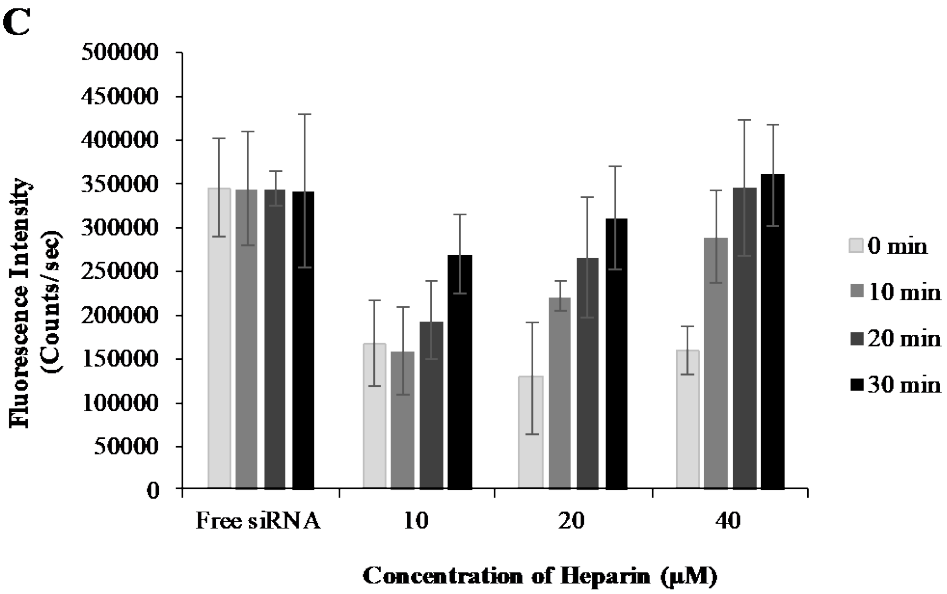
C
Fluorescence Intensity (Counts/sec)
500000
450000
400000
350000
300000
250000
200000
150000
100000
50000
0
Free siRNA
10
20
40
Concentration of Heparin (μM)
0 min
10 min
20 min
30 min

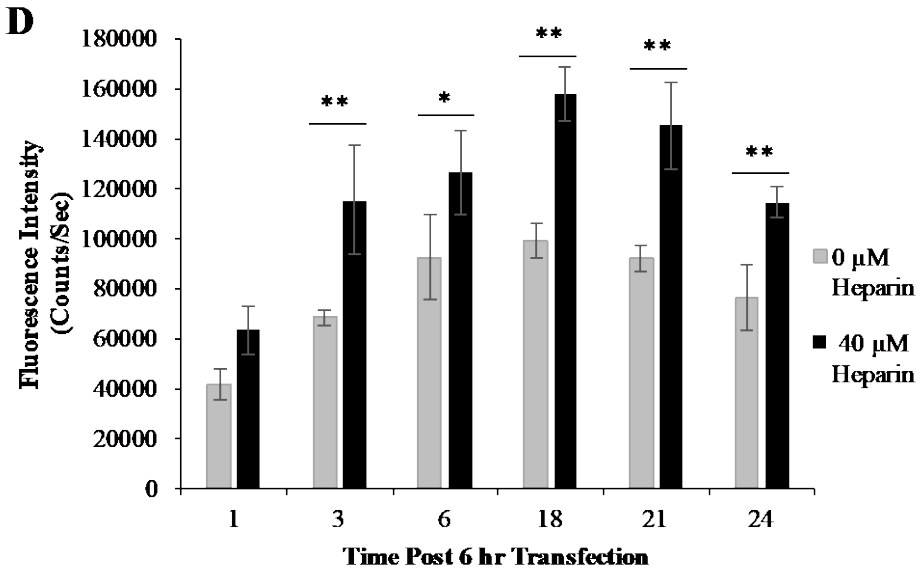

Figure 11. Exocytosis study of the Alexa flour 647 based SSCP siRNA nanocomplex. (A) Fluorescence intensity of the transfection medium at various time points post-transfection. (B) The fluorescence quenching effect of nanocomplex and optiMEM medium on Alexa Fluor 647-labeled siRNA. (C) Heparin incubation dissociates siRNA from the nanocomplex and reverses the fluorescence quenching effect. (D) HSC-T6 cells were incubated with Alexa Fluor 647-labeled siRNA nanocomplex for 6h, and the medium was replaced. The medium was then collected at 1, 3, 6, 18, 21 and 24h post-incubation for fluorescence analysis. Fluorescence intensities of the medium samples were determined with and without 40 µM heparin treatment. (n=3). Statistics was performed using Student t-test where, * = $P < 0.05$.

3.3.5 Silencing Activity of PCBP2 Streptavidin Nanocomplex

Figure 12 illustrates the silencing activity of the streptavidin nanocomplex in HSC-T6 cells. The silencing activity reaches the highest level (80% at 12 h) and then decreases with time (Figure 12). This is in accordance with our previous findings showing a similar time-dependent silencing activity.[205, 223] Decreased silencing activity could be due to the following: i) saturation of silencing machinery and cellular uptake; ii) siRNAs entrapped in late endosomes undergo degradation in lysosomes; iii) cellular recycling of nanocomplex; and iv) cell division as the classic example of transient silencing activity.

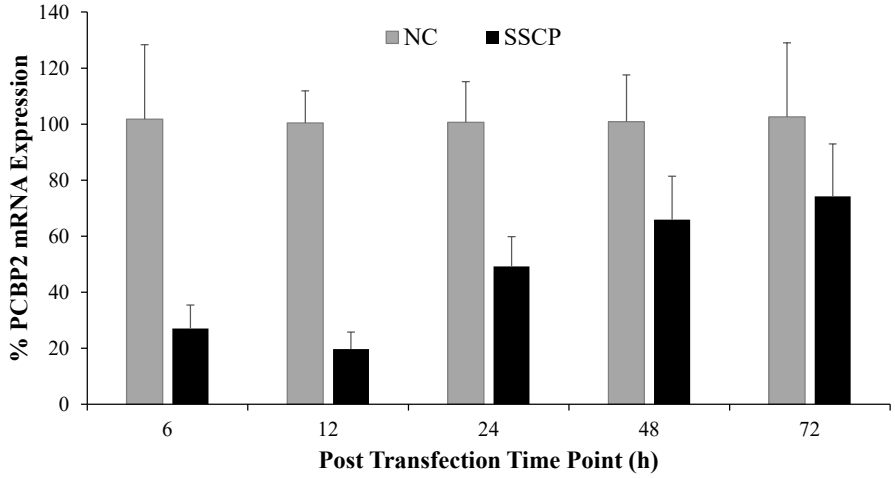

Figure 12. Time course of the silencing activity mediated by SSCP nanocomplex. SSCP formulated with PCBP2 siRNA or negative control siRNA was incubated with HSC-T6 cells for various time points (6, 12, 24, 48 and 72h). Total RNA was isolated and the silencing effect was evaluated by qRT-PCR (n=3).

A small amount of siRNA/streptavidin complexes are entrapped in lysosomes at extended time intervals, contributing to the decrease in silencing effect (Figure 12). We therefore studied the effect of endosome disrupting agents like chloroquine on the silencing activity of the streptavidin nanocomplex. We transfected the cells with the streptavidin nanocomplex in the presence of chloroquine (50 and 100 μM). Researchers have regularly used chloroquine as a control for the endosomal escape reagent at 100 μM concentration. However, these concentrations are toxic, which is why, chloroquine is not used in clinical trials to enhance endosomal escape. Lönn et al has utilized the chloroquine to compare the TAT peptide for efficient endosomal escape. Figure 13A shows that chloroquine treatment significantly increases silencing activity of the nanocomplex, indicating endosomal entrapment is one of the reasons accounting for the low silencing activity at 24 h post-transfection. Chloroquine acts by swelling endosomes and lysosomes and further neutralizing their pH. In Figure 13B, confocal images reveal that after chloroquine treatment, siRNA intensity increases in the cytoplasm with several swollen black circular organelles (endosomes and lysosomes) without siRNA (indicated with white arrows). This result suggests that even a tiny amount of siRNA in the cytoplasm is enough to induce silencing activity. This is in accordance with a previous report showing only a very small fraction of delivered siRNA can exhibit its activity.[224]

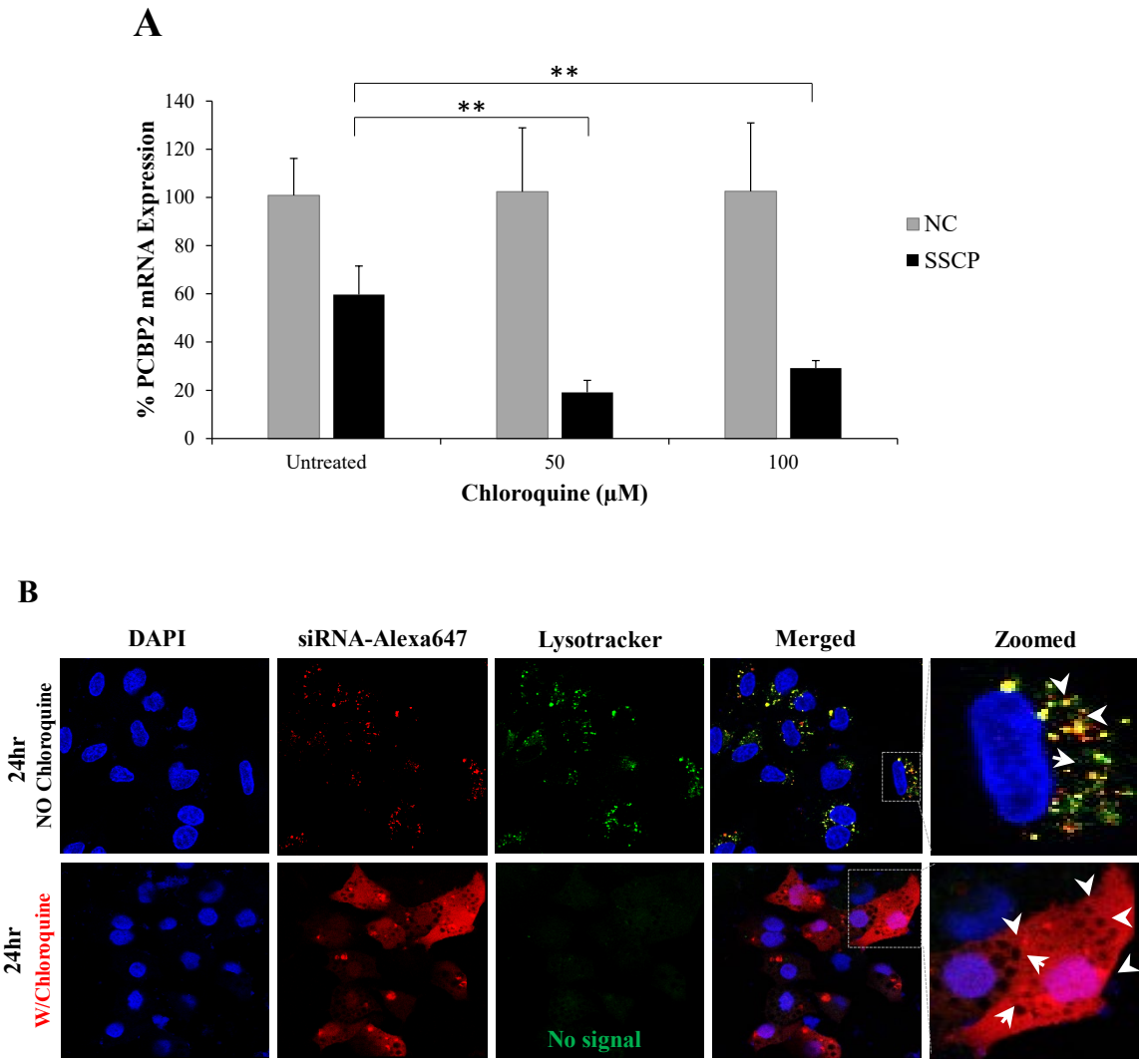

Figure 13. A. The effect of chloroquine on the silencing activity and B. cellular uptake.

HSC-T6 cells were transfected with siRNA nanocomplex with or without chloroquine for 24h (n=3). Statistics was performed using Student t-test where, * = P< 0.05. Scale bar = 20 µm

3.3.6 Early Cellular Trafficking of the SSCP Nanocomplex

We examined how the SSCP nanocomplex traffics inside the cells after one hour transfection. Early endosomes and Golgi complex were stained with antibody and golgi specific ceramide respectively to examine how the siRNAs traffic in these organelles. As Figure 14A shows, one hour after the transfection, a significant amount of the siRNAs are entrapped inside early endosomes (indicated with white arrows). However, after two hours, nearly all the siRNAs escape from early endosomes. Figure 14B illustrates co-localization of the siRNAs with Golgi complex inside the cells. One hour after the transfection, negligible siRNAs are localized in the Golgi complex. By contrast, a significant amount of the siRNAs are co-localized with the Golgi complex 2 h post-transfection (indicated with white arrows), suggesting that a fraction of the siRNAs translocate into the Golgi complex for recycling as time elapses.

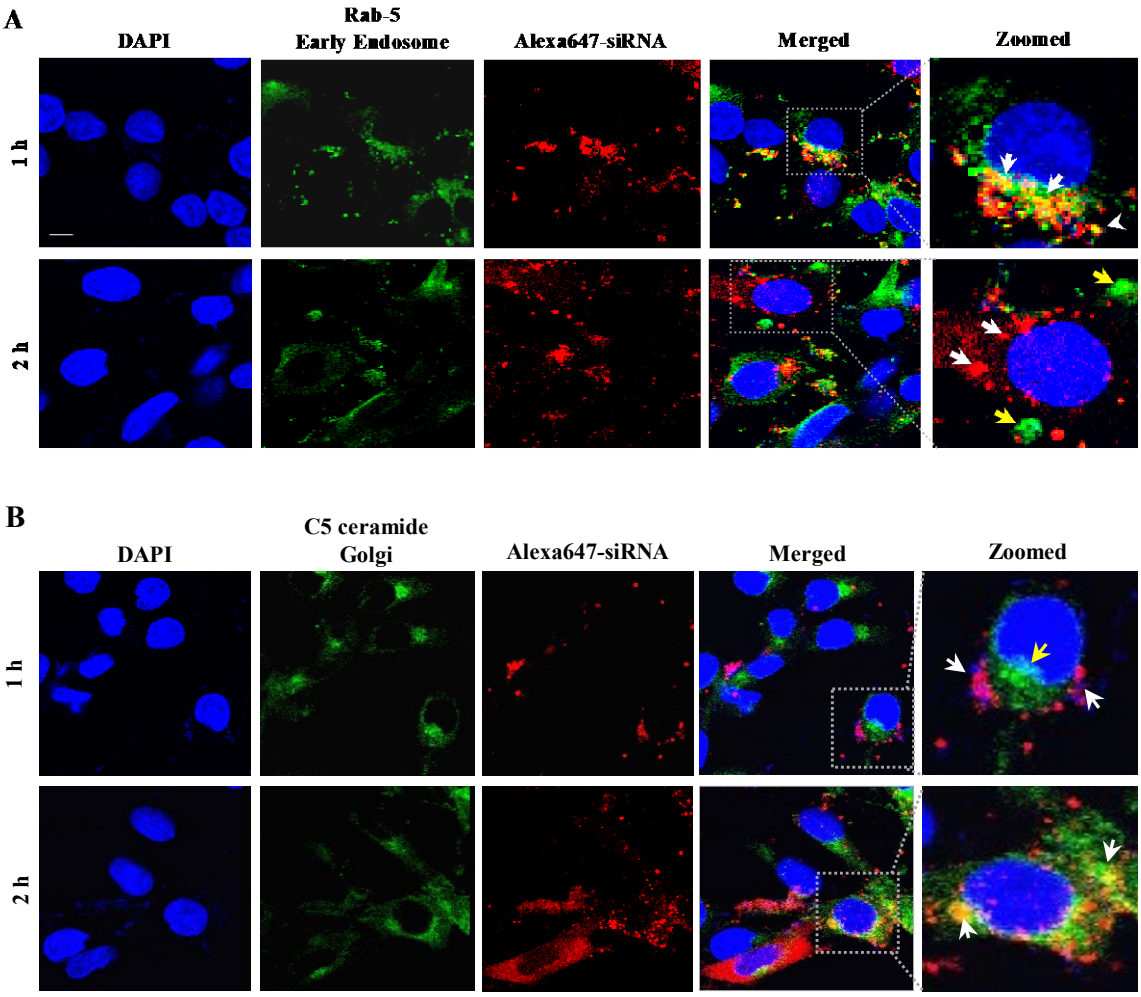

Figure 14. Early cellular trafficking of the SSCP nanocomplex in HSC-T6 cells.
(A) Early endosome (Rab5 antibody, Green) and Alexa Fluor 647 siRNA tracking (Red). (B) Golgi complex (BODIPY-FL-C5 Ceramide, Green) and Alexa Fluor 647 siRNA (Red) tracking. HSC-T6 cells were incubated with SSCP for 1h and further incubated with fresh OptiMEM for 0 or 1h before fixation and staining. Scale bar = 20 μm

3.4 Discussion

Despite the tremendous interest in using siRNA as therapeutics for various diseases, efficient delivery still remains the major obstacle to fully exploit the therapeutic potential of siRNA.[209, 211] To overcome the various biological barriers *in vivo*, an efficient siRNA delivery system should contain multiple components to address these challenges simultaneously.[213, 225] The multiple components in the system should not interfere with the silencing activity of siRNA. Our previous work has demonstrated that the nanocomplex can safely and efficiently deliver the siRNA via receptor-mediated uptake.[68] However, it is not clear how these multiple components dissociate and traffick inside the cells. Understanding the behaviors of the multiple components and siRNA inside cells is fundamental to further improve its efficacy for future *in vivo* studies. Recently there has been an increasing interest in studying the extravasation or exocytosis of nanocarriers.[216, 220, 226-227] As a result, we studied intracellular trafficking of each of the components of the siRNA nanocomplex using confocal microscopy and flowcytometry.

Based on the findings of this study, we hypothesize an intracellular trafficking mechanism of the multi-component SSCP nanocomplex in HSC-T6 cells. As Figure 15 illustrates, SSCP is first entrapped in early endosomes and commutes intracellularly through three possible routes: 1) the early endosomes are recycled through Trans Golgi network or recycling endosomes; 2) the endosomes undergo endosome maturation to lysosomes; 3) SSCP escapes from the early endosomes, and protamine dissociates from the SSCP nanocomplex to form the SSC complex, which releases free siRNA by the action of glutathione reductase in the cytoplasm. This is in accordance with a recent study reporting similar recycling pathways for nanoparticles.[204] Significant amount of siRNA

dissociates from the SSCP nanocomplex and distributes in the cell cytoplasm to exert silencing activity. As time elapses, protamine is either co-localized with SSC in lysosomes or stays free in the cytoplasm (Figure 3A). A fraction of the siRNA translocate into the nucleus, which is in accordance with a previous report.[228] A very small fraction of the siRNA remains complexed with streptavidin and entrapped in lysosomes for degradation or recycling. A significant amount of siRNA and nanocomplex are exocytosed, which may explain the transient silencing activity of synthetic siRNA delivered by nonviral vectors. However, exocytosis of the siRNA could be beneficial to its transcytosis and tissue penetration *in vivo*.

Protamine has been widely used to neutralize the negative charge of the siRNA and enhance the complexation of the siRNA with other components in delivery systems.[68, 229-231] The presence of high arginine content (~67%) in protamine and its inherent characteristics to condense nucleic acid in sperm has been extensively exploited in nucleic acid delivery to promote cellular internalization.[232] It is known that peptides containing high arginine content promote not only cellular internalization but also nuclear entry of its cargo through the nuclear pore complexes (NPC).[233] As shown in Figure 10A, Alexa Fluor 350 labeled protamine dissociates from the SSCP at early time points and slowly accumulates around the nucleus. However, we did not observe nuclear entry of protamine, which is different from the reports postulating nuclear uptake of protamine/DNA or polyarginine/DNA complex.[234] Nuclear import of siRNA may not be induced by protamine as several research groups have demonstrated that siRNA itself can translocate inside and out of the nucleus.[228, 235] We believe that protamine being a large molecule is unable to penetrate the nuclear pore complex (NPC).

Streptavidin is used as a "backbone" to form a complex with biotin-conjugated siRNA and ligands in the SSCP nanocomplex.[68] Alexa Fluor 350-labeled streptavidin distributes in the cytoplasm at 3 h but is slowly taken up by lysosomes at 6 h (yellow arrows) and converts into granular structures at 24 h post-transfection (Figure 10B). Interestingly, these granular structures co-localize with siRNA, suggesting inefficient endosomal escape of the SSCP complexes or reuptake or SSC complex by lysosomes from the cytoplasm in a similar way as auto-phagosomes.[236] Retention of the SSCP in endosomes or reuptake by lysosomes may lead to lysosomal degradation[237] or recycling by exocytosis.[238] Reports from others also shown that after endosomal escape nanocomplexes can again be taken up by either lysosomes or recycling vesicles.[236] Inefficient cleavage of the siRNA from SSC complex can be another reason for reduced activity at extended time. This could be attributed to low glutathione concentration in HSC-T6 cells because cells undergoing oxidative stress, such as activated HSCs, have low GSH levels.[239] To overcome this problem, other stimuli-responsive cleavable linkers, such as protease labile peptide sequences[240-241] and pH labile (hydrazone) groups [242-243] may be used for efficient release of the siRNA inside cells.

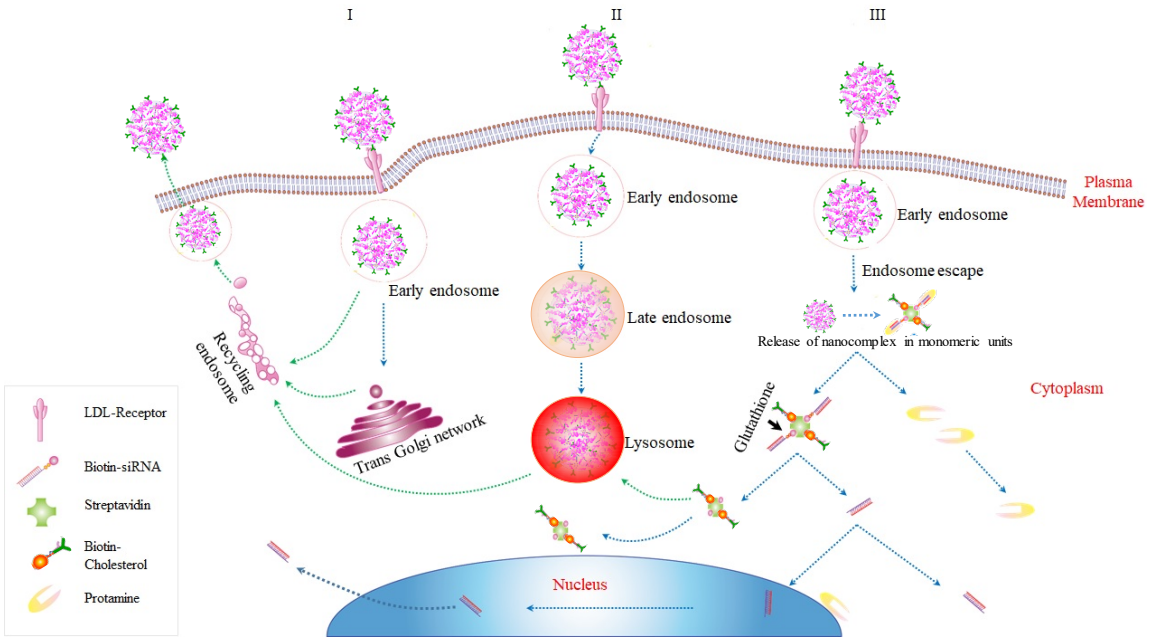

Figure 15. Schematic diagram of the intracellular trafficking of SSCP nanocomplex. Once internalized, SSCP commutes intracellularly through three possible routes: I) SSCP entrapped early endosomes are recycled through Trans Golgi network or recycling endosomes, II) SSCP entrapped endosomes undergo endosome maturation to lysosomes; III) SSCP escapes from early endosomes, and protamine dissociates from the SSCP nanocomplex to form the SSC complex, which releases free siRNA by the action of glutathione reductase in the cytoplasm.

Although endocytosis of nanocarriers has been extensively studied, exocytosis of nanocarriers has always been elusive and ignored.[216, 244] We therefore studied the exocytosis of siRNA and demonstrated the dynamic transport of siRNA across cell membrane with elapse of time. Alexa Fluor 647 is accepted as a highly stable probe for tracking siRNAs and remains attached to siRNA under physiological conditions.[245] In the exocytosis study (Figure 11D), the trend of increasing fluorescence in extracellular medium is in agreement with the basic endocytic machinery and recycling circuit proposed by Huotari.[204] Recycling of nanoparticles starts as soon as uptake occurs in early endosomes, but the rate of endocytosis exceeds the rate of exocytosis.[204] Our results (Figure 11A-D) further demonstrate that exocytosis dominates the endocytosis/exocytosis kinetics with lapse of time. Heparin treatment shows that a significant amount of the exocytosed siRNA is still entrapped in the nanocomplex, suggesting a similar recycling pathway as described by Langer and his colleagues.[220] Efforts have been made to overcome nanocarrier recycling by downregulating NPC1 (Niemann-Pick type C1)[220] or lipid recycling regulators.[246]

Transient gene silencing has been a major shortcoming of synthetic siRNA delivered by nonviral systems. Multiple factors, such as endogenous nucleases mediated degradation,[63, 247] dilution due to cell division,[248] and inefficient release from delivery systems [249] are considered to be the classic reasons for the transient silencing effect. Here we have demonstrated that exocytosis and recycling circuit (Early endosome, Golgi body and Lysosomes) mediated recycling is another possible pathway that accounts for the transient silencing activity of siRNA. Although exocytosis is one of the reasons accounting for the decreased cellular uptake and silencing activity *in vitro* in a monolayer

cell culture system, it may be beneficial for transcytosis and tissue penetration *in vivo* in a 3D environment. Recent studies indicate that exocytosis is an essential step for transcytosis of macromolecules or nanocarriers across cell membranes to neighboring cells.[216, 250-251] For example, transcytosis is the underlying mechanism for the delivery of drug and macromolecules across blood brain barrier (BBB) and other complex physiological systems.[252-254]

3.5 Conclusion

We elucidated the intracellular trafficking and fate of the streptavidin based siRNA delivery system. By using fluorescent labeled siRNA, streptavidin and protamine, we monitored their distinct behaviors inside the cells. Cytoplasmic and nuclear translocation of the different components of SSCP have been elucidated. A systemic stability and aggregation study of nanocomplex requires further investigation for better understanding of the role of aggregation on uptake and silencing activity. A different cleavable linker between biotin and siRNA may be more efficient to release siRNA from the nanocomplex inside the cells. Moreover, the use of an endosomolytic agent may further enhance the silencing activity of the nanocomplex.

CHAPTER 4

COMPARISON OF AVIDIN, NEUTRAVIDIN, AND STREPTAVIDIN AS NANOCARRIERS FOR EFFICIENT SIRNA DELIVERY

4.1 Introduction

Protein-based drug delivery carrier has been one of the most employed modalities in the biopharmaceuticals. Since the inception of RNA interference (RNAi), siRNA has proven to be the most specific and efficient molecule to knockdown a target gene. A tremendous amount of work has been devoted to explore this phenomenon for therapeutic purposes. A safe and efficient delivery of siRNA, however, is still the major stumbling block for its clinical translation regardless of its therapeutic potential.[209] Lipids [255], peptides [213, 256-257] polymers [258] proteins [68, 259] oligonucleotide [260-261] and inorganic materials [262-263] have been developed for siRNA delivery. Among these carriers, protein-based delivery systems are promising carriers because of ease of construction, good solubility and low toxicity compared to synthetic materials [264]. In our previous work, we developed a streptavidin-based nanocomplex to deliver PCBP2 siRNA. During liver fibrogenesis, overexpression of PCBP2 gene results in the accumulation of type I collagen in fibrotic liver. Streptavidin-based nanocomplex demonstrated a very efficient PCBP2 gene silencing at 6 h but efficiency lowered at extended time point (24h).[68, 265] Also, due to its bacterial origin, streptavidin could be arguably immunogenic, and several efforts have been made to develop less immunogenic analogs of streptavidin.[266]

Avidin, streptavidin, and neutravidin are functional and structural analogues that bind to biotin with extremely high affinity. Avidin is derived from eggs of oviparous vertebrates [267], while streptavidin is derived from *Streptomyces avidinii.* Neutravidin is a

chemically modified avidin without glycosylation. Although the three analogues share a similar tetramer structure and binding affinity to biotin, their physical and chemical structures are different. Depending upon their specific physical and chemical characteristics, these avidin analogues are utilized frequently in the field of nanotechnology and biotechnology.[268] For example, streptavidin and neutravidin lack the four mannose and three N acetyl glucosamine residues in each unit, which are present in avidin. In the absence of the carbohydrate moieties, the pI of neutravidin and streptavidin are slightly acidic, which prevents the nonspecific binding property of avidin (pI ~10). The higher pI of avidin is responsible for the positive charge at physiological pH and non-specific binding to the negatively charged molecules and surfaces, such as silica and cell membrane [37]. As described by Zhao et al [269] and Nguyen et al [37], avidin, neutravidin and streptavidin show positive cooperativity (affinity toward the biotin) with an increasing order (avidin<streptavidin<neutravidin). Nearly neutral charge on neutravidin keeps it from nonspecific protein-protein interaction.

With the knowledge of what we have previously reported[68], in this study we compared the avidin-, neutravidin- and streptavidin-based nanocomplexes in delivering PCBP2 siRNA to hepatic stellate cells. Protein-based delivery systems are critical and face challenges such as interactions with intrinsic proteins present in systemic circulation, pro-inflammatory response from innate immune system [270] and cytotoxic effect, aggregation.[271-272] We therefore compared the serum stability, cellular uptake, silencing activity, exocytosis, and pro-inflammatory cytokine induction of these nanocomplexes. Biodistribution of the neutravidin-based nanocomplex in rats with CCl_4-induced liver fibrosis was evaluate using a small animal imaging system.

4.2 Materials and Methods

4.2.1 Materials

Avidin, neutravidin and streptavidin were obtained from Pierce (Rockford, IL). Dulbecco's phosphate buffered saline (DPBS) and protamine sulphate (Salmon X grade) were purchased from Sigma-Aldrich (St. Louis, MO). Dulbecco's Modified Eagle's Medium (DMEM), Opti-MEM reduced serum medium, scrambled siRNA (negative control, sense sequence: 5'-ACUACCGUUGUUAUAGGUGtt-3'), and Alexa Fluor 647-labeled siRNA were purchased from Invitrogen (*Carlsbad*, CA). GelRed™ was obtained from Biotium (Hayward, CA). Non-enzymatic cell dissociation reagent was purchased from MP Biomedicals LLC (Solon, Ohio). Annexin V–Propidium iodide apoptosis assay kit was obtained from Thermo Fisher Scientific (Grand Island, NY). iTaq™ Universal SYBR® Green One-Step Kit was purchased from Bio-Rad (Hercules, California). The rat hepatic stellate cell line (HSC-T6) was kindly provided by Dr. Scott L. Friedman (Mount Sinai School of Medicine, New York University).

4.2.2 Preparation of the siRNA Nanocomplexes

The siRNA nanocomplexes were prepared as we previously described.[68] Biotin conjugated cholesterol was synthesized as we described,[68] and the biotin labeled PCBP2 siRNA (sense sequence 5'-GUCAGUGUGGCUCUCUUAUtt-3') was purchased from Gene Pharma (Shanghai, China). Briefly, the nanocomplex was formed by mixing biotin-siRNA, biotin-cholesterol and avidin/neutravidin/streptavidin in a 2:2:1 molar ratio. The complex was incubated for 10 min at room temperature and then condensed with protamine (N/P ratio of 10:1) for 30 min. Particle size and zeta potential of nanocomplexes were measured in HEPES buffer (pH 7.4) using a Malven Zetasizer Nano

ZS (Malvern Instruments Ltd, United Kingdom). Silencing activity of the siRNA nanocomplex was examined as we reported.[68]

4.2.3 Enhanced Serum Stability of siRNA Protected by Nanocomplexes

Nanocomplexes were incubated with 50% rat serum at 37°C for indicated time intervals, followed by electrophoresis through a 20 % native PAGE gel and visualization with GelRed™ staining under UV light. To further confirm that the siRNAs encapsulated inside nanocomplex are intact, the siRNA nanocomplexes treated with rat serum were incubated with 40 μM heparin and 100 mM Dithiothreitol (DTT) for 10 min to release the free siRNA from nanocomplex. Dissociated siRNA samples were electrophoresed in 2% agarose gel and 20% native PAGE and visualized with GelRed™ under UV light.

4.2.4 Cellular Uptake of Nanocomplexes

Cellular uptake of the siRNA nanocomplexes was examined by confocal microscopy and flow cytometry as described.[11, 213] HSC-T6 cells were incubated with nanocomplexes for various time intervals and washed with PBS containing 1 mM heparin to remove nonspecifically bound nanocomplex. The cells were stained with LysoTracker DND 99, fixed with 10% formalin, and examined under a confocal microscope (Leica TCS SP5). Similarly, HSC-T6 cells were treated with nanocomplexes, washed with PBS containing 1 mM heparin, detached using trypsin, and centrifuged to recover the cells. The resulting cell pellet was washed, suspended, and subjected to fluorescence analysis using a BD FACS II flow Cytometer (Bectone Dickinson Instruments, Franklin Lakes, NJ).

4.2.5 Exocytosis Study of the siRNA Nanocomplexes

Previously we developed a method to examine the exocytosis of siRNA nanocomplex from hepatic stellate cells.[265] Briefly, HSC-T6 cells were seeded in a 96 well plate at a density of 5000 cells/well. The cells were transfected with nanocomplex containing Alexa Fluor 647-labeled siRNA for 6 h, followed by washing with DPBS (3 times) and there after replacement with fresh Opti-MEM medium. The fresh medium was then collected at various time intervals (3, 6, 18, 21 and 24 h) and treated with 40 μM heparin for 30 min to release free Alexa Fluor 647-siRNA from nanocomplex. Fluorescence of the siRNA samples was measured using a VICTOR X Multilabel Plate Reader (Perkin Elmer, Waltham, MA).

4.2.6 Apoptosis and Necrosis Study

Apoptosis and necrosis of the cells transfected with nanocomplexes were evaluated using the Dead Cell Apoptosis Kit with Annexin V Alexa Fluor® 488 & Propidium Iodide (Thermo Fisher Scientific, Grand Island, NY) as described.[273] After transfection with the avidin, neutravidin, and streptavidin nanocomplexes (100 nM PCBP2 siRNA) for 24 h, HSC-T6 cells were harvested using non-enzymatic cell dissociation agent and re-suspended in annexin-binding buffer at a concentration of 1×10^6 cells/mL. Five microliters of Alexa Fluor® 488 annexin V and 1 μL of PI working solution (100 μg/mL) were added to 100 μL of the cell suspension and incubated in dark for 15 min. After addition of 400 uL annexin-binding buffer, the samples were analyzed using a BD FACSCanto™ II Flow Cytometry Analyzer System (BD bioscience, San Jose, California). The excitation wavelength is 488 nm, and the emission wavelengths are 530 and 575 nm for Alexa Fluor 488 and Propidium Iodide (PI), respectively. Untreated

HSC-T6 cells were used as the negative control, and HSC-T6 cells treated with 2% Triton X-100 were used as the positive control.[274]

4.2.7 Inflammatory Cytokine Induction Study

Pro-inflammatory cytokine induction by the siRNA nanocomplexes in rat whole blood was examined as reported. [275-277] Briefly, the siRNA nanocomplexes were incubated in 2 mL rat whole blood at 37°C for 24 h or 48 h. Untreated blood was used as a negative control. The plasma was extracted from the blood by centrifugation at 1500 g for 10 min. The concentrations of proinflammatory cytokine including IL6, IFNγ and TNFα were determined using Picokine ELISA kits according to the manufacturer's protocol.

4.2.8 *In-Vivo* Biodistribution Study

The animal protocol was approved by the Institutional Animal Care and Use Committee (IACUC) at the University of Missouri-Kansas City. Male Sprague Dawley rats were purchased from Charles River Laboratories, Inc. (Raleigh, NC) and housed in a temperature and humidity controlled room with a 12 h light–dark cycle. The 1:1 (v/v) mixture of CCl_4 and olive oil was intra-peritoneally (i.p) administered at a dose of 1 mL/kg twice a week for six consecutive weeks. The rats were then randomly divided into two groups. One group was intravenously (i.v.) injected with Cy5-labeled siRNA (0.1 mg/kg), and the second group was i.v. injected with neutravidin-based nanocomplexes encapsulating Cy5 labeled siRNA (0.1 mg/kg). After 2h, the rats were euthanized and major organs including the liver, spleen, kidneys, lungs, heart, and muscle (thigh) were harvested and imaged using a Bruker MS FX PRO Imaging System (Billerica, MA).

4.2.9 Statistical Analysis

Statistical analysis was performed using a two-way analysis of variance (ANOVA) with Tukey's Post Hoc test. $P<0.05$ was considered statistically significant.

4.3 Results

4.3.1 Characterization of the siRNA Nanocomplexes

The hydrodynamic size and zeta potential of the siRNA nanocomplexes were measured using the Malven Zetasizer. The siRNA nanocomplexes were diluted in HEPES buffer (pH 7.4) during the characterization. As shown in Figure 16, the particle sizes of the avidin, neutravidin, and streptavidin nanocomplexes are 225, 237, and 263 nm, respectively. The polydispersity index (PDI) values of the avidin, neutravidin, and streptavidin nanocomplexes are 0.103, 0.07, and 0.151, respectively. These results indicate that the avidin and neutravidin- nanocomplexes exhibit nearly monodisperse particles, while the streptavidin nanocomplex shows a relatively wide size distribution.

Zeta potentials of the avidin, neutravidin, and streptavidin nanocomplexes are +25, +22, and +18 mV, respectively (Figure 16). Obviously, cationic protamine provides the basis of positive surface charge. The difference in zeta potential can be explained by the different isoelectric point (pI) of avidin, neutravidin and streptavidin. With a pI of ~5, streptavidin is slightly negatively charged under physiological condition, which neutralizes some of the protamine in nanocomplex. On the contrary, avidin has a basic pI of ~10 and therefore contributes more positive charges to nanocomplex, leading to a relatively high zeta potential. The zeta potential of neutravidin is also consistent with its slightly acidic pI 6.3. Figure 17 illustrates the respective capabilities of the avidin, neutravidin and streptavidin to form nanocomplexes. After formation of nanocomplexes,

gel retardation was performed and it is clearly visible that the all the nanocomplexes were able to hold the siRNA efficiently without releasing them into the PAGE gel.

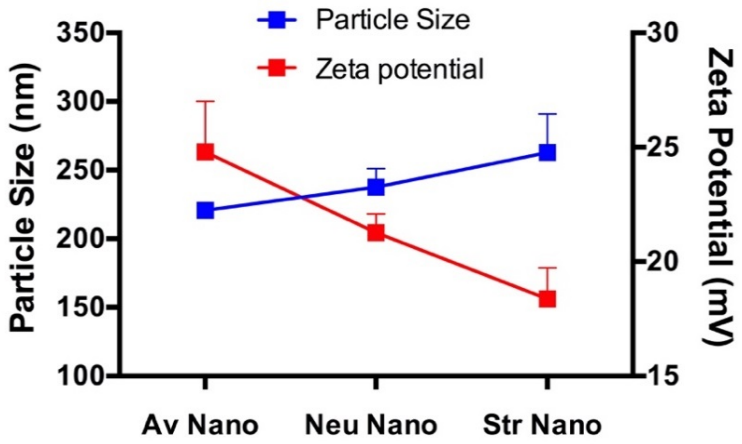

Figure 16. Particle size and Zeta potential analysis of SACP, SNCP and SSCP. Nanocomplexes were formulated in avidin, neutravidin and streptavidin in 10mM HEPES buffer (pH 7.4)

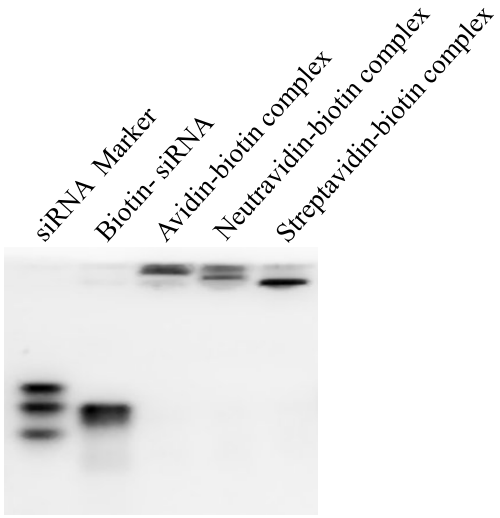

Figure 17. Evaluation of Nanocomplex forming ability of avidin, neutravidin and streptavidin with biotin siRNA and Biotin cholesterol by using 20% Native PAGE.

4.3.2 Enhanced Serum Stability of siRNA Protected by Nanocomplexes

Because of the widely distributed nucleases in the body, stability is always a major concern in developing siRNA delivery systems. We therefore examined the serum stability of the avidin, neutravidin, and streptavidin nanocomplexes in 50% rat serum. After incubation in the serum, nanocomplexes were treated with heparin and DTT for 30 min to dissociate and release free siRNA from nanocomplexes. As Figure 18 illustrates, native siRNA is completely degraded in the serum after 12 h. On the contrary, the avidin, neutravidin, and streptavidin nanocomplexes protect the siRNA from degradation for up to 24 h.

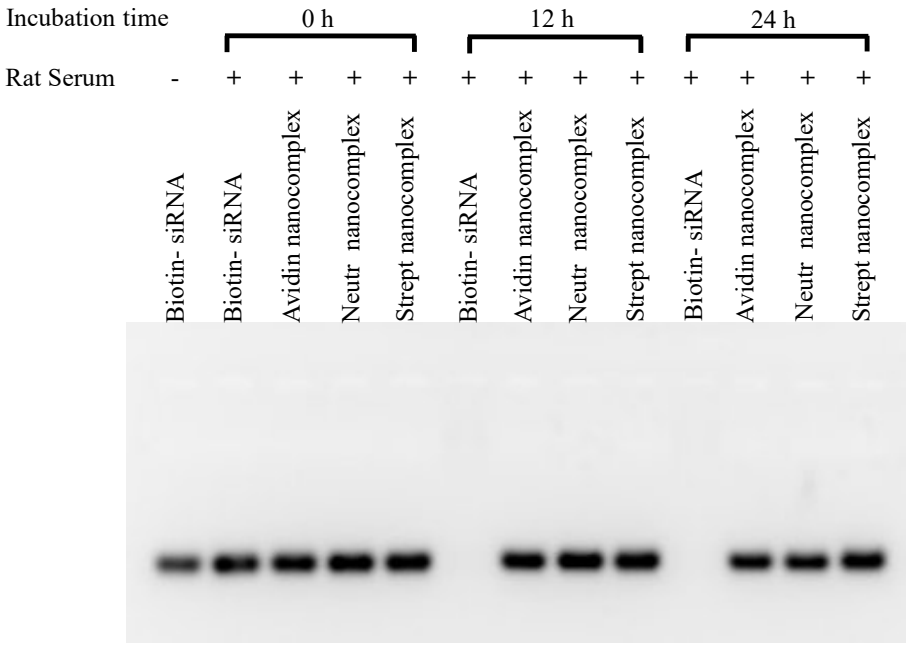

Neutr: neutravidin
Strept: streptavidin

Figure 18. Enhanced stability of siRNA by nanocomplexes in 50% rat serum.
The avidin-, neutravidin-, and streptavidin-based nanocomplexes were incubated with 50% rat serum for 0, 12 and 24 h. The samples were incubated with 40 μM heparin and 100 mM DTT for 30 min to release free siRNA from the nanocomplex and then analyzed with 2% agarose gel.

4.3.3 Silencing Activity of Nanocomplexes

Having shown that the avidin, neutravidin, and streptavidin nanocomplexes can form nanoscale particles with siRNAs and efficiently protect them from serum degradation, we next compared their silencing activity in HSC-T6 cells at the mRNA level by real time RT-PCR. The cells were transfected with the avidin, neutravidin, and streptavidin nanocomplexes for 6 and 24 h. A scrambled siRNA (negative control) was used as the negative control for each group. As show in Figure 19A, the neutravidin based nanocomplex exhibits the highest silencing activity at both time intervals (79% at 6h and 81% at 24h). The avidin based nanocomplex shows the lowest silencing activity among the three nanocomplexes. Moreover, both avidin and streptavidin based nanocomplexes show reduced silencing activity with time, which is consistent with our previous finding with the streptavidin nanocomplex.[265] On the contrary, the neutravidin based nanocomplex exhibits sustained silencing activity over 24 h. The silencing activity of the neutravidin nanocomplex at 24 h post-transfection is similar to that at 6h post-transfection.

Nonspecific protein binding is one of the barriers that may limit the cellular uptake and silencing activity of siRNA nanocomplex in the body. We therefore examined the silencing activity of nanocomplexes in DMEM supplemented with 10% FBS. As Figure 19B illustrates, addition of FBS in the medium does not compromise the silencing activity of neutravidin and streptavidin based nanocomplexes. Their silencing activities are similar to that in the Opti-MEM reduced serum medium (Figure 19A). However, the silencing activity of the avidin nanocomplex is dramatically reduced in the presence of FBS (Figure 19B), indicating its high protein binding with serum protein. This is

consistent with the findings that avidin is more prone to nonspecific interaction because of its basic pI and glycosylation. [37, 278] It has already been proven that the FBS or serum protein are one of the biggest factors that influences the transfection efficiency.[279] Whereas, serum proteins have negligible effect on the silencing activity of the neutravidin and streptavidin nanocomplexes because of their nearly neutral pI.

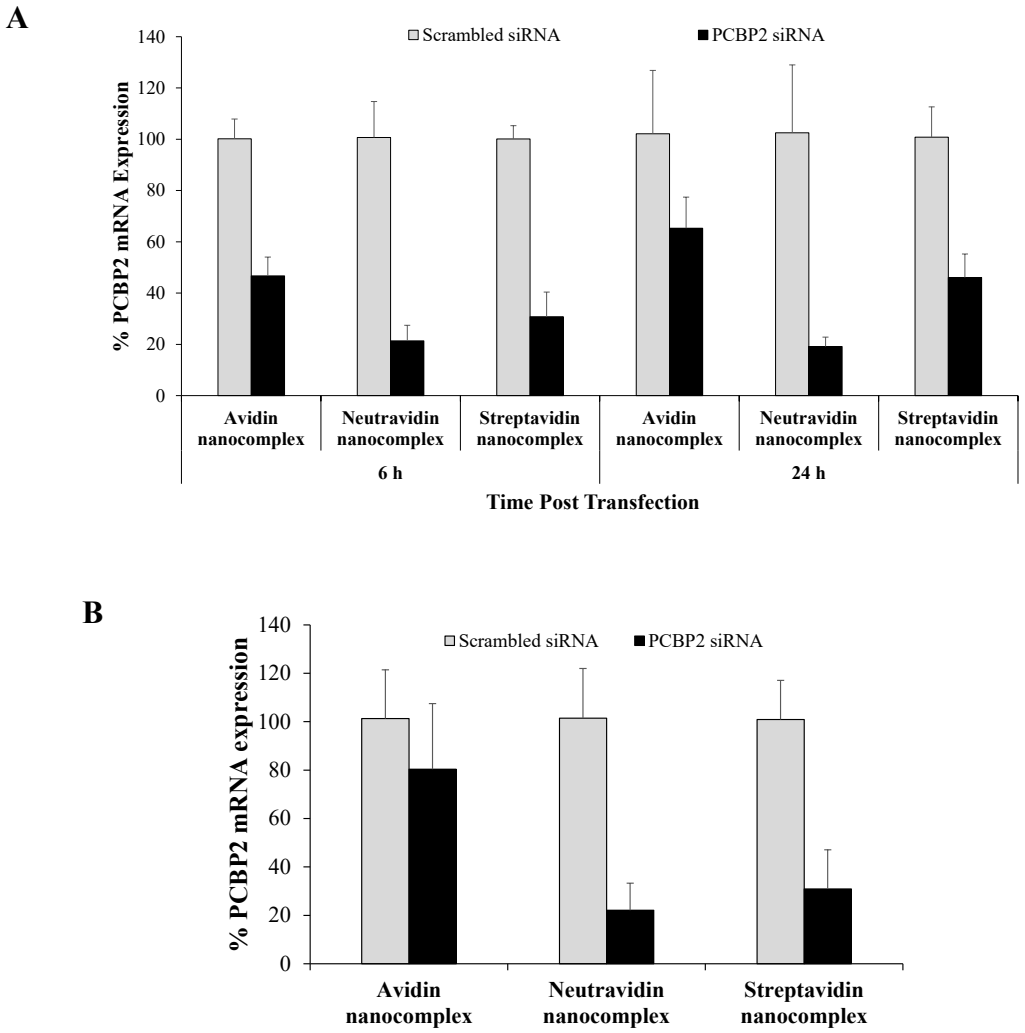

Figure 19. Silencing activity of avidin-, Neutravidin-, Streptavidin Nanocomplexes at 6 and 24 h; A. incubation in OptiMEM; B. incubation in DMEM with 10% FBS. Nanocomplexes formulated with PCBP2 siRNA or scrambled siRNA (negative control) were incubated with HSC-T6 cells in OptiMEM or DMEM supplemented with 10% FBS. Total RNA was isolated and silencing activity was evaluated by Real Time RT-PCR. Results are represented as the mean±SD (n=3).

4.3.4 Cellular Uptake of Nanocomplexes

Confocal microscopy was used to compare cellular uptake of the avidin, neutravidin, and streptavidin nanocomplexes in HSC-T6 cells at 3, 6, and 24 h post-transfection. The avidin nanocomplex (Figure 20A) shows consistently lower uptake in comparison to neutravidin- (Figure 20B) and streptavidin- (Figure 20C) based nanocomplexes. The neutravidin nanocomplex shows the highest uptake over a 24-hour time period. This finding is consistent with the silencing activity results in Figure 19, where the avidin nanocomplex exhibits the lowest silencing activity, and the neutravidin nanocomplex exhibits the highest activity. Time courses of the cellular uptake for the three nanocomplexes are also different. Both the avidin (Figure 20A) and streptavidin (Figure 20C) nanocomplexes exhibit higher cellular uptake at early time points but much lower uptake at 24 h post-transfection. On the contrary, the neutravidin nanocomplex (Figure 20B) exhibits consistently high cellular uptake over 24 h. At extended timepoints (24 h), lysosome (green) and siRNA (red) showed very high colocalization (indicated by white arrows) in case of streptavidin nanocomplex (Figure 20C). On the other hand, neutravidin nanocomplex treated group showed negligible lysosome and siRNA colocalization.

Endosomal release of siRNA nanocomplex is always a major barrier for its silencing activity. We therefore examined co-localization of siRNA and lysosomes in the cells. As Figure 20 illustrates, the neutravidin nanocomplex shows the lowest endosomal entrapment inside the cells, while the streptavidin nanocomplex shows the highest endosomal entrapment.

We further quantitated cellular uptake using flow cytometry analysis. As shown in Figure 21, nearly 100% of the cells were transfected with the three nanocomplexes at 3 and 6 h post-incubation, indicating that nanocomplexes can rapidly deliver siRNA into the cells. However, the percent of transfected cells decreases at 24 h post-incubation in the cells treated with avidin and streptavidin nanocomplexes. Meanwhile, the neutravidin nanocomplex exhibits the same transfection efficiency throughout 24 h.

Neutravidin nanocomplexes showed significantly higher uptake in comparison to avidin- and streptavidin-- based nanocomplexes at extended time point (24 h). Figure 21A shows that all nanocomplexes show rapid uptake, but differ quantitatively. As time progresses, Neutravidin nanocomplex treated groups showed significantly higher Alexa Fluor 647- siRNA mediated fluorescence intensities (Figure 21B) in comparison to the other nanocomplexes (avidin and streptavidin nanocomplexes) at all the timepoints. At early timepoint (3h), neutravidin and streptavidin nanocomplexes showed similar fluorescence intensity but after 6h neutravidin nanocomplexes showed consistently higher uptake of Alexa Fluor 647-siRNA. Figure 21C clearly shows the peak shift of siRNA mediated fluorescence intensity with time for respective nanocomplex treated groups.

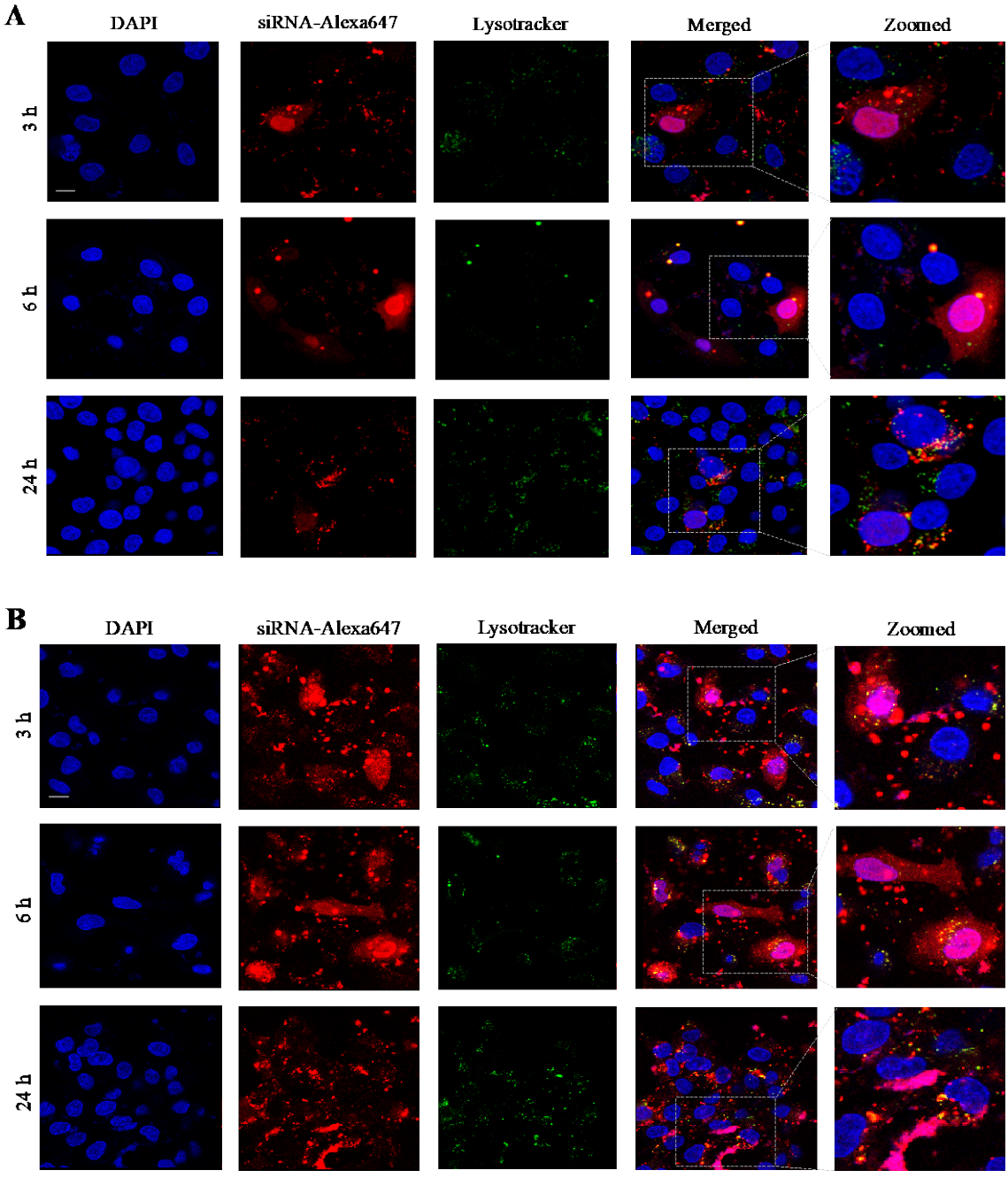
A
DAPI
siRNA-Alexa647
Lysotracker
Merged
Zoomed
3 h
6 h
24 h
B
DAPI
siRNA-Alexa647
Lysotracker
Merged
Zoomed
3 h
6 h
24 h

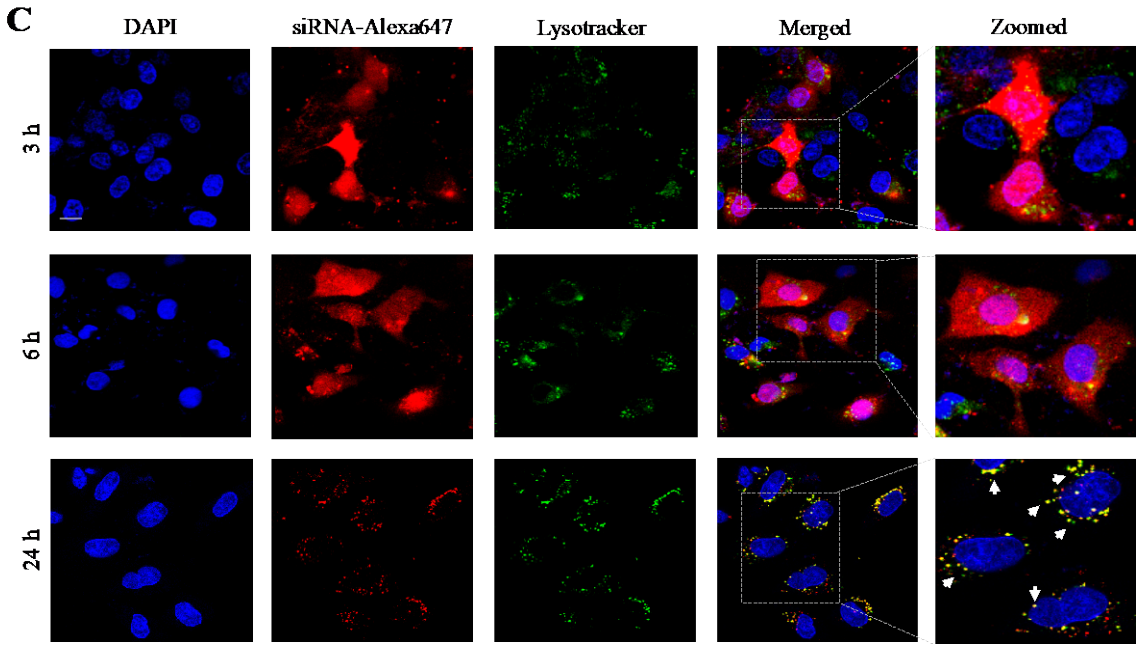

Figure 20. Cellular uptake of the various avidin nanocomplexes in HSC-T6 cells. Avidin nanocomplex(A), neutravidin nanocomplex (B), and streptavidin nanocomplex (C) in HSC-T6 cells at various time points. Alexa Fluor-647 labeled siRNA was encapsulated in nanocomplexes and confocal microscopy was used to monitor the cellular uptake at different time intervals (3, 6, and 24 h). Scale bar = 20 μm.

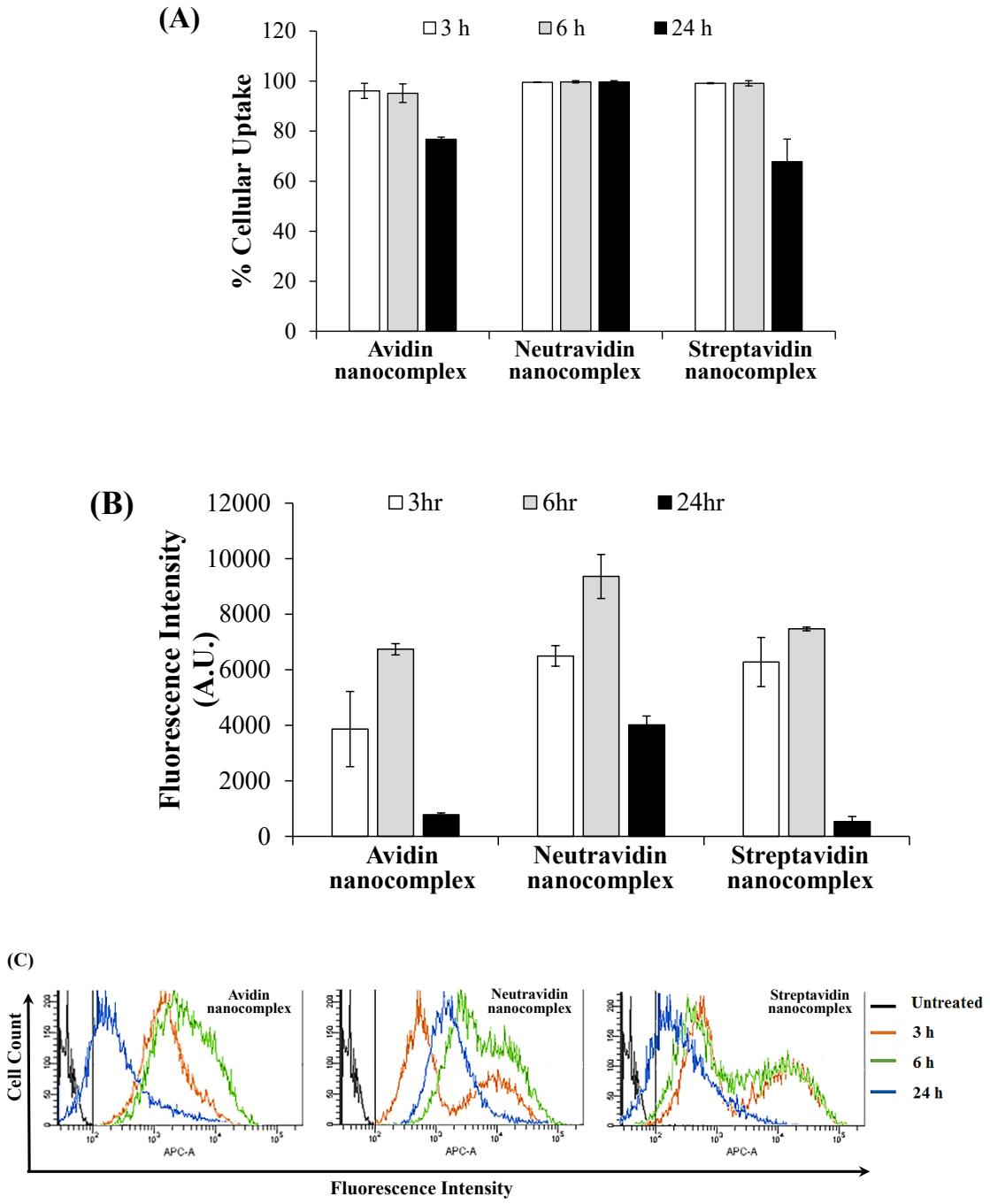

Figure 21. Quantitative cellular uptake study of PCBP2 siRNA with the avidin-, neutravidin- and streptavidin-based nanocomplexes using flow cytometry.
(A) Percent of cells that take up the nanocomplex; (B) Fluorescence intensity of the cells at various time points; (C) Histogram Plot for the Alexa Fluor-647 siRNA mediated intensity peak shift by avidin-, neutravidin- and streptavidin- based nanocomplexes at various time points.

4.3.5 Exocytosis Study of Nanocomplexes

We have previously reported an intriguing phenomenon of exocytosis of streptavidin-based nanocomplex with the progression of time.[265] However, cellular uptake studies such as confocal microscopy (Figure 20) and flow cytometry (Figure 21) indicated an extensive uptake of the neutravidin-based nanocomplex at extended time points. We therefore compared the exocytosis of the avidin-, neutravidin-, and streptavidin-based nanocomplexes in HSC-T6 cells. As shown in Figure 22, the neutravidin-based nanocomplexes exhibit the lowest exocytosis compared with the avidin- and streptavidin-based nanocomplexes, which explains the prolonged cellular uptake of siRNA at extended time points. The avidin-based nanocomplex showed lower exocytosis compared to the streptavidin-based nanocomplex (Figure 22).

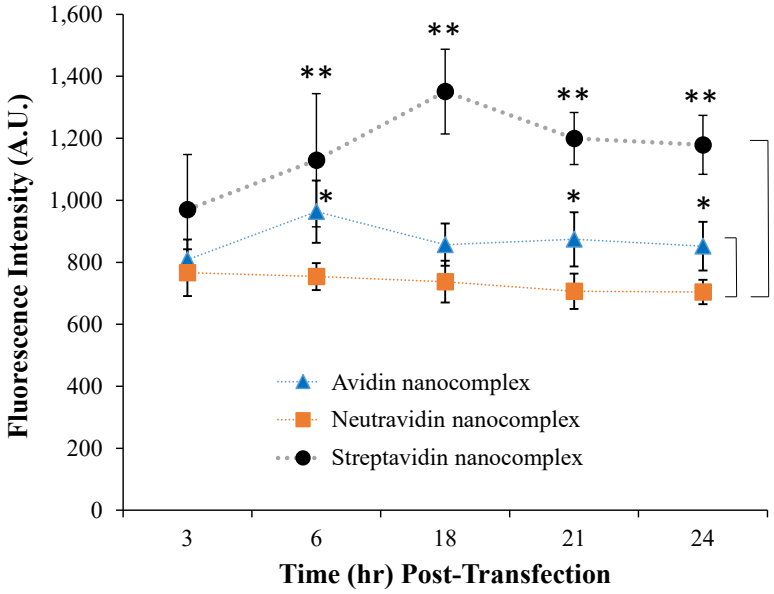

Figure 22. Exocytosis study of avidin, neutravidin, and streptavidin nanocomplexes HSC-T6 cells were transfected with nanocomplex containing Alexa Fluor 647-siRNA for 6 h, and the medium was replaced with fresh OptiMEM medium. The fresh medium was collected at various time intervals and treated with heparin for 30 min and further analyzed for fluorescence intensity using a Victor X fluorescence plate reader. Results are represented as the mean ± SD (n = 3; * $P \leqslant 0.05$; ** $P \leqslant 0.01$).

4.3.6 Apoptosis and Necrosis Study

A safe siRNA delivery system should not induce nonspecific apoptosis and necrosis. We therefore evaluated the apoptotic effect of nanocomplexes in HSC-T6 cells. Untreated HSC-T6 cells were used as the negative control, and HSC-T6 cells treated with 2% Triton X-100 were used as the positive control. As illustrated in Figure 23A&B, all three different nanocomplexes did not induce apoptosis, late apoptosis or necrosis in comparison to the untreated control group. By contrast, 2% Triton X-100 induced significant apoptosis and necrosis in HSC-T6 cells. Accordingly, morphology of the cells treated with nanocomplexes is similar to the untreated group and did not show any sign of wear or cell death that was observed in the cells treated with Triton (Figure 23C).

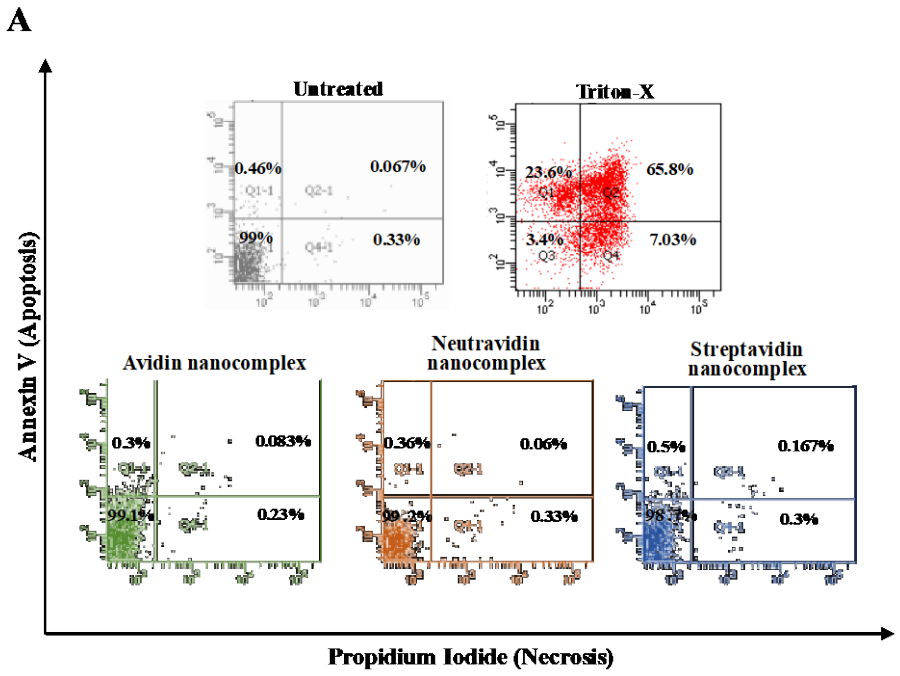

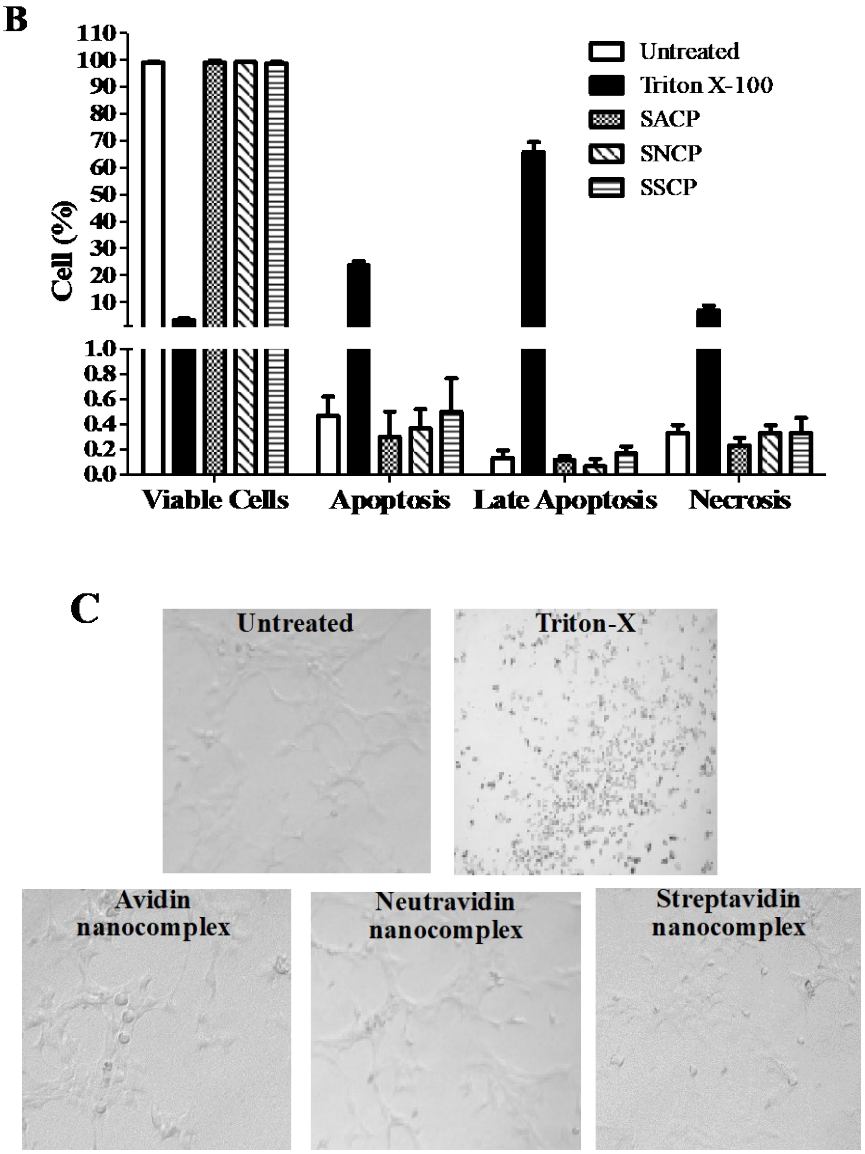

Figure 23. Analysis of apoptosis by Annexin V and Propidium iodide staining. HSC-T6 cells were treated with the avidin-, neutravidin- and streptavidin-based nanocomplexes (100 nM PCBP2 siRNA) for 24 h and then subjected to the analysis of apoptosis and necrosis. The acquisition data were divided into four quadrants according to the type of fluorescence emitted from the cells: Q1-1 calculates the percent of cells undergoing apoptosis (Annexin V), Q2-1 calculates the percent of cells undergoing late apoptosis or induced necrosis (Annexin V and Propidium Iodide), Q3-1 calculates the percent of cells with no fluorescence and Q4-1 calculates the percent of cells undergoing necrosis induced by the nanocomplex. Results are represented as the mean±SD (n=3).

4.3.7 Inflammatory Cytokine Induction Study

Nonspecific stimulation of immune system is always a concern for protein-based therapeutics and delivery systems. Cytokine and chemokine assays are commonly used to evaluate the immunotoxicity of nanoparticles or any sort of biopharmaceutical therapeutic agents.[280] Recently, investigators have been using whole blood assay for the *in-vitro* analysis of immunogen-mediated cytokine responses. [275, 277, 281-282] Moreover, whole blood assay is preferred over the PBMC (Peripheral Blood Mononuclear Cell) assay because whole blood assay requires less blood volume for the analysis.[283] Therefore, we incubated the whole blood of Sprague-Dawley rats with nanocomplexes for 24 and 48 h. Plasma was then isolated from the whole blood, and the levels of primary proinflamatory cytokines were measured using a PicoKine^{TM} ELISA assay kit (Bosterbio Pleasanton, CA). IL6 and TNFα are considered very important cytokines among the whole pro-inflammatory cytokine family because they are involved in most inflammatory states and overexpressed even after a small infection or fever.[284-285] As shown in Figure 24, the streptavidin-based nanocomplex stimulated the highest expression of IFNγ, TNFα, and IL6 after 24 and 48 h incubation. On the contrary, the neutravidin-based showed the lowest stimulation of IFNγ, TNFα, and IL6 among the three nanocomplexes. Moreover, the cytokine expression levels of the cells treated with the neutravidin-based nanocomplex are similar to the negative control group, indicating the low cytokine induction by the neutravidin-based nanocomplex and safety. Moreover, this level of cytokine in all the groups was insignificant if compared with the Lipopolysaccharide (LPS) as a positive control. We did not however used the LPS positive control. It is just our postulation.

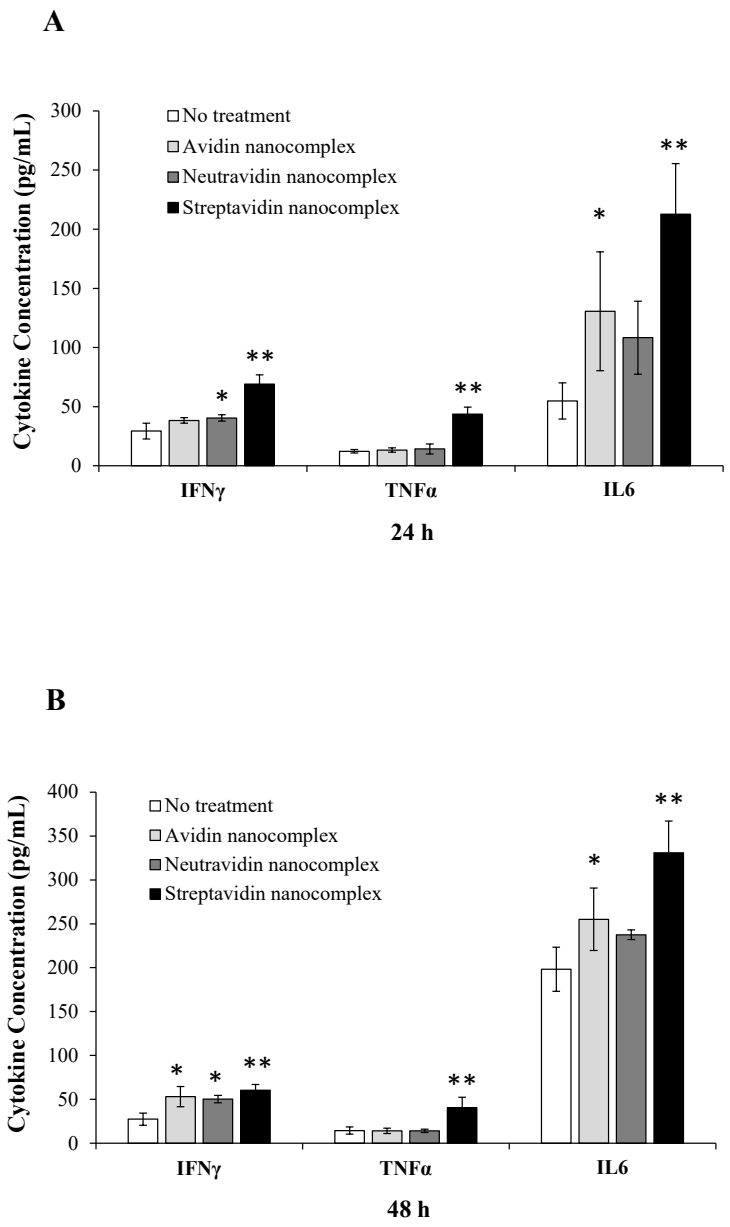

Figure 24. Inflammatory cytokine induction by avidin-, neutravidin-, and streptavidin- based nanocomplexes nanocomplexes in blood for A. 24h; B. 48h (B). Sprague-Dawley rat whole blood was incubated with the avidin-, neutravidin- and streptavidin-based nanocomplexes at 37°C for 24h (A) and 48h (B). The plasma was collected and quantified for the expression of IFNγ, TNF α and IL6 ELSA kits. Results are represented as the mean ± SD (n=3; * $P \leqslant 0.05$; ** $P \leqslant 0.01$).

4.3.8 *In-Vivo* Biodistribution Study

Neutravidin-based nanocomplex exhibited significantly high cellular uptake, better silencing efficacy, and insignificant inflammatory cytokine induction compared to avidin- and streptavidin-based nanocomplexes. These results suggest that neutravidin could be a potentially safe and efficient carrier for siRNA delivery. We thereafter studied the biodistribution of neutravidin-based nanocomplex encapsulating Cy5-labeled siRNA in rats with CCl_4-induced liver fibrosis (Figure 25). The free Cy5-labeled siRNA was rapidly eliminated from the body and showed very low liver accumulation at 2 h after tail vein injection. It has been previously reported that the cholesterol-modified siRNA delivery systems show higher liver accumulation after 60 min whereas free siRNA is readily eliminated from the systemic circulation.[286] It is also well known that the oligonucleotides show very short half-life of less than 60 min[287-288]; therefore, we used 2 h time point for comparing free siRNA and neutravidin nanocomplex for biodistribution studies. We also performed preliminary studies in live animals (data not shown) to optimize the timepoint for biodistribution studies. Compared to the free siRNA, the neutravidin-based nanocomplex increased the siRNA uptake in the liver by approximately 2.7 fold. On the other hand, the neutravidin-based nanocomplex and free siRNA did not show significant differences in the fluorescence in other major organs, such as the spleen, kidneys, lungs, heart and muscle. These results clearly demonstrated that the neutravidin-based nanocomplex does not have nonspecific binding after systemic administration and the biotin-cholesterol in the nanocomplex can efficiently guide the nanocomplex to fibrotic liver. This is in accordance with our previous finding, in which cholesterol was used to achieve targeted delivery of an oligonucleotide to fibrotic liver.[289]

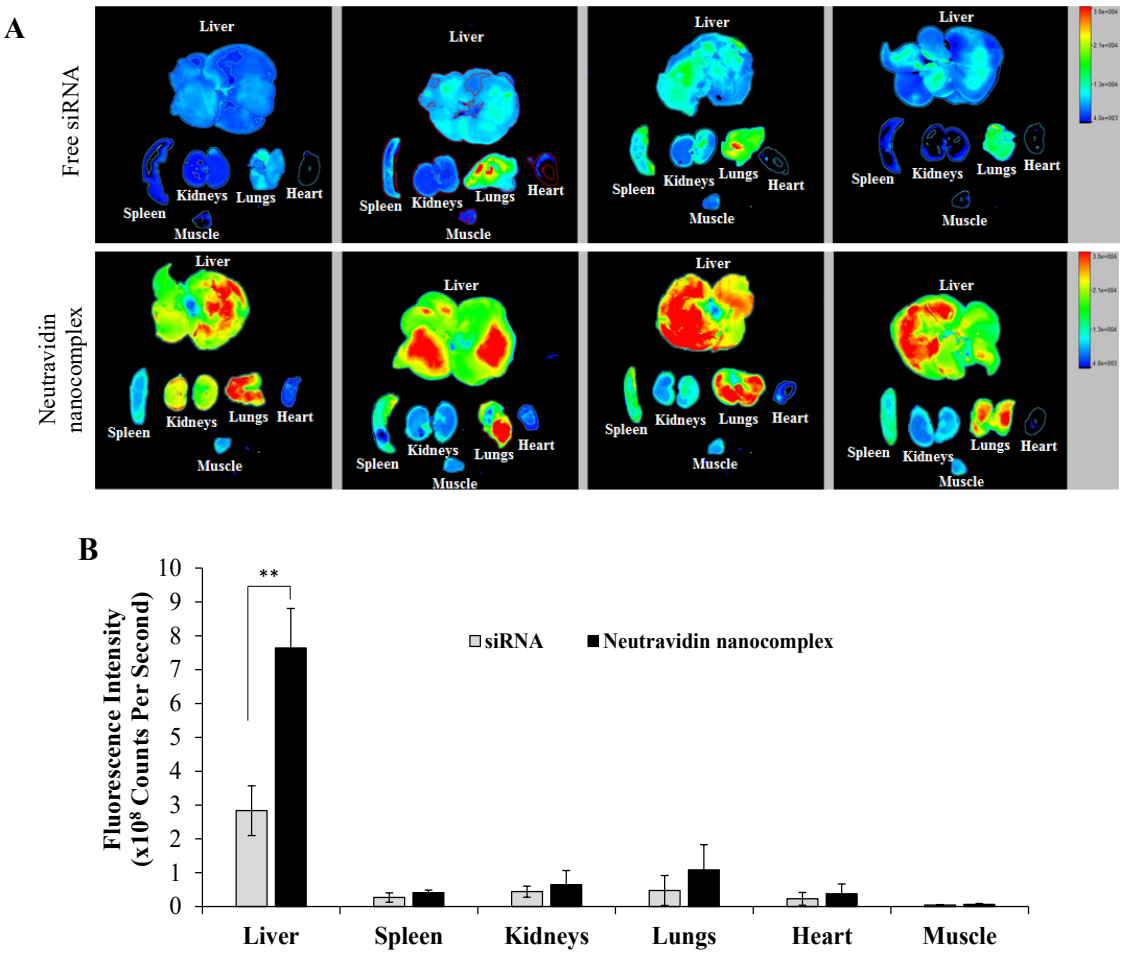

Figure 25. Biodistribution of the neutravidin-based siRNA Nanocomplex in CCL_4 induced liver fibrosis rat model

Cy-5 labeled siRNA was used in this study. The rats were euthanized two hours post tail vein injection, and major organs including the liver, spleen, kidneys, lungs, heart, and muscle were harvested for fluorescence imaging analysis using a Bruker MS FX PRO Imaging System. Fluorescence images of the major organs of four rats per group were presented in (A). (B). Region of interest (ROI) was determined by the Bruker molecular imaging software. Fluorescence intensities with respect to the area under the ROI were plotted for the liver, spleen, kidneys, lungs, heart and muscle. Results are represented as the mean $\pm$ SD (n=4; ** $P \leqslant 0.01$).

4.4 Discussion

Protein-based nanocomplexes have a high potential for the targeted delivery of siRNA as a therapeutic agent. However, the protein carriers for the delivery of siRNA have been limited only to polycationic peptides, which have shown unfavorable biological and physiological properties when tested *in vivo*.[290] In this work, we evaluated various avidin analogues and critically investigated their efficiency and safety for the delivery of siRNA to HSC. To perform this unbiased evaluation, all nanocomplexes were prepared and compared for physical properties under the same chemical and physiological conditions. The particle size analysis demonstrated that the avidin nanocomplexes were the smallest in size and had the highest positive zeta potential (Figure 16). Avidin has a pI value of 10, which suggests that at a physiological pH, it exhibits a net positive charge. Therefore, protamine and avidin synergistically contribute to the net positive charge of this nanocomplex, resulting in the smallest hydrodynamic size compared to the neutravidin- and streptavidin-based nanocomplexes. However, all nanocomplexes have sizes that were in the optimum range of 200-275 nm.

Avidin and the other tetravalent derivatives effectively formed stable nanocomplexes with biotinylated siRNA and biotinylated cholesterol (ligand). The serum stability studies demonstrated that the siRNA remained stable and condensed in nanocomplexes after prolonged incubation with serum. After 24 h of serum incubation, the amount of siRNA released from nanocomplexes by DTT and heparin was found to be stable (Figure 17), which demonstrated that all of the avidin analogues produced equally stable nanocomplexes. However, in contrast to the avidin- and streptavidin-based nanocomplexes, only the neutravidin-based nanocomplex demonstrated a sustained

silencing activity through 24h (Figure 18A). This sustained silencing could be attributed to the efficient internalization and higher endosomal release.

Despite having similar serum stability and a smaller size, the avidin-based nanocomplex exhibited poor activity, which could be the result of their positive charge at physiological pH. The higher positive charge of avidin makes it more prone to nonspecific interactions with negatively charged molecules and proteins. As described by Trang T. Nguyen and co-workers[37], avidin, neutravidin and streptavidin show a cooperativity coefficient (η) greater than unity. This contributes to the tight interaction of avidin with biotin, but the relatively higher positive charge makes avidin more prone to non-specific interactions. We therefore tested for the non-specific binding and impact of serum protein interaction on the efficiency of the nanocomplex. Interestingly, the efficiency of the avidin nanocomplex was significantly compromised when they were incubated with HSC-T6 cells in the presence of 10% FBS for 6 h at 37^{o} C. On the other hand, the neutravidin and streptavidin nanocomplexes showed consistent silencing activity after 6 h in the presence of serum, which suggested that neutravidin and streptavidin did not interact with the serum proteins. However, unlike the neutravidin nanocomplexes, the activity of streptavidin nanocomplex could not be sustained at later time points because of its high exocytosis, which could be due to its bacterial origin

In addition to its intrinsic protein-binding ability, the higher net positive charge of the avidin nanocomplexes might have contributed to the aggregation of these nanocomplex in the extracellular medium. However, more detailed study is yet to be performed to provide a strong conclusion. As shown in Figure 20, the avidin nanocomplex (Figure 20A) has the lowest uptake compared to neutravidin (Figure 20B)

and streptavidin (Figure 20C) nanocomplexes at all time points. In contrast, the neutravidin nanocomplexes showed a consistently higher cellular uptake, which was consistent with the sustained silencing activity at the extended time intervals. Interestingly, the groups treated with the neutravidin nanocomplex showed extremely low co-localization of the siRNA with the lysosomes, whereas the streptavidin-treated groups demonstrated higher siRNA co-localization with the lysosomes at the extended time points (24 h). Higher lysosomal co-localization of the streptavidin nanocomplexes in the cells could be due to the bacterial origin of streptavidin on the basis that the cells undergo auto-phagocytosis to degrade intrinsic or foreign proteins derived from bacteria.[291] The cellular uptake and efficiency of various nanocomplexes were found to be greatly affected by their physical and chemical properties. The confocal microscopy results were confirmed by flow cytometry (Figure 21). This process revealed that the Alexa Fluor 647-based fluorescence remained significantly higher in case of the neutravidin nanocomplex-treated group at the later time points than that in the avidin and streptavidin nanocomplex-treated groups.

The activity of siRNA in any type of delivery system is compromised due to cellular recycling and exocytosis. We have previously demonstrated that exocytosis and cellular recycling negatively impacts the silencing activity of streptavidin based nanocomplex [265]. The exocytosis analysis revealed that the neutravidin nanocomplexes showed very low Alexa Fluor 647 associated fluorescence in the extracellular medium. In other words, the neutravidin nanocomplex showed significantly lower exocytosis than the streptavidin based nanocomplex.

In addition to their therapeutic activities, biologics are required to be safe, and their administration must not cause any toxicity. Especially for protein therapeutics, toxicological studies are imperative and several efficient tools to evaluate the toxicity have been developed in the past decade.[292] We therefore evaluated the cytotoxic effect of the avidin, neutravidin and streptavidin nanocomplexes in HSC-T6 cells *in vitro*. None of nanocomplexes showed significant apoptotic or necrotic effect on the cells compared to the untreated control group (Figure 23). However, the safety of nanoparticles cannot be determined using only apoptosis/ necrosis (cytotoxicity) studies. The level of pro-inflammatory cytokines act as a marker of the nanoparticle-induced immunotoxicity and thus indicate the safety of a drug molecule or a delivery system.[293] A potential immunotoxic response caused by a nanocarrier indicates that it is unsafe and therefore not a viable candidate for translational research. Among all of the cytokines, IL6, TNF α and IFN γ play vital roles in the primary inflammatory response of a body against any foreign agent. [293-294] Therefore, we tested all of nanocomplexes for the ability to increase the levels of these selected proinflamatory cytokines and found that the levels of the cytokines following administration of the neutravidin nanocomplexes were the same as the negative control group. However, the streptavidin nanocomplexes produced a statistically significant immunogenic response in comparison to the negative control group (Figure 24).

Regardless of promising *in-vitro* efficacy, many nanocarriers fail to succeed *in-vivo* because of their poor pharmacokinetics and targeting efficacy. Moreover, free siRNAs after administration have shown unfavorable PK profiles and extremely poor systemic stability.[295] Groups treated with Free Cy5-siRNA was rapidly eliminated from

the body and showed very low liver accumulation at 2 h after tail vein injection. In contrast, the neutravidin-based nanocomplex exhibited significantly higher siRNA uptake in the fibrotic liver (Figure 25), suggesting that this system can dramatically improve the serum stability and pharmacokinetic profile of siRNA *in-vivo.*

4.5 Conclusion

The siRNA nanocomplexes that were formulated using various avidin analogues showed similar morphological characteristics. However, the neutravidin-based nanocomplex demonstrated the most efficient and sustained silencing activity *in-vitro*. Moreover, this formulation showed the highest uptake at extended times compared to avidin- and streptavidin-based nanocomplexes. In addition, the neutravidin-based nanocomplex exhibited excellent liver retention in comparison to free siRNA. Hence, neutravidin is the best avidin analogue that can be potentially used for siRNA delivery. *in vivo* gene silencing and reversal of liver fibrosis by neutravidin nanocomplex is yet to be explored and represents our future direction. Efforts will be made to improve siRNA loading and further reduction in the particle size and zeta potential to further improve pharmacokinetic profile of nanocomplex and better targetability.

CHAPTER 5

IN VIVO DELIVERY OF siRNA BY PROTEIN BASED NANOCOMPLEX TO TREAT AGGRESSIVE LIVER FIBROSIS

5.1 Introduction

Liver fibrosis is the dynamic process of fiber accumulation on the scars caused by the acute or chronic liver injury. The whole process is called dynamic because of cascade of factors acting as the contributing factor for the disease. After acute or chronic injury, hepatocytes produce apoptotic bodies which are engulfed by the resident kupffer cells, followed by the recruitment of the natural killer cells, macrophages and T cells.[3] In this cascade, recruitment of immune cells and instigation of upregulatory signaling of the proinflamatory and profibrogenic cytokines and chemokines leads to the activation of hepatic stellate cells. This activation of hepatic stellate cells (HSCs) also augments this inflammatory cascade and promotes more fibrogenesis.[3] Discovery of HSCs as the major fibrogenic myofibroblast, during the event of liver injury and evidence of reversibility of liver fibrosis has motivated scientists to investigate the molecular mechanisms to discover novel therapeutic strategies.

Despite extensive knowledge of the molecular mechanisms and pathogenesis of the disease, there is no first line of treatment approved by FDA. Liver fibrosis and cirrhosis are the major cause of morbidity in developing as well as developed countries irrespective of the cause such as nonalcoholic fatty liver disease (NAFLD), nonalcoholic steatohepatitis (NASH), cholestasis, hepatitis c virus, alcohol etc.[296] There is an urgent need for a potent first line therapy that can specifically and efficiently target the core of the disease. Clinical trials have revealed that the resolution of liver fibrosis can be

attained by collagenase activity and clearance of activated hepatic stellate cells.[297] Reduction of the extracellular matrix (collagen) is believed to be most effective strategy to target the liver fibrosis.[298 299]

PCBP2 (poly(rC)-binding protein) siRNA works by targeting the PCBP2 mRNA that help in the stabilization of the collagen I mRNA and promotes collagen I protein synthesis. PCBP2 gene is overexpressed during in profibrogenic cells such as hepatic stellate cells during liver fibrosis, therefore, resulting in accumulation of type I collagen in extra cellular matrix in fibrotic liver.[5, 69] PCBP2 siRNA has proven to be highly effective *in vitro*.[5] There are compelling evidences of siRNA's therapeutic potential, systemic delivery of the siRNA remains the biggest challenge. Previously we demonstrated the *in vitro* delivery of PCBP2 siRNA with the help of neutravidin protein based nanocomplexes.[300-301]

In this study, we utilized an IGF2R peptide ligand discovered by our group that has shown tremendous promise in HSC targeting.[11] Biotinylated IFG2R peptide ligand and biotinylated PCBP2 siRNA molar ratios in the nanocomplexes were optimized to achieve maximum siRNA loading and exquisite HSC targeting. We tested various molar ratios of siRNA and IGF2R peptide ligand with keeping neutravidin concentration constant. In efforts to keep siRNA stable and prevent degradation during formulation operations, we non-covalently coupled the biotin to the PCBP2 siRNA with the help of peptide nucleic acid positioned beside the 3' end of the antisense strand of PCBP2 siRNA. To support the Peptide nucleic acid (PNA), sense strand was designed with a PNA complementary sticky end. Nanocomplexes prepared from various molar ratios of multiple components were further condensed with protamine (N/P=2.5:1). We examined

the various formulations of nanocomplexes for morphological characteristics, serum stability, *in vitro* cellular uptake to screen the best candidate for *in vivo* activity studies. Selected nanocomplex candidate was further used for the treatment of the CCL4 induced liver fibrosis rat model. After the completion of the study and liver from different treatment groups and normal control were analyzed for the fibrosis molecular markers.

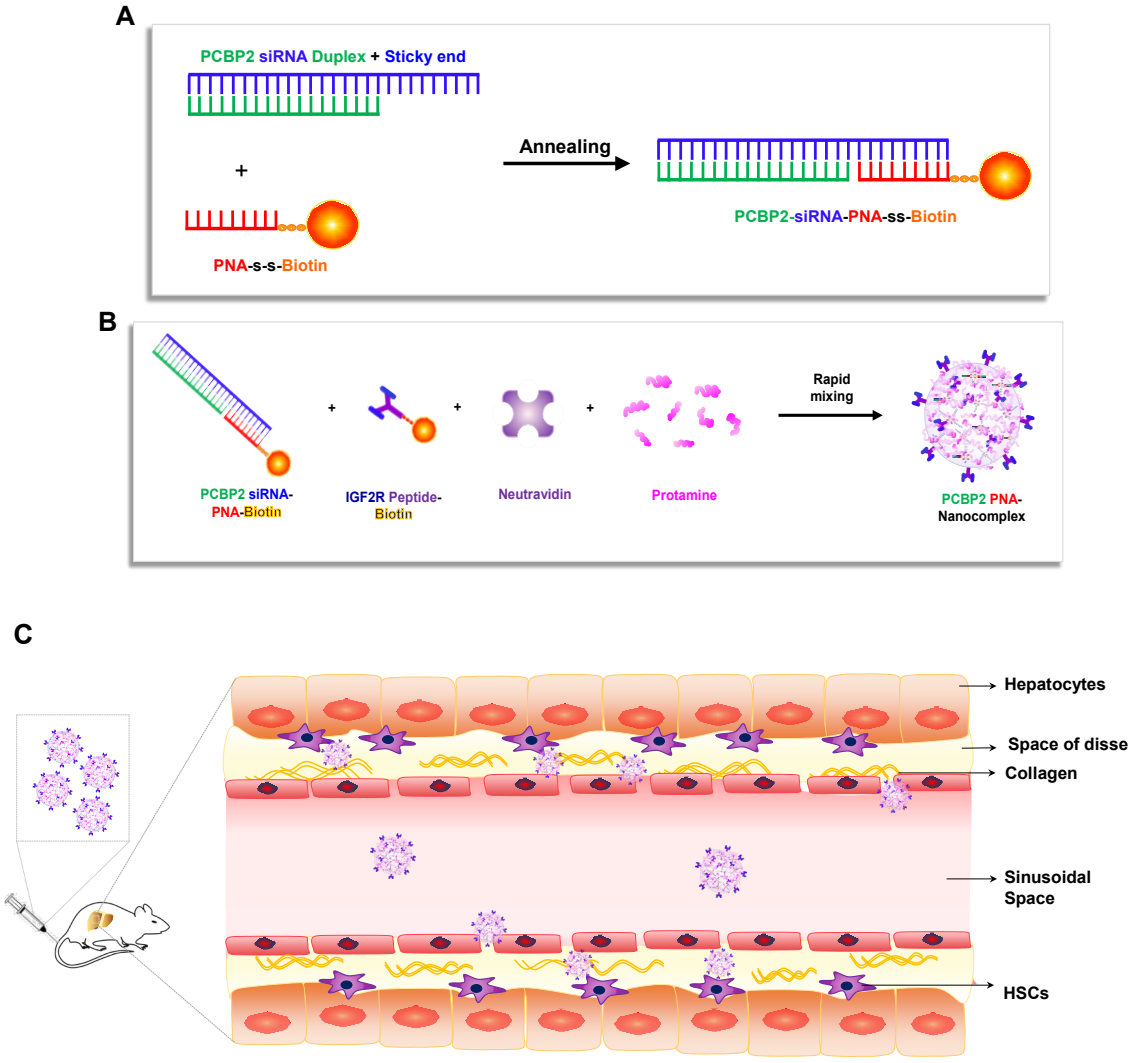

Figure 26. Schematic diagram of PCBP2 siRNA nanocomplex formulation and *in vivo* targeting.

5.2 Materials and Methods

5.2.1 Materials

Biotin-S-S-PNA (Sequence: Biotin-S-S-O-CAC CAC CAC) was purchased from PNA Bio, Inc., Newbury Park, CA. PCBP2 Sense strand with sticky end (Sequence: 5' GUC AGU GUG GCU CUC UUA UGU GGU GGU G dTdT 3') and PCBP2 anti sense strand (Sequence: 5' AUA AGA GAG CCA CAC UGA C dTdT 3') was purchased from GE Healthcare Dharmacon, Inc. Chicago, IL. Neutravidin, CCL4 was purchased from thermos fisher scientific. Bioplex assay kit was purchased from biorad inc.

5.2.2 Formulation of PCBP2-PNA-Nanocomplex

PCBP2 siRNA duplex with sticky end was prepared by annealing the sticky sense end with antisense along with anneling buffer. In the PCBP2 siRNA duplex with sticky end equimolar biotin-S-S-PNA was mixed and incubated in water bath at 37^{o}C for 30 min. Various molar ratios of PCBP2 PNA biotin: Neutravidin: biotin IGF2R peptide, such as 2:1:2, 3:1:1, 3.5:1:0.5, 3.8:1:0.2, 3.9:1:0.1 and 3.99:1:0.01 were mixed together to keep the final siRNA concentration as 100 nM and incubated for 10 min at room temperature. Further, protamine was added along with the respective nanocomplexes (N/P ratio as 2.5/1) and incubated for 30 min at RT.

5.2.3 Morphological Analysis of PCBP2-PNA Nanocomplex

Nanocomplexes were prepared as above and diluted in the HEPES buffer (pH 7.4). Nanocomplexes were analyzed for mean diameter and mean zeta potential of the dispersed nanocomplexes using Malvern zeta sizer. Nanocomplex with molar ratio 2:1:2, 3:1:1, 3.5:1:0.5, 3.8:1:0.2, 3.9:1:0.1 and 3.99:1:0.01 were re-analyzed for the mean particle size with the help of transmission electron microscopy. Briefly, nanocomplex

was prepared as described above and negative stained using 1% phosphotungstic acid with pH 7.2 on carbon electron microscope grid. After drying, the sample was analyzed under the electron microscope.

5.2.4 Gel Retardation and Serum Stability Assay

PNA-s-s-Biotin was annealed with the duplex PCBP2 siRNA with sticky end as described above. To confirm the annealing and nanocomplex formation, PCBP2-s-s-biotin, PCBP2 siRNA with sticky end, PCBP2 siRNA-PNA-s-s-biotin and PCBP2-PNA nanocomplex were ran on 20% native poly acrylamide gel electrophoresis (native PAGE) at 80V constant voltage for 4 h in cold room (4C). After 4 h, gel was visualized under UV with the help of gel red.

To confirm the release of the PCBP2 siRNA from the biotin-s-s-PNA and PNA nanocomplex, Biotin-s-s-siRNA, Biotin-s-s-PNA, Neutravidin-siRNA nanocomplex and PCBP2 PNA nanocomplex were formulated as described above and in our previous work[300] were incubated with 40uM heparin and 100mM Dithiothreitol (DTT) for 10 min to reduce the disulfide bond and release the PCBP2 siRNA free. Samples were further analyzed by native PAGE as described above.

To evaluate the serum stability of PNA nanocomplexes, free biotin s-s-PNA-$PCBP_2$ and various ratios of PNA nanocomplexes were formulated as mentioned above and incubated with 50% rat serum at 37C for 0h, 12h and 24h. After respective incubations, samples were incubated with 40uM heparin and 100mM DTT for 10 min as described above and analyzed using the native PAGE and visualized using gel red.

5.2.5 Cellular Uptake of Nanocomplexes

Various PCBP2 siRNA to IGF2R ligand ratios of nanocomplexes were evaluated for the cellular uptake efficacy by using Alexa 647 labeled PCBP2 siRNA. Sample preparation and analysis was done by confocal microscopy and flow cytometry as described as previously described.[11, 213] Briefly, HSC-T6 cells were transfected with various nanocomplexes for 1 h and washed with 1 mM heparin containing PBS. The acidic organelles like endosomes and lysosomes in cells were stained with LysoTracker DND 99 followed by formalin fixation. The cells were further examined under confocal microscope (Leica TCS SP5). To validate the cellular uptake results from confocal microscopy, HSC-T6 cells were incubated with nanocomplexes for 1 h as described above, washed with 1 mM heparin containing PBS, detached using non-enzymatic cell dissociation agent, and centrifuged to recover the cells. The resulting cell pellet was washed with PBS, re-suspended, and analyzed for Alexa 647 positive cells using a BD FACS II flow Cytometer (Bectone Dickinson Instruments, Franklin Lakes, NJ).

5.2.6 *In Vivo* Biodistribution Study

Liver fibrosis model was developed as mentioned above in accordance with UMKC-IACUC approved protocol. 12 rats were randomly divided into 2 groups. Rats in first group were intravenously (i.v.) administered with Cy5- labeled siRNA (0.1 mg/kg), and the rats in another group were i.v. administered with PCBP2 PNA nanocomplexes (3.5:1:0.5) encapsulating Cy5 labeled siRNA (0.1 mg/kg). Post 2 h of circulation, the animals were euthanized and vital organs including the liver, lungs, spleen, kidneys, heart, and thigh muscle were harvested and immediately imaged using a Bruker MS FX PRO Imaging System (Billerica, MA).

5.2.7 *In Vivo* Treatment of CCL_4 Induced Liver Fibrosis Rat Model

CCL_4 induced liver fibrosis animal model was developed as described previously and in accordance with the animal research protocol approved by the Institutional Animal Care and Use Committee (IACUC) at the University of Missouri Kansas City.[300, 302-303] Briefly, 32 Sprague dawley rats were purchased from the Charles river laboratories, Inc. (Raleigh, NC) and caged in the humidity and temperature controlled room with controlled 12h day-night cycle. Liver fibrosis was induced by intraperitoneal injections of mixture of 1 μL of CCl_4 per gram of body weight of rat and olive oil (1:1 v/v) every consecutive third day for 28 days. 32 Sprague dawley rats were randomized in four groups as named below and treatment mentioned in parenthesis, 1. Blank (No CCL_4/No PCBP2 PNA nanocomplex treatment, blank control), 2. CCL_4 (CCL_4 only, positive control), 3. Scrambled-PNA nanocomplex (CCL_4/Scrambled PNA nanocomplex, negative control), 4. PCBP2-PNA nanocomplex (CCL_4/ PCBP2 PNA nanocomplex). All groups underwent CCL_4 -mediated fibrosis induction except blank control group. PNA nanocomplex were formulated either with scrambled siRNA or PCBP2 at molar ratio of 3.5:1:0.5, keeping the final siRNA dose at 1mg/kg. On 14^{th}, 18^{th}, 23^{rd} and 27^{th} day of CCL_4 induction, PNA Nanocomplexes (PCBP2 or scrambled) were prepared at final volume of 200 uL and injected via tail vein of the respective rats of each group. On day 31^{st}, 6-8 mL blood was drawn from rats by cardiac puncture and rats were euthanized. Serum was immediately separated from the blood and stored in -80C freezer. Liver of respective animals from each group were harvested and cut into two parts, one was frozen in -80^{o}C and other part was stored with formalin for future analysis.

5.2.8 Serum ALT and AST Assay

ALT was measured according to the manufacturer's protocol (Sigma Aldrich). Briefly, 20 uL (V) of serum samples, positive control and pyruvate standards were added to the two separate 96 well plates. 100 uL of master mix was added to each well and briefly mixed by horizontal plate shaker. Initial measurement was taken after 2 minutes ($T_{initial}$) at 570 nm ($A_{initial}$). Plate reader was set at 37^{o}C and measurements were taken kinetically at every 5 min until 60 mins (T_{final}). Change in absorbance was calculated by subtracting the final absorbance (A_{final}) with the initial absorbance ($A_{initial}$). From the pyruvate standard, the concentration of the pyruvate (B) generated in samples from $T_{initial}$ to T_{final} was measured. ALT activity was determined by using the following equation: ALT Activity = (B × Sample dilution factor)/(T_{final}-$T_{initial}$) × V. ALT activity value is equivalent to the 1.0 nmol of pyruvate generated by the amount of ALT enzyme per minute at 37 °C.

AST assay was performed as per the manufacturer's protocol (Biovision). Briefly, 50 uL (V) of serum samples, positive control and glutamate standards were added to the two separate 96 well plates. 100 uL of reaction mix was added to each well and briefly mixed by horizontal plate shaker. Initial measurement was taken after 2 minutes ($T_{initial}$) at 450 nm ($A_{initial}$). Plate reader was set at 37^{o}C and measurements were taken kinetically at every 10 min until 60 mins (T_{final}). Change in absorbance was calculated by subtracting the final absorbance (A_{final}) with the initial absorbance ($A_{initial}$). From the pyruvate standard, the concentration of the glutamate (B) generated in samples from $T_{initial}$ to T_{final}. AST activity was determined by using the following equation: AST Activity = (B x

Sample dilution factor)/(T_{final}-$T_{initial}$) × V. AST activity value is equivalent to the 1.0 µmol of glutamate generated by the amount of AST enzyme per minute at 37 °C.

5.2.9 Hydroxyproline Assay

Collagen content in the liver was colorimetrically quantified as total hydroxyproline per gram of liver. One frozen liver sample from each group was weighed (50 mg) and homogenized with 250 uL PBS. After homogenization, homogenate was transferred to the glass vial and 500 uL of 12N HCL was added. The glass vial was tightly capped and hydrolyzed overnight at 120C on a dry bath incubator. Using the PVDF filter, hydrolyzed homogenate was filtered to remove the hydrolyzed tissue particles. 5 uL of the standard and sample supernatant were added in a 96 well plate and gently mixed with 50 µl of citrate/acetate buffer (pH 6.0) by taping on the side of the 96 well plate. Chloramine T (100uL) was added to each well and mixed gently. The plate was incubated at RT for 30 min. Further, DMAB-Ehrlich´s reagent (100 µl) was added in each well and incubated for 30 min at 65°C. Absorbance was measured at 550 nm in a microplate reader. Total hydroxyproline (µg/liver weight) was calculated based on the hydroxyproline (µg) per liver sample weigh (mg).

5.2.10 Histological Studies

Liver tissues in each group were stained with hematoxylin and eosin (H&E), Picro sirius red and Masson's trichrome staining. Briefly, formalin fixed liver tissues were embedded in paraffin and sectioned at thickness of 5 µm and mounted on the microscope glass slides. For staining, the respective slides were deparaffinized by three changes of histosol for 5 min; Further, slides were rehydrated by incubation in the series of alcohol (100% > 100% > 95% > 70%) incubation for a minute each and finally

hydrated with running water for 2 min. To stain the nucleus, rehydrated slides were incubated in the Wiegert's hematoxylin for 30 min followed by washing the slides in running water for 10 min. To stain the collagen in the section, the slides were subjected to the incubation with Picro Sirius red for 60 min. To differentiate the red stained collagen from other components of tissues and remove the unbound dye, slides were dipped 3 times in 1% acetic acid; followed by dehydrating the slides with 100% alcohol and 2 changes of histosol before tissues were mounted by Cytoseal^{TM} XYL (Richard Allan Scientific^{TM})

For Masson's trichrome staining, NovaUltra Special Stain Kit was used (IHC world) and manufacturer's protocol was followed. Briefly, tissue section slides were deparaffinized and rehydrated as described above. The slides were fixed after washing in bouin's solution at 56ºC for 60 min to improve the staining quality. After washing under running tap water, nucleus was stained with Weigert's iron hematoxylin working solution for 10 minutes followed by washing in DI water. Further, slides were incubated in the Biebrich scarlet-acid fuchsin solution for 15 minutes. After washing in DI water, differentiated in phosphomolybdic-phosphotungstic acid solution for 15 minutes. Slides were transferred directly to the aniline blue solution for 10 min to stain the collagen. After brief rinsing in DI water, slides were differentiated in 1% acetic acid solution for 2-5 min. Slides were washed in DI water and dehydrate in 95% alcohol and 100% alcohol to wipe off Biebrich scarlet-acid fuchsin staining. Slides were cleared in two changes of histosol and mounted with Cytoseal^{TM} XYL.

5.2.11 Collagen I Immunostaining

Formalin fixed paraffin embedded liver tissue sectioned slides were incubated in the histosol clearing agent followed by sequential lowering concentration of ethanol for rehydration (100% > 100% > 95% > 70% > 50%). The slides were incubated in water for full rehydration for 5 min. To expose the epitope from the deep paraffin embedded section, heat induced antigen retrieval was performed using citrate buffer (pH 6). Dehydrated tissue slides were placed in a boiling citrate buffer (antigen retrieval buffer) for 45 min. After cooling down the slides with DI water and tris buffered saline (TBS) tissues were blocked by protein blocking buffer for 1 h. Followed by incubation with primary anti collagen 1 antibody (rabbit-polyclonal) over night at 4C. After washing in PBST, tissue sections were incubated with biotinylated anti-rabbit IgG-HRP secondary antibody for 2 h at room temperature. Streptavidin HRP was sufficiently spread over the tissues followed by color development with Diaminobenzidine (DAB) chromogen. Counterstained with Mayer's hematoxylin and mounted with cytoseal XYL.

5.2.12 Total RNA Isolation and *In Vivo* PCBP2 and Collagen I Silencing Activity from Liver Tissues

Section from liver tissue samples from four groups were taken and homogenized in 500 uL Trizol using hand handled tissue homogenizer. Tissue homogenate was mixed with 250 uL of chloroform and mixed vigorously and incubated at RT for 10 min followed by centrifugation at 12000g for 15 min (4ºC). The supernatant was collected and mixed gently with 500 uL Isopropanol and incubated at RT for 10 min and further centrifuged at 12000 g for 15 min. RNA palette was washed with 75% ethanol and centrifuged at 7500g for 10 min, this step was repeated twice. RNA palette was dissolved

in nuclease free water and incubated in 37C water bath for 10 min to dissolve the RNA completely. RNA was quantitated using Nano drop UV spec. Total RNA isolated was diluted to make 50 ng/uL concentration. Forward and reverse primers of PCBP2 and Collagen I were obtained from Integrated DNA technology. Biorad iTaq universal SYBR green one step PCR kit was used to evaluate $PCBP_2$ and collagen I mRNA expression in the in vivo samples with the help of Biorad CFX Connect™ Real-Time PCR Detection System.[69]

5.2.13 Bioplex Cytokine Assay

To evaluate the serum cytokine levels in vivo samples, Bio-Plex Pro™ rat cytokine assay kit was used and manufacturer's protocol was followed. Briefly, serum samples were diluted with sample diluent buffer (1:4). The 96 well filter plate was diluted with diluent buffer. 20X coupled beads stock was diluted to 1X and 50 uL was added to the each well of the filter bottom 96 well filter plate. After vacuum washing (2 times) with wash buffer, 50 uL of standard and samples were added to appropriate wells. Plate was sealed and incubated on plate shaker for 1h. Respective wells were washed three times with wash buffer, followed by addition of 25 uL 1X detection antibody per well. Plate was further incubated on plate shaker at room temperature (RT) for 30 min. Wells were washed again as described above followed by addition of 50 uL of streptavidin-PE (1X) per well and incubated for 10 min on plate shaker at RT. After subsequent washing, 125 uL assay buffer added to the 96 well filter plate to resuspended the beads followed by 30 sec incubation on plate shaker. Finally, 96 well filter plate was analyzed on Bio-Plex MAGPIX system at high PMT, RP1 setting.

5.2.14 TUNEL Assay

Liver tissues embedded in paraffin were analyzed for the degree of apoptosis among groups. TUNEL assay was performed according to manufacturer's protocol (Click-iT™ Plus TUNEL Assay, Thermo Fisher Scientific). Briefly, paraffin was removed from the tissue slides by incubation with histosol. Followed by hydration with sequentially reducing ethanol immersion. Tissue sections were fixed with 10% formalin, followed by permeablization with Proteinase K and fixed in formalin again. Further, terminal deoxynucleotidyl transferase (TdT) enzyme catalyzed incorporation of terminal deoxynucleotidyl transferase-EdUTP in the double stranded DNA breaks for fluorescent detection of apoptotic cells in the liver tissue section. Counterstained with DAPI. Images were captured by using Leica microscope and analyzed using ImageJ software.

5.2.15 Statistical Analysis

All groups were divided into 8 samples. For every statistical analysis, at least 8 samples per group were used. Assays were performed 3 independent times for each group. Analysis was performed using a two-way analysis of variance (ANOVA) with Tukey's Post Hoc test. $P<0.05$ was considered statistically significant. GraphPad Prism software was used.

5.3 Result

5.3.1 Morphological Analysis of Nanocomplexes

Nanocomplexes of various molar ratios (siRNA: Neutravidin: IGF2R peptide) were used to investigate the particle size and zeta potential of nanocomplexes when dispersed and diluted in HEPES buffer (pH 7.4). Results shown in Figure 27A, demonstrated that the increase in the ratio of siRNA with respect to the PEG modified

peptide ligand leads to the reduction in particle size. As expected, the zeta potential for nanocomplexes with higher siRNA molar ratio showed direct proportionality with the zeta potential. Particle size data was validated with the scanning electron microscopy (Figure 27B). Nanocomplexes showed similar texture but different particle size similar to what observed in dynamic light scattering (DLS). Nanocomplexes were polydispersed and showed spherical morphology with slight distortions on surface demonstrating the protamine being electrostatically attached to the Nanocomplex.

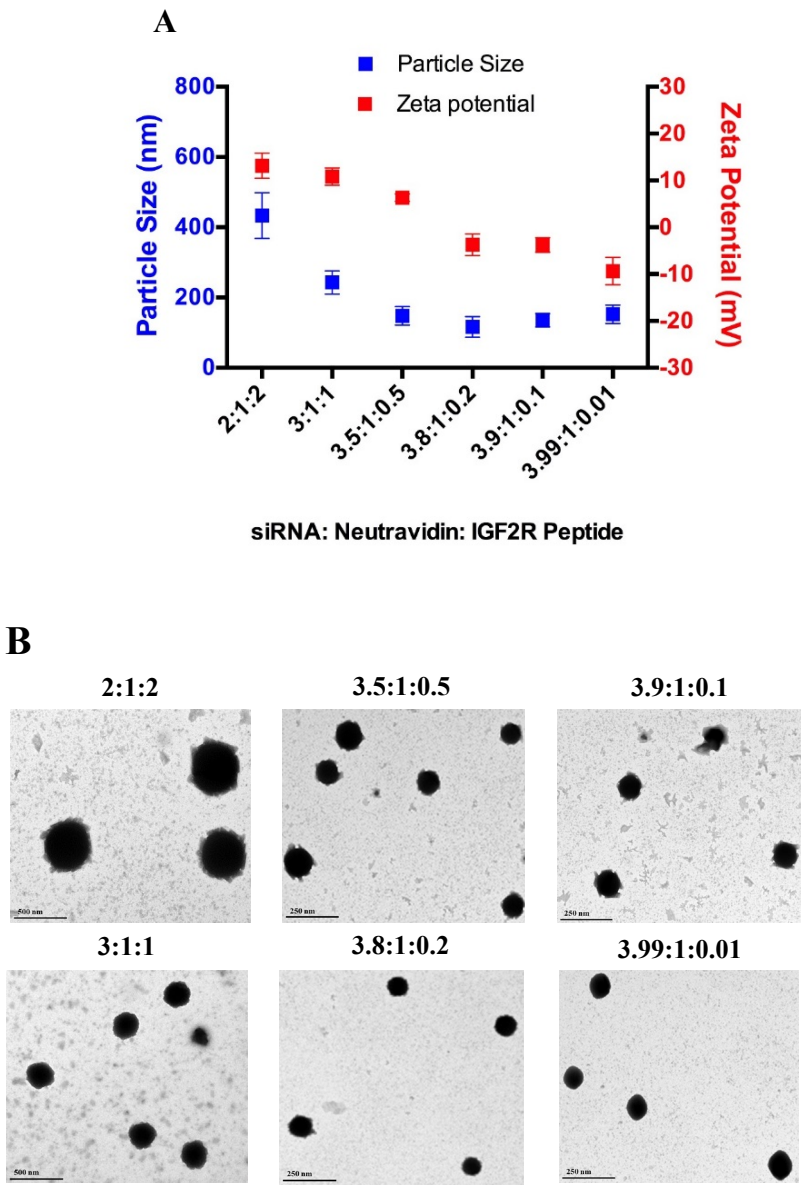

Figure 27. Particle size and zetapotential analysis of PCBP2 siRNA nanocomplex.
A. Particle size and zeta potential of PCBP2 siRNA nanocomplexes with various ratios were compared was analyzed in HEPES (pH: 7.4) buffer and analyzed by Diynamic light scattering; B. PCBP2 siRNA nanocomplexes were stained with phosphotungstic acid, imaged and analyzed in transmission electron microscope.

5.3.2 Annealing and Serum Stability of Nanocomplexes

Although, PCBP2 siRNA-biotin conjugated with disulfide linkage has already been reported, our core concept was to non-covalently attach the IGF2R ligand to the siRNA with the help of peptide nucleic acid (PNA). To confirm the annealing of the PCBP2 siRNA (plus sticky end) with the PNA-ss-Biotin, we analyzed the annealed products in 20% native poly acrylamide electrophoresis (PAGE). In figure 28A, from lane 1 to 3, PCBP2 siRNA-S-S-Biotin, PCBP2 siRNA with sticky end and PNA-S-S-Biotin annealed to the PCBP2 siRNA with sticky end were resolved on the native gel in the order of their respective molecular weight. In lane 4. PCBP2-PNA-S-S-Biotin was completely complexed with neutravidin Nanocomplex and resided on the interface of the gel shown as a thin and sharp band (highlighted by the red circle).

Similarly, release of siRNA from the PCBP2 siRNA-S-S-Biotin, PCBP2-PNA-S-S-Biotin, PCBP2-Nanocomplex and PCBP2-PNA-Nanocomplex was investigated by incubating all the modalities in the 40 uM heparin and 100 mM DTT. DTT reduced the disulfide linkage and heparin competed with the siRNA to bind with protamine. This resulted in the release of the siRNA or siRNA PNA from the Nanocomplex and conjugated biotin. Resulting crude release products were resolved using native PAGE. In figure 28B, it is clearly visible that the PCBP2 siRNA and PCBP2-PNA, free or complexed, were successfully released. This demonstrates that, upon reaching endosomal acidic pH, disulfide bonds in nanocomplexes will be effectively reduced to release the PCBP2 siRNA-PNA in the cytoplasm.

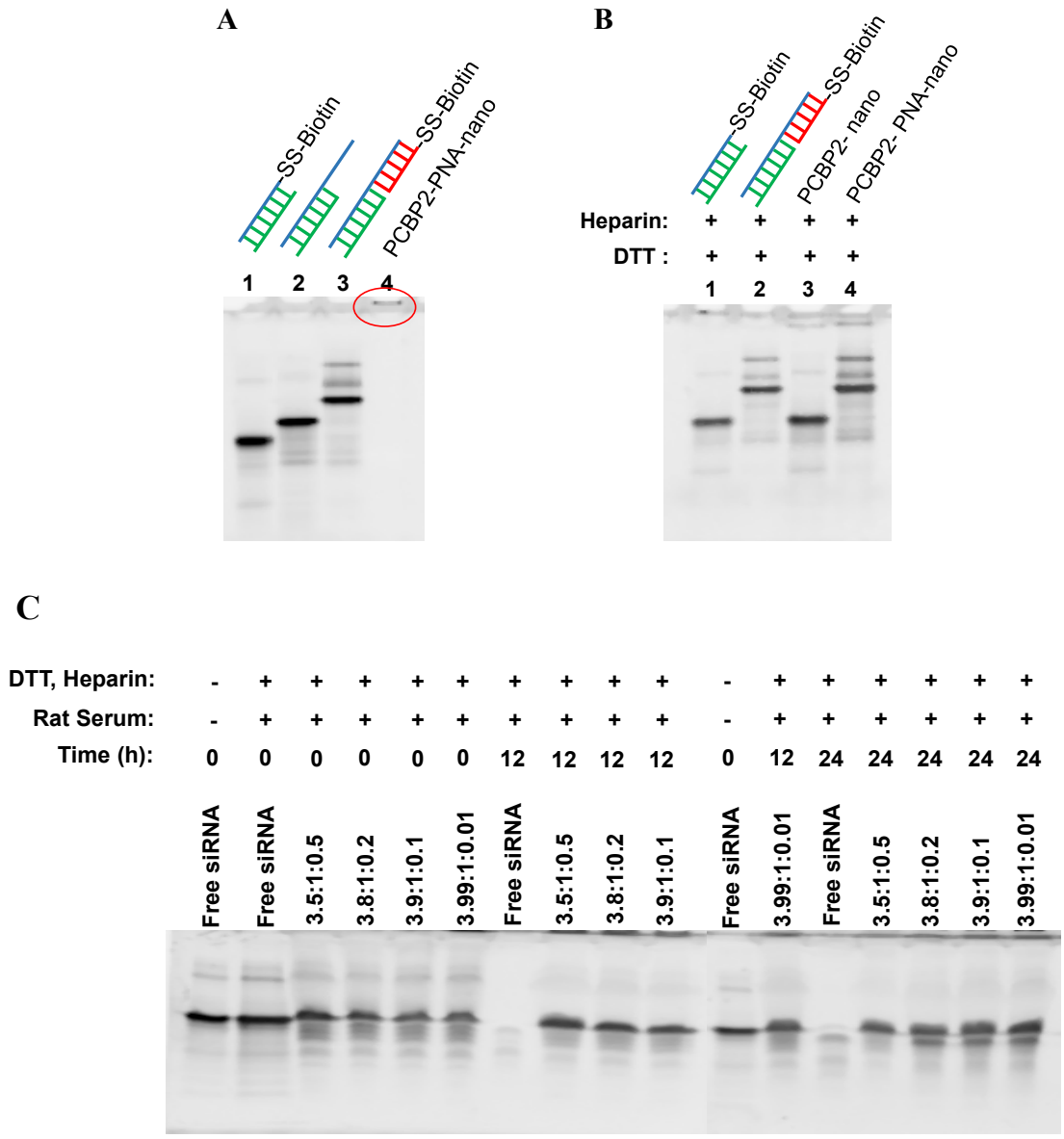

Figure 28. Gel retardation and serum stability of the various siRNA modifications
A. Lane 1: Biotin covalently attached to the sense strand of PCBP2 siRNA duplex by disulfide bond, Lane 2: PCBP2 siRNA duplex with sticky sense strand, Lane 3: PCBP2 siRNA duplex with sticky sense strand annealed to peptide nucleic acid-s-s-biotin, Lane 4: PCBP2 siRNA nanocomplex; B. Release of siRNA by reduction of disulfide bond by 100mM DTT. Lane 1: Biotin covalently attached to the sense strand of PCBP2 siRNA duplex by disulfide bond, Lane 2: PCBP2 siRNA duplex with sticky sense strand annealed to peptide nucleic acid-s-s-biotin, Lane 3: PCBP2 noncomplex with covalently attached biotin to sense strand of siRNA dulplex, Lane 4: PCBP2 siRNA nanocomplex with biotin attached noncovalently to the PNA; C. Various molar ratios of PCBP2 Nanocomplexes (with PNA-biotin) incubated with 50% rat serum for 0, 12 and 24 h followed by 40 uM heparin and 100mM DTT. Samples were analyzed in the 20% native PAGE.

Serum stability is one of the biggest challenges for siRNA delivery systems. After incubation of the four different nanocomplexes ratios (3.5:1:0.5, 3.8:1:0.2, 3.9:1:0.1 and 3.99:1:0.1) in 50% rat serum for 0 h, 12 h and 24 h, the mixture was further incubated with 100 mM DTT and 40 uM heparin to release the total PCBP2-siRNA-PNA from the nanocomplex. The mixture was subsequently analyzed using the 20% native PAGE. Results indicated that the siRNA was highly stable in rat serum at extended hours at 37ºC. In Figure 28C, the band from siRNA was clearly visible in the same horizon as the control free siRNA. At early time points such as 0 h and 12 h there was no visible degradation of the siRNA. However, at 24 h, a secondary band was observed in the case of 3.8:1:0.1, 3.9:1:0.1 and 3.99:1:0.01 molar ratio Nanocomplex formulations. This indicates that the 3.5:1:0.5 molar ratio for Nanocomplex formulation is in fact more stable and keeps siRNA intact for longer period of time.

5.3.3 Higher Ligand Ratio Increases Cellular Uptake of Nanocomplexes

Nanocomplexes of various ratios, 3.5:1:0.5, 3.8:1:0.2 and 3.9:1:0.1, were also examined for the cellular uptake. After incubation with hepatic stellate cells for 1 h at 37ºC, 3.5:1:0.5 ratio showed significantly higher uptake in comparison to other molar ratios when analyzed by flow cytometry. As shown in Figure 29 A, nanocomplexes with various ratios showed 100% uptake in hepatic stellate cells. Interestingly, the fluorescence intensity imparted by the CY-5- PCBP2 siRNA was significantly higher in case of the 3.5:1:0.5 molar ratio (Figure 29B).

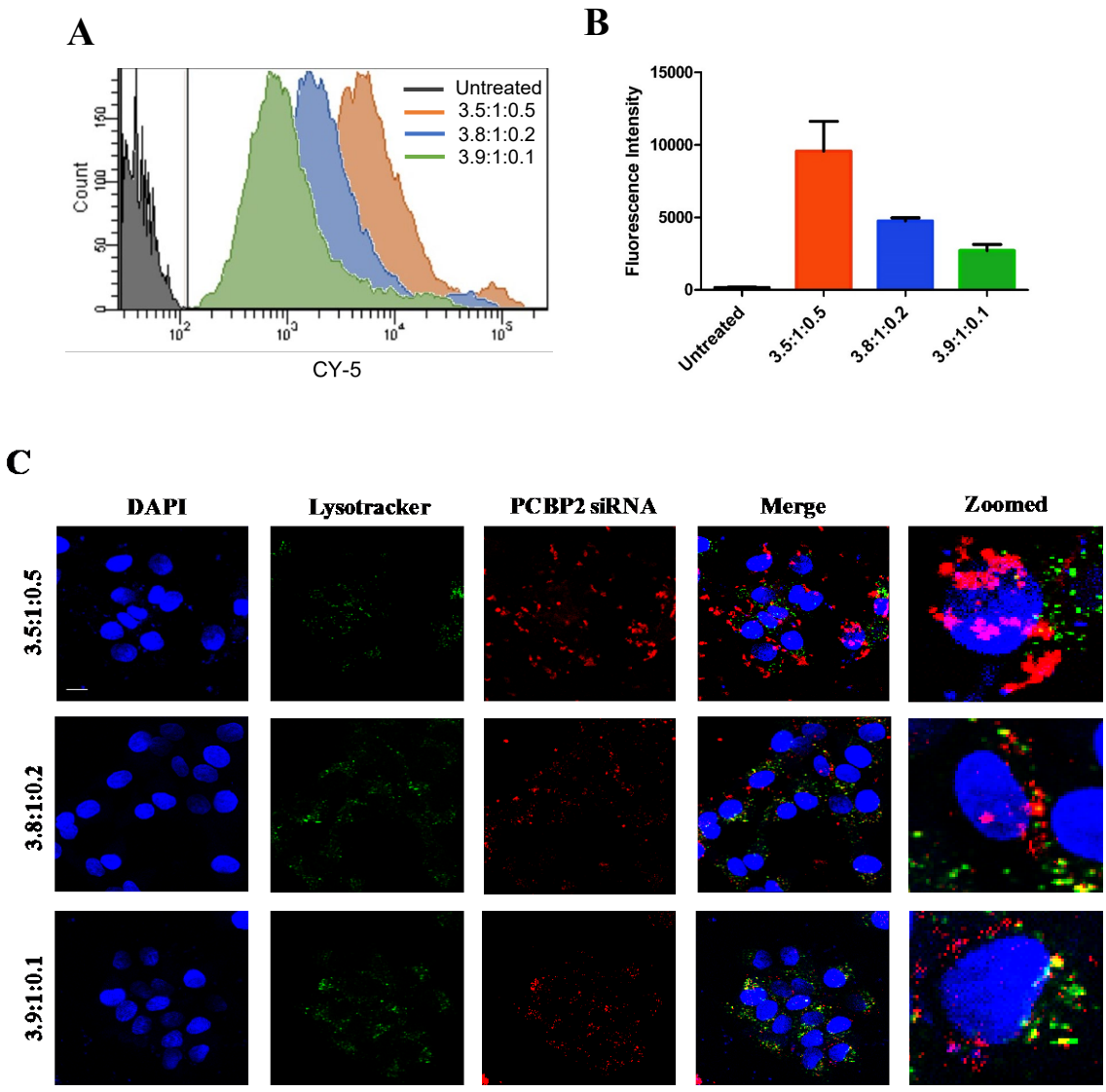

Figure 29. Analysis of rapid cellular uptake of PCBP2 siRNA nanocomplexes in HSC.

A. CY-5 labeled PCBP2 siRNA was formulated in various ratios (3.5:1:0.5, 3.8:1:0.2, 3.9:1:0.1) and HSC-T6 cells for 1 h and analyzed by Flow Cytometry. B. Fluorescence intensity data from flow cytometry was quantitated for each nanocomplex treatment group. C. CY-5 labeled PCBP2 siRNA was formulated in various ratios (3.5:1:0.5, 3.8:1:0.2, 3.9:1:0.1) and HSC-T6 cells for 1 h. after incubation, acidic organelles were stained with 100 nM lysotracker and counterstained with DAPI to stain the nuclei. Followed by formalin fixing and imaged in confocal microscopy. Scale bar = 20um.

Flow cytometry results were validated by the incubating the HSC-T6 with nanocomplexes with various ratios (3.5:1:0.5, 3.8:1:0.2 and 3.9:1:0.1). After 1 h of incubation, cells were fixed and imaged under the confocal microscope using the red channel for CY-5-PCBP2 siRNA, green channel for the lysotracker and blue channel for the DAPI. As demonstrated in Figure 29C, CY-5-PCBP2 siRNA-mediated signal intensity was significantly higher in case of the 3.5:1:0.5 molar ratio nanocomplex. Results confirmed that the 3.5:1:0.5 molar ratio has high siRNA loading along with optimum IGF2R ligand for extensive targeting and rapid cellular uptake.

5.3.4 Nanocomplex Show Enhanced *In-Vivo* Biodistribution

PCBP2 siRNA nanocomplex with molar ratio 3.5:1:0.5 molar ratio has shown significantly higher cellular uptake and HSC-T6 targeting *in vitro* in comparison to the other molar ratios. In addition to it *in vitro* superiority, 3.5:1:0.5 molar ratio was evaluated for its *in vivo* liver uptake in the liver fibrosis model. CY5-PCBP2 siRNA condensed in the nanocomplex at molar ratio of 3.5:1:0.5 and free CY5-PCBP2 siRNA was injected through the tail vein of CCL_4 -induced liver fibrosis rat model. After 2h of circulation, animals were euthanized and vital organs such as liver, kidneys, spleen, heart, lung and muscle (thigh) were harvested and organs were immediately imaged and analyzed for fluorescence. In contrast to the free PCBP2 siRNA, PCBP2 siRNA condensed in the nanocomplex showed significantly higher liver distribution and free PCBP2 siRNA-CY5 was rapidly eliminated by renal clearance. CY5 mediated fluorescent signal were statistically significant in case of the free CY5 PCBP2 siRNA.

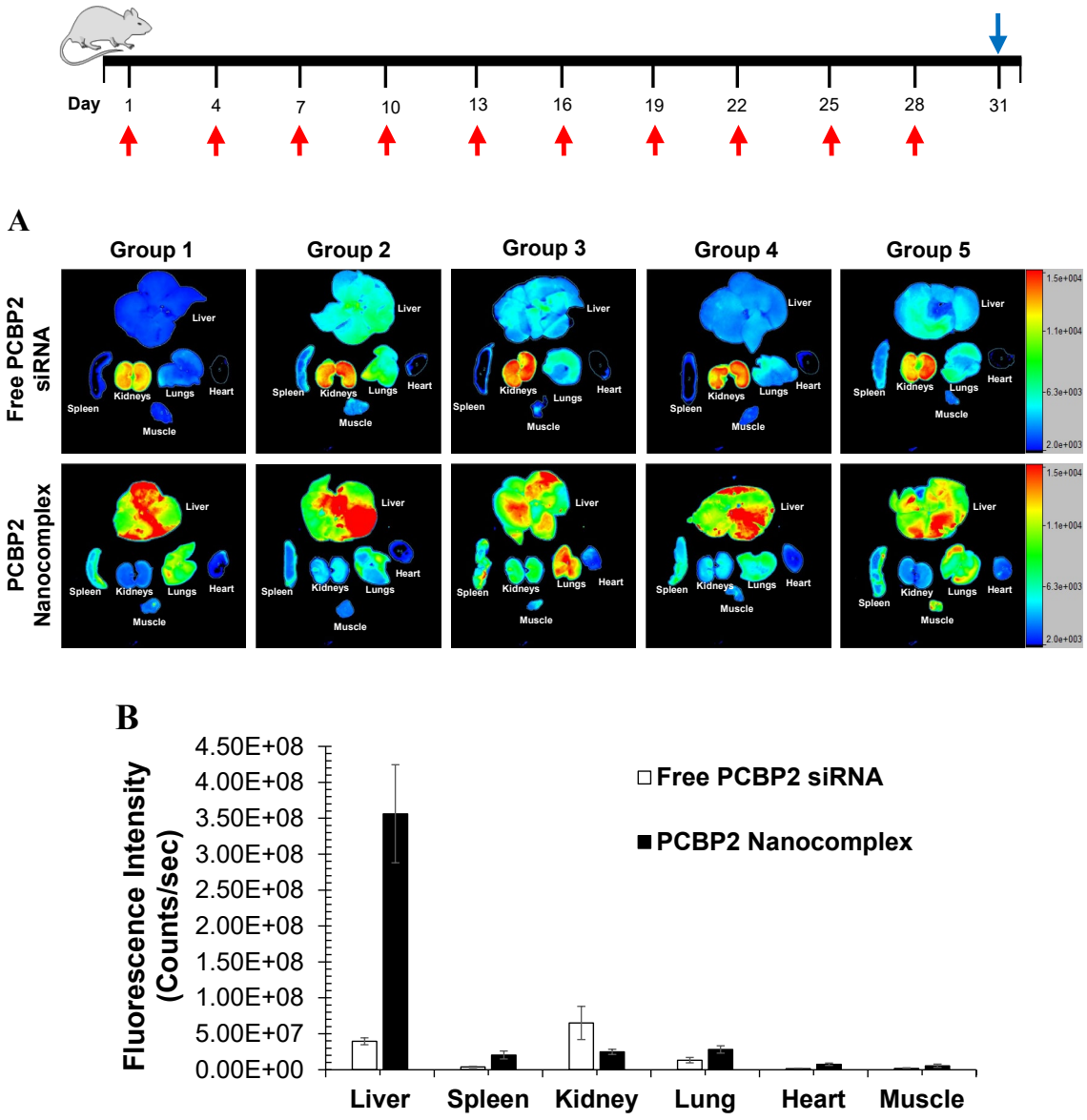

Figure 30. ***In vivo*** **biodistribution of PCBP2 siRNA and PCBP2 siRNA Nanocomplex.**

CY5 labeled PCBP2 siRNA (0.1 mg/kg) after 1 h of systemic circulation post tail vein injection (blue arrow) in CCL_4/Olive oil (red arrow) induced liver fibrosis model. A. Liver, spleen, kidney, lung, heart and muscle were harvested and imaged for fluorescence mediated by CY5 labeled PCBP2 siRNA. B. Fluorescence intensity in various organs in different treatment groups was quantitated by GraphPad PRISM.

5.3.5 PCBP2 Nanocomplex Reduces the Fibrosis Serum Markers

To evaluate the extent of fibrosis in the control and treatment groups, blood (after the treatment regimen) was collected from each animal before euthanizing. Blood was centrifuged at 2000 g for 5 min to separate the serum. Serum was used to evaluate the primary markers of liver fibrosis, ALT and AST. As depicted in figure 31A and 31B, in comparison to the blank/no treatment group, ALT and AST levels in serum were significantly higher in case of no treatment/CCL_4 group (ALT = 499.96 IU/L, AST = 463.7 IU/L) and scrambled siRNA/CCl4 group (ALT = 451.01 IU/L and 498.08IU/L). Interestingly, after periodic treatment with PCBP2 siRNA nanocomplex, fibrotic rat showed significantly lower levels of ALT and AST (218.07 IU/L and 214.9 IU/L respectively). However, the liver enzyme levels were statistically significant when compared to normal control (blank/no treatment).

To examine the amount of the collagen in a tissue, hydroxyproline assay is performed as hydroxyproline constitutes of the 13.5% of the total collagen protein. The liver samples harvested from the different treatment groups were subjected to hydroxyproline assay. Results revealed that the hydroxyproline content after the liver fibrosis induction escalated dramatically in comparison to the normal control (Blank/no treatment). It was observed that after receiving the scrambled siRNA treatment, there was no significant difference in the hydroxyproline levels in comparison to the CCL_4-induced fibrosis group with no treatment. In contrast to no treatment and scrambled siRNA treatment group, PCBP2 siRNA nanocomplex treated group with fibrosis showed significantly lower hydroxyproline content (figure 31C).

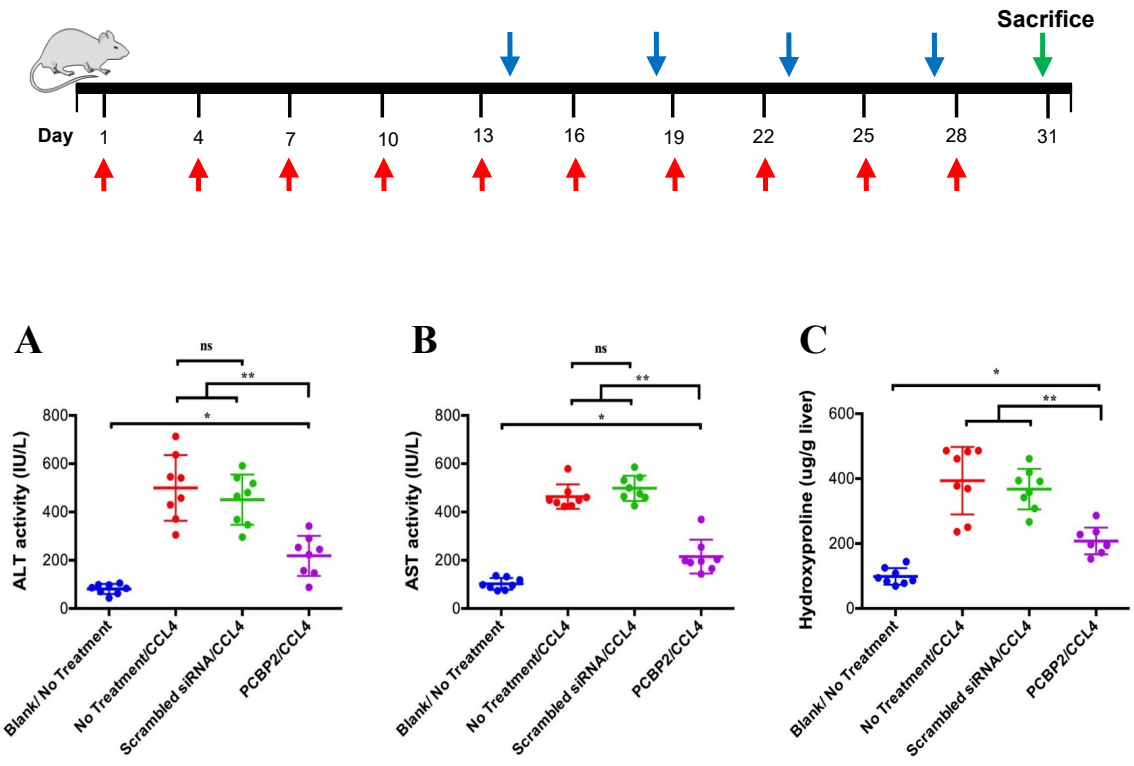

Figure 31. Analysis of fibrosis markers after PCBP2 nanocomplex *in vivo* delivery. Treatment timeline: Liver fibrosis was induced in Sprague dawley rats by administering intraperitoneal injection of CCL4: olive oil (1:1 v/v) indicated by red arrows. After 2nd week of fibrosis induction, animals separated in different groups either received no treatment, scrambled siRNA nanocomplex (1mg/kg), or PCBP2 siRNA nanocomplex (1mg/kg), indicated by blue arrows. Series of assays were performed to examine the fibrosis. A. Serum ALT levels (IU/L); B. Serum AST levels (IU/L); C. Liver Hydroxyproline content (ug/g liver).

5.3.6 Nanocomplex Reduces the PCBP2 and Collagen I mRNA Expression

To investigate the *in vivo* effect of PCBP2 siRNA Nanocomplex on the PCBP2 and Collagen type I mRNA expression, the frozen liver tissues from all the animals were homogenized in the DNase and RNase free water and total RNA was isolated. qRTPCR results revealed that the PCBP2 (Figure 32A) and Collage I (Figure 32B) mRNAs were

significantly downregulated in comparison to the no treatment and scrambled siRNA treatment fibrotic rat groups. This downregulation is the key for the regression of the collagen fiber production in the extra cellular matrix.

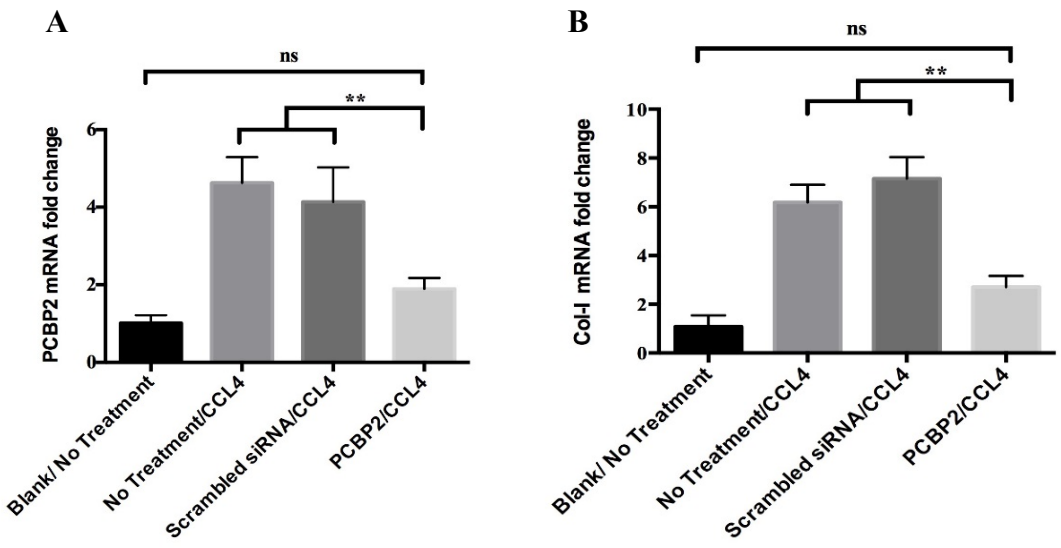

Figure 32. qRTPCR analysis of the mRNA fold change in different treatment groups.
A. PCBP2 mRNA fold change in liver; B. Type I Collagen mRNA fold change in liver.

5.3.7 PCBP2 Nanocomplex Mitigates the Aggressive CCL4 Induced Liver Fibrosis

To assess the anti-fibrotic effect of PCBP2 nanocomplex on the aggressive fibrogenesis, fibrotic rats were injected (i.v.) with the scrambled siRNA or PCBP2-siRNA Nanocomplex with concurrent CCL4 IP injection. After formalin fixation and tissue sectioning, liver tissues were subjected to staining and subsequently imaged (Figure 4F). Hematoxylin and Eosin (H&E) staining showed that the CCL4 induced fibrosis group that received no treatment or scrambled siRNA treatment was heavily scared and showed remarkable signs of injury. Intriguingly, PCBP2 treatment group not

only demonstrated substantially less hepatic scarring, but signs of wound healing. Although, this assumption needs to be further investigated.

Tissue slides from each group were also stained for collagen fibers by Picro-sirius red staining and masons trichrome staining. Picro-sirius red and Masson's trichrome stains collagen type I, III, IV. As CCL4 induces extensive damage to the liver architecture and tissues providing the structural integrity to the liver, activated hepatic stellate cells produce larger volumes of collagen to keep the liver architecture stable. Treatment with PCBP2 siRNA Nanocomplex substantially reduced the collagen fibers in comparison to the no treatment and scrambled siRNA treatment group. In figure 33B, picro sirius staining of no treatment and scrambled siRNA treatment group showed portal to portal and portal to central vein bridging with significant nodules. This demonstrates that the fibrosis in our study was late stage as per Ishak score of fibrosis. [304] In case of PCBP2 treatment groups, we saw significant thinning of the collagen fiber bridging with no signs of nodules. To elucidate the fibrosis (collagen staining) the images from different groups were processed in ImageJ software and the collagen positive stained area was calculated. As shown in Figure 33C, percent area stained with collagen fiber in no treatment and scrambled siRNA treatment group was significantly different when compared to the PCBP2 siRNA treatment. However, there was statistically significant collagen staining in PCBP2 siRNA nanocomplex treatment samples compared to the blank/no treatment (normal control) group.

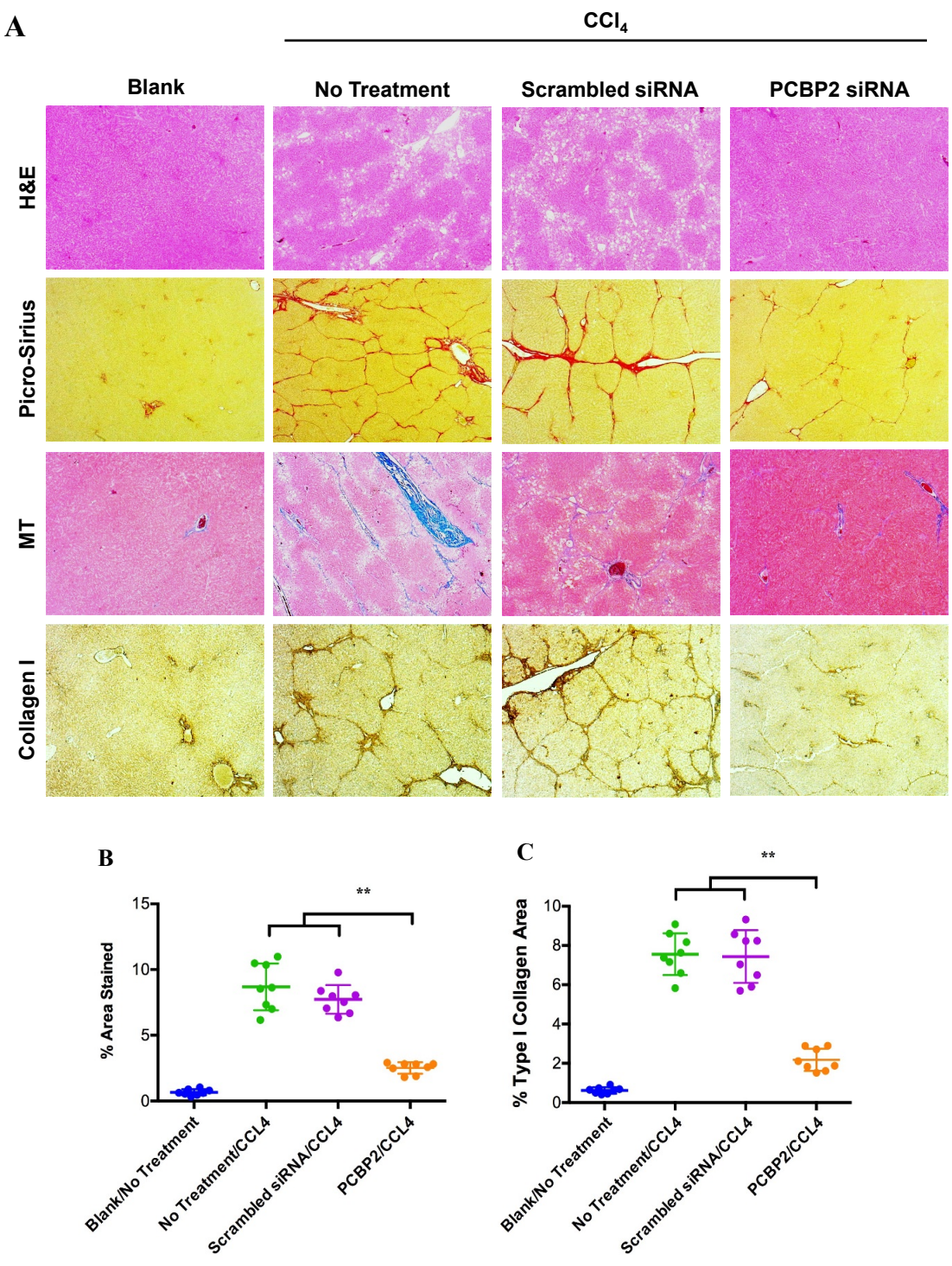

Figure 33. A. Histological analysis of liver tissue after the treatment of liver fibrosis. A. Hematoxylin and Eosin staining, Picro-sirius red staining, Masson's Trichrome staining, and Type I collagen immunohistochemistry staining by light microscopy; B. Collagen I, III and IV (Picro-sirius red) stainied area quantified by ImageJ; C. Type I collagen (immunohistochemistry) stained area quantified by ImageJ.

As PCBP2 siRNA specifically downregulates the collagen I mRNA, we examined its effect at protein level in the liver tissue sections by collagen I immunohistochemistry. As highlighted by arrows in figure 33A, collagen I protein staining was significantly lower in PCBP2 nanocomplex treatment group. Since picrosirius stains all collagen fibers, collagen I immunostaining validated the specific downregulation of collagen I fibers (protein) upon PCBP2 nanocomplex treatment in fibrotic rats. Images were analyzed from each sample by ImageJ and collagen I staining was quantified. Collagen I positive areas were approximately 8 % of total tissue area in case of the liver fibrosis model, whereas PCBP2 treated fibrotic rats showed less than 3 % collagen staining (figure 33C).

5.3.8 Effect of Fibrosis and Its Resolution on Apoptotic Cells

Paraffin embedded liver tissues from each group were examined for the apoptosis. Apoptosis is one most significant events during liver injury and many events such as cytokine induction, reactive oxygen species, immunological damage etc. are prime reasons for the liver injury.[3] Also, Apoptosis is a sign of chronic liver injury and its intervention has proven to be beneficial for the resolution of liver fibrosis/injury in clinical trials. [305-306] As indicated in Figure 34A, PCBP2 siRNA-treated groups showed significantly lower TUNEL positive (apoptotic) cells in comparison to the no treatment or scrambled siRNA treatment groups. We also quantified the TUNEL positive cells from 5 different areas per slide of 5 independent samples per group. As shown in figure 34 B, count of TUNEL positive cells of No treatment and scrambled siRNA was significantly higher than PCBP2 treatment groups.

This also supports the assertion derived from the literature that the regression in the apoptosis leads to the resolution of fibrosis and liver injury.[305] This result also

confirms the resolution of fibrosis shown by molecular serum markers and histology studies (collagen staining). There was some apoptosis visible in the normal liver (blank/no treatment) group which can be attributed to the homeostasis.[307]

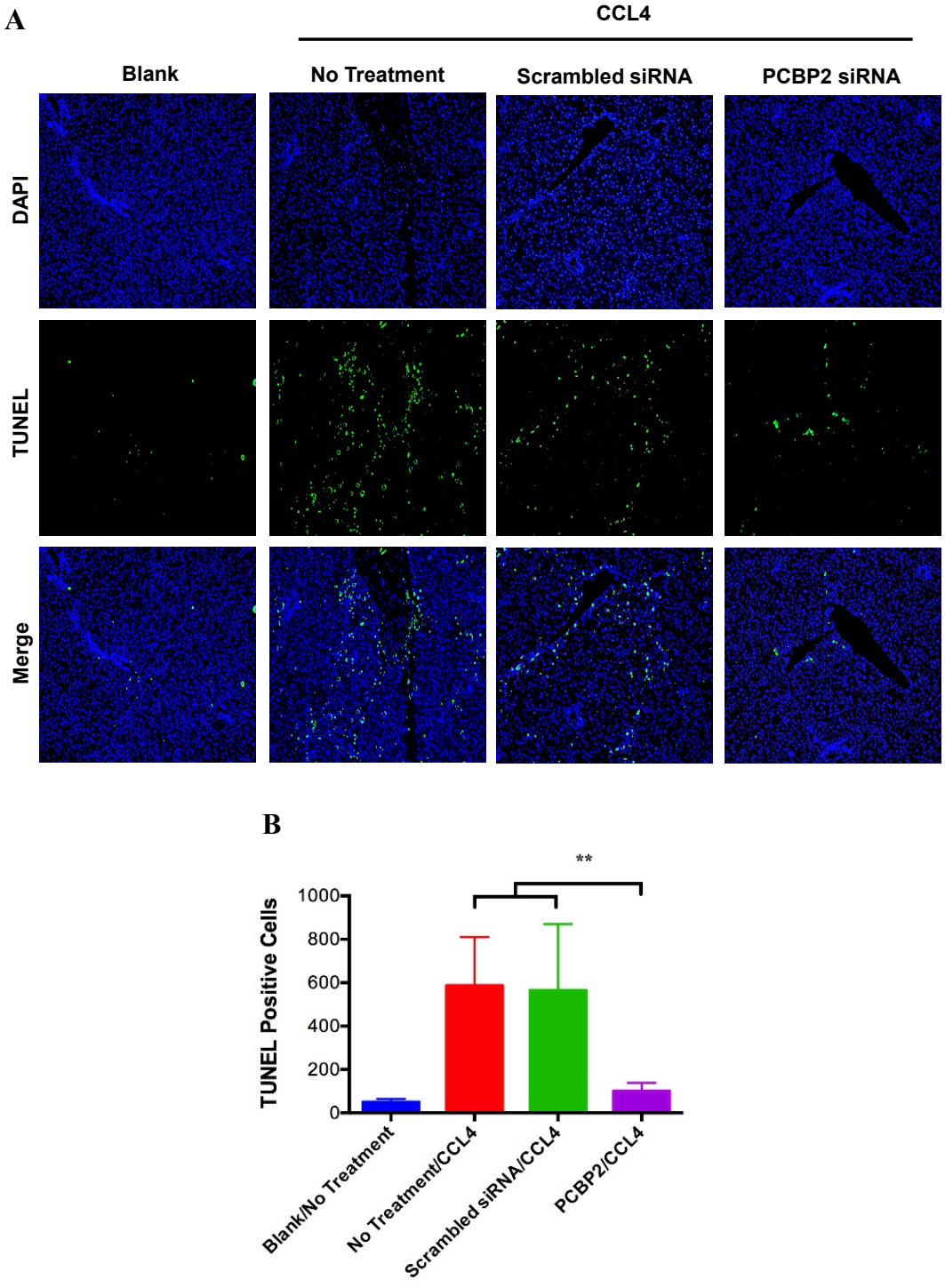

Figure 34. Evaluation of apoptosis in liver tissue in different groups of treatment
A. Images taken for TUNEL assay by fluorescence microscopy; B. Quantification of TUNEL positive cells (apoptotic cells) in liver section by ImageJ

5.3.9 Resolution of Fibrosis by PCBP2 siRNA Downregulates Cytokine Production

Cytokine upregulation is the most important event post liver injury which regulates the fibrogenesis. Cytokines such as TGF β-1 and PDGF are primary cytokines which drive hepatic stellate cell differentiation.[308-310] We investigated the proinflamatory cytokines level changes in the serum of the fibrotic rats and normal (blank) control rats. Serum from each group analyzed by bioplex cytokine assay kit for detecting the concentration of the proinflamatory cytokines and chemokines. Interleukins (such as IL-1β, IL-4, IL-6 and IL-18), TNFα are highly elevated in the progression of fibrosis as they govern the proliferation of the fibroblasts, T cells and macrophages.[308, 311] It is important to note that due to induction of fibrosis with CCL_4, serum levels of cytokines were upregulated in comparison to the healthy control (blank/no treatment). With periodic treatment with PCBP2 siRNA nanocomplexes, expression of cytokines like IL-1β, IL-4, IL-6 and IL-18), TNFα was significantly lowered if not the same as the healthy control. All interleukins were downregulated in PCBP2 siRNA nanocomplex- treated groups by 2-3 fold approximately except that of the IL-18. Levels of IL18 were lower in some samples but cumulatively the expression was found to be statistically insignificant. Moreover, chemokines such as MCP-1 (CCL2) and RANTES (CCL5) are known to be profibrogenic in nature and potent chemoattractants which further the inflammation by interacting with the T lymphocytes, monocytes, NK cells etc. [293, 312-313] It has also been reported that the targeting the RANTES and MCP-1 helps in amelioration of liver fibrosis.[314] As shown in figure 35 F-G, MCP-1 and RANTES were significantly downregulated in the groups treated with PCBP2 siRNA Nanocomplex.

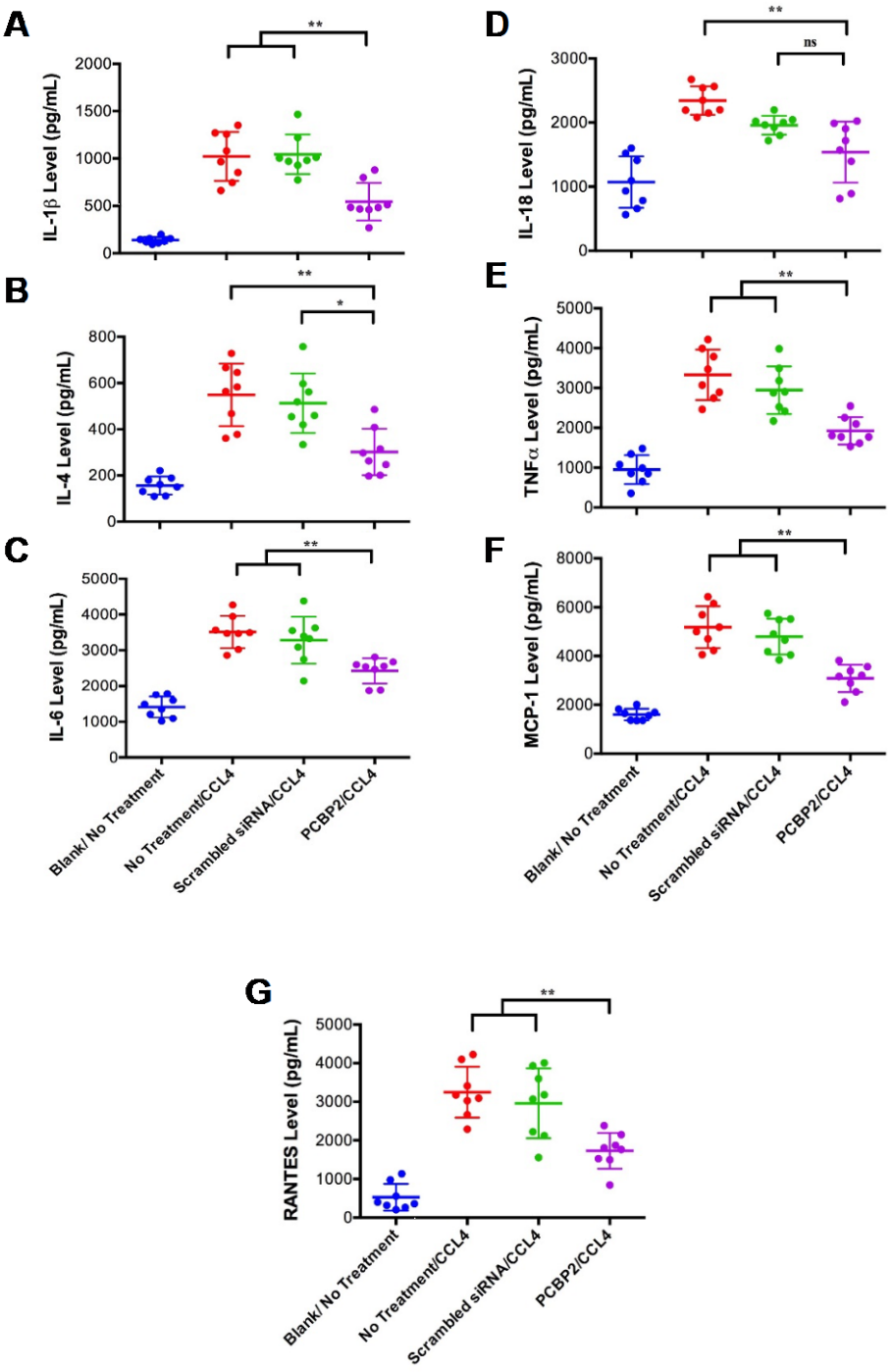

Figure 35. Multiplex assay for the evaluation of cytokines and chemokines in serum. A. Serum IL-1β cytokine level; B. Serum IL-4 cytokine level; C. Serum IL-6 cytokine level; D. Serum IL-18 cytokine level; E. Serum TNFα cytokine level; F. Serum MCP-1 chemokine level; G. Serum RANTES chemokine level.

5.4 Discussion

Effective treatment for liver fibrosis has remained a challenging endeavor because of the following major reasons: 1. Complex and dynamic nature of the molecular mechanisms contributing to fibrosis; 2. Lack of targets for the delivery of drug cargo; 3. Obstructive vascular passage in the fibrotic liver resisting the efficient delivery and targeting of drug. Due to the apparent rise in scar tissue during liver fibrosis, it is imperative and ideal to develop drug delivery carrier of size less than 200 nm. Reduced size of hepatic sinusoidal fenestration[315] and splenic clearance[316] are two major reasons for the smaller particle size of delivery carriers. PCBP2 siRNA nanocomplex developed in our study was evaluated on such parameters to fit the stringent requirements for the ideal delivery system. Various nanocomplex formulations prepared were having average particle size lower than 200 nm except the formulation with molar ratio of 2:1:2 (Figure 27). Regardless of the mild cationic to neutral charge and absence of large aggregates (PDI < 0.05), this particle size was ideal for the distribution in the liver instead of the spleen. Addition of PNA in the siRNA allows a highly efficient noncovalent coupling of the biotin. As PNAs are extensively stable and resistant to the harsh pH, DNase and RNase, it helped us to maintain the therapeutic potency of the PCBP2 siRNA. PNA not only assists in the noncovalent coupling of the chemical moiety such as biotin, but provides superior stability to the siRNA in comparison to the naked siRNA. In addition to the small size, presence of the IGF2R receptor also contributed to the uptake in the activated hepatic stellate cells *in vitro* and *in vivo*.

There are three major molecular receptor targets for liver fibrosis therapy that have been substantially investigated: 1. Low density lipoprotein receptor (LDLR)[69, 317]; 2.

Cellular retinol binding receptor protein 1 (CRBP-1)[318-319]; and 3. Insulin-like growth factor 2 receptor (IGF2R)[320-321]. We previously demonstrated that the IGF2R targeting is significantly higher in comparison to the CRBP-1 (ligand: Vitamin A) and LDLR (Ligand: Cholesterol).[302] Notably, increasing IGF2R ligand proportion in different nanocomplexes had direct proportionality with the cellular uptake, however, increasing molar ratio of IGF2R from 0.5 to 2 enhanced the particle size significantly. Regardless of the delivery obstacles across the fibrotic hepatic sinusoidal architecture, PCBP2 nanocomplexes preferentially distributed in the liver. High rate of renal clearance is also a contributing factor for the oligonucleotides and its delivery systems to be translated in to the clinics. As shown in figure 30 A and B, nanocomplexes targeted with IGF2R peptide demonstrated exceptionally higher liver uptake regardless of the increased portal pressure and portal resistance. This shows that the nanocomplexes were highly efficient in liver uptake and hepatic stellate cell targeting. In comparison to the free siRNA-PNA, nanocomplex showed nearly 10 times higher CY5-PCBP2 siRNA mediated fluorescence. Apart from efficient target specificity, small size of the nanocarrier is supposedly another reason responsible for the optimal extravasation and retention of the therapeutic payload in complex and dense matrix containing tissues.[322] macromolecular drugs alone or delivered by nanocarriers have evidently shown rapid renal clearance which substantially compromises the efficiency of the macromolecule drugs. PCBP2 siRNA Nanocomplex on the other hand shows no significant kidney uptake and demonstrated improved liver retention.

The core objective of this study was to inhibit the collagen type I production and suppress the profibrogenic factors of liver fibrosis. To accomplish this objective, PCBP2

siRNA must be delivered efficiently to the HSCs after bypassing all the systemic hurdles. PCBP2 siRNA nanocomplex suppressed the overexpression of PCBP2 mRNA and collagen type I mRNA (Figure 32 A-B). Moreover, primary serum markers of liver fibrosis such as ALT and AST were significantly reduced (Figure 31A-B). Furthermore, Nanocomplex containing dosage of 1 mg/Kg (PCBP2 siRNA) injected in the fibrotic rat models for 4 times during the course of 3 weeks generated extensive fibrosis resolution in comparison to other research where 8-160 mg/kg dosage was utilized.[323-326] Moreover, given the total blood volume in rats as 20 mL, it was unrealistic to prepare an injection volume as 10:1 ratio of total blood volume to drug injection volume, as used by other researchers who use mouse model.[327] In contrast, we used the 100:1 ratio for the total blood volume to drug injection volume to make the final volume of the injection as 200 μL. This is a very important factor as larger volumes may contribute to the hydrodynamic pressure in vasculature and transduce the siRNA *in vivo*.[328]

It is noteworthy that we provided the nanocomplex treatment to the rat fibrosis model by just four injections; whereas, the animals were still under constant CCL_4 mediated fibrosis induction. As PCBP2 siRNA indirectly suppressed the collagen type I protein production and possibly concomitantly induced degradation of predeposited collagen fibers. As highlighted in figure 31C, PCBP2 siRNA nanocomplex treated groups showed statistically lower levels of hydroxyproline content in the liver tissue in comparison to the fibrotic rats that received no treatment or scrambled siRNA complexed nanocomplex. This finding was consistent with the Picro-sirius red (PS red), Masson's trichrome (MT) and collagen type I immuno-staining where significant reduction of collagen fibers (PS red and MT) and collagen type I (IHC) fibers. Moreover, collagen

fiber anchoring and bridging was also diminished after treatment with PCBP2 siRNA nanocomplex, whereas groups with no treatment and scrambled siRNA showed advanced fibrotic symptoms with extensive portal to portal and portal to central vein collagen fiber anchorage and bridging with occasional nodules.

Hepatic stellate cells are the primary executioners of liver fibrosis in general and are the principle source of myofibroblast in CCL_4 induced fibrosis.[329] They are susceptible of wide range molecular signals such as cytokines, chemokines, apoptotic bodies (hepatocytes), macrophages and other fibrosis instigator cells.[329-331] It has been proven that the apoptosis of the HSCs has anti-fibrogenic response and on the other hand, enhanced apoptosis in the liver tissue potentiates the HSC activation.[332-334] To examine the difference between apoptosis in the liver of different treatment groups, we performed the TUNEL assay. It revealed that there was substantial apoptosis across the liver tissue of liver fibrosis model with no treatment or scrambled siRNA treatment (Figure 34). Interestingly, apoptotic cells (TUNEL positive) were present in a pattern which we believe to be aligned with collagen fiber or scar tissue (As shown in Figure 34). It can be postulated that the cells near the collagen matrix and scar tissue were exposed to more resistance, hypoxia and CCL_4, as the collagen fibers underlie and bridge between the hepatic vasculature. Healthy group (blank/no treatment) also showed some TUNEL positive region, which possibly could be the result of cellular homeostasis (normal cell death). However, PCBP2 siRNA treatment group showed significantly lower apoptotic cells which suggests that PCBP2 nanocomplex not only reduces the collagen production but significantly diminishes the apoptotic cells that participate in the perpetuation signals to maintain the HSC activation.[335]

Apart from the apoptotic bodies, cytokines and chemokine are the other major players for the regulation of fibrosis. Autocrine signals coming from the inflammatory cells or HSCs themselves are the reason for the survival and maintenance of the activated HSCs.[336] To examine the effect of liver fibrosis therapy on the serum cytokine and chemokine levels, we investigated serum from the respective treatment and control groups for cytokine and chemokine bioplex panel assay. It has been proven that the TGFβ and PDGF expression is elevated in the fibrotic rats and their expression is dramatically lowered upon regression of the fibrosis.[337-339] We tested the expression of other pro inflammatory cytokines (IL-1β, IL-6, IL-18 and TNFα) that mediate the regulation of the fibrogenic pathway. As IL-1β, IL-6, and TNFα are highly over expressed in the patients with advanced liver fibrosis and cirrhosis, they are considered the primary molecular markers of fibrosis progression except IL-18. These cytokines directly or indirectly promote HSC survival and activation, promote hepatocyte apoptosis and lipid accumulation in the liver. It has also been reported that the NF-κB is the key regulator of the liver fibrosis. Moreover, IL-1β, IL-6 and TNF α, are key mediators of HSC survival and activation and are selectively regulated by NF-κB. Selective inhibition of NF-κB diminishes the CCL4 mediated liver fibrosis.[340]

Furthermore, chemokines such as MCP-1 (CCL2) and RANTES (CCL5), involved in the liver injury, are considered potential profibrogenic factors. These chemokines are major contributors of the macrophage recruitment and HSC activation.[341] As explained by Michal Cohen –Naftaly and Scott L. Friedman[3], hepatic injury, activation and maintenance of the HSCs, activation of inflammatory cells and fibrosis is vicious circle and every step is one way or the another way codependent.[3] After PCBP2

siRNA nanocomplex treatment, we found significant reduction of the cytokine and chemokine levels suggesting the reversal of progression of fibrosis.

5.5 Conclusion

Taken together, we invented a highly specific and efficient therapeutic delivery system for siRNA. As simple as it is in its fundamental concept, PCBP2 siRNA nanocomplex is potent in the reversal of fibrosis progression and inhibition of collagen in CCL_4 induced liver fibrosis model. Successful delivery of the PCBP2 to the target site, not only reversed the fibrosis but functionally treated the symptoms by significantly reducing the molecular serum markers such as ALT, AST, cytokine and chemokines. Therefore, it holds great promise for clinical translation for advanced liver fibrosis treatment. This siRNA delivery system is diverse in its applicability and has higher potential for broader application in targeting other complex molecular target and delivering potent therapeutic modalities.

CHAPTER 6

SUMMARY AND CONCLUSIONS

6.1 Summary

Oligonucleotide delivery is the greatest challenge and especially if the target is too complex, it makes it even more difficult. Liver fibrosis for instance, is developed due to increased sinusoidal resistance and closure of the sinusoidal pores. Regardless of how small the drug molecule may be, the resistance in the lumen creates a great obstacle for the delivery system to be able to produce the desired therapeutic effect. Not just liver fibrosis, but other complex delivery targets such as various types of cancer and blood brain barrier are some of the most difficult to target sites. An efficient delivery system that induces negligible side effect and produces maximum therapeutic effect is the most important goal for the field of pharmaceutical science.

In this work, we first tried to evaluate the problems associated with the siRNA delivery to the target cells and worked backwards to improve the system. In chapter 3 we first investigated the basic mechanism of intracellular trafficking of siRNA nanocomplex. At higher incubation time points post transfection to the hepatic stellate cells with siRNA nanocomplex, silencing activity reduced drastically. Our curiosity led us to unveil some intriguing mechanisms of siRNA intracellular trafficking and cellular recycling. This knowledge helped us understand the possible ways to improve the system to circumvent the reduction in therapeutic efficacy over the extended period.

In chapter 4, we utilized novel avidin and variants of avidin proteins for the delivery of siRNA to hepatic stellate cells. Avidin, neutravidin and streptavidin were compared for morphological characteristics, in vitro cellular uptake and silencing

activity. The performance of the PCBP2 siRNA in silencing the PCBP2 mRNA was significantly improved at elevated time intervals. We also tested avidin, streptavidin and neutravidin nanocomplexes for inflammatory cytokine induction in rat blood and in vivo biodistribution. We also found that the neutravidin nanocomplexes were more efficiently distributed in the liver than other avidin counterparts.

In chapter 5 we further improved the delivery system by introducing IGF2R specific peptide ligand for targeted delivery of the siRNA. We optimized the formulation of the neutravidin based delivery system for PCBP2 siRNA. We observed that various ligand to siRNA ratio yield variable morphological characteristics and thereby show different cellular uptake. We examined the optimized ratio of nanocomplex (3.5:1:0.5) for the treatment of the liver fibrosis model. Data revealed that the major markers of the liver fibrosis such as ALT, AST, hydroxyproline, PCBP2 and Type 1 collagen were significantly reduced after the treatment with PCBP2 siRNA complexed neutravidin nanocomplex. Very insignificant collagen was stained in the liver tissue samples after the end of the PCBP2 dosage regimen. Only 1mg/kg siRNA was enough to produce a significant reversal of fibrosis in vivo.

6.2 Future Directions

1. Employing the immunotherapy to co-deliver PCBP2 siRNA along with the check point inhibitor as the apoptosis of the hepatic stellate cells is the best way to ameliorate the liver fibrosis.

2. Develop mouse model for the liver fibrosis by using alcohol or CCL_4 as inducer of fibrosis and hepatic injury.

3. Develop lipid based delivery system as lipids are metabolized in liver, which may also enhance the liver localization of the nanoparticulate delivery system and siRNA.

REFERENCES

1. Tsuchida, T.; Friedman, S. L., Mechanisms of Hepatic Stellate Cell Activation. *Nat Rev Gastroenterol Hepatol* **2017,** *14* (7), 397-411.

2. Borkham-Kamphorst, E.; Weiskirchen, R., The Pdgf System and Its Antagonists in Liver Fibrosis. *Cytokine Growth Factor Rev* **2016,** *28*, 53-61.

3. Cohen-Naftaly, M.; Friedman, S. L., Current Status of Novel Antifibrotic Therapies in Patients with Chronic Liver Disease. *Therap Adv Gastroenterol* **2011,** *4* (6), 391-417.

4. Bataller, R.; Brenner, D. A., Liver Fibrosis. *J Clin Invest* **2005,** *115* (2), 209-18.

5. Shukla, R. S.; Qin, B.; Wan, Y. J.; Cheng, K., Pcbp2 Sirna Reverses the Alcohol-Induced Pro-Fibrogenic Effects in Hepatic Stellate Cells. *Pharm Res* **2011,** *28* (12), 3058-68.

6. van Rijt, S. H.; Bolukbas, D. A.; Argyo, C.; Wipplinger, K.; Naureen, M.; Datz, S.; Eickelberg, O.; Meiners, S.; Bein, T.; Schmid, O.; Stoeger, T., Applicability of Avidin Protein Coated Mesoporous Silica Nanoparticles as Drug Carriers in the Lung. *Nanoscale* **2016,** *8* (15), 8058-69.

7. Mishina, M.; Minamihata, K.; Moriyama, K.; Nagamune, T., Peptide Tag-Induced Horseradish Peroxidase-Mediated Preparation of a Streptavidin-Immobilized Redox-Sensitive Hydrogel. *Biomacromolecules* **2016,** *17* (6), 1978-84.

8. Bataller, R.; Brenner, D. A., Liver Fibrosis. *Journal of Clinical Investigation* **2005,** *115* (2), 209-218.

9. Llorente-Cortes, V.; Barbarigo, V.; Badimon, L., Low Density Lipoprotein Receptor-Related Protein 1 Modulates the Proliferation and Migration of Human Hepatic Stellate Cells. *J Cell Physiol* **2012,** *227* (10), 3528-33.

10. Lu, L.; Zeng, M.; Li, J.; Hua, J.; Mao, Y.; Fan, Z.; Qiu, D., Effects of Lipid on Low-Density and High-Density Lipoprotein Receptors in Hepatic Stellate Cell from Rat Liver. *Zhonghua Gan Zang Bing Za Zhi* **2000,** *8* (3), 164-6.

11. Chen, Z.; Jin, W.; Liu, H.; Zhao, Z.; Cheng, K., Discovery of Peptide Ligands for Hepatic Stellate Cells Using Phage Display. *Mol Pharm* **2015,** *12* (6), 2180-8.

12. Ma, D., Enhancing Endosomal Escape for Nanoparticle Mediated Sirna Delivery. *Nanoscale* **2014,** *6* (12), 6415-25.

13. Livnah, O.; Bayer, E. A.; Wilchek, M.; Sussman, J. L., Three-Dimensional Structures of Avidin and the Avidin-Biotin Complex. *Proc Natl Acad Sci U S A* **1993,** *90* (11), 5076-80.

14. Diamandis, E. P.; Christopoulos, T. K., The Biotin-(Strept)Avidin System: Principles and Applications in Biotechnology. *Clin Chem* **1991,** *37* (5), 625-36.

15. Laitinen, O. H.; Hytonen, V. P.; Nordlund, H. R.; Kulomaa, M. S., Genetically Engineered Avidins and Streptavidins. *Cell Mol Life Sci* **2006,** *63* (24), 2992-3017.

16. Rybak, J. N.; Scheurer, S. B.; Neri, D.; Elia, G., Purification of Biotinylated Proteins on Streptavidin Resin: A Protocol for Quantitative Elution. *Proteomics* **2004,** *4* (8), 2296-9.

17. Elia, G., Biotinylation Reagents for the Study of Cell Surface Proteins. *Proteomics* **2008,** *8* (19), 4012-24.

18. Pan, J.-f.; Liu, N.-h.; Shu, L.-y.; Sun, H., Application of Avidin-Biotin Technology to Improve Cell Adhesion on Nanofibrous Matrices. *J Nanobiotechnology* **2015,** *13*, 37.

19. Shimoni, O.; Postma, A.; Yan, Y.; Scott, A. M.; Heath, J. K.; Nice, E. C.; Zelikin, A. N.; Caruso, F., Macromolecule Functionalization of Disulfide-Bonded Polymer Hydrogel Capsules and Cancer Cell Targeting. *ACS Nano* **2012,** *6* (2), 1463-1472.

20. Gao, J.; Reibetanz, U.; Venkatraman, S.; Neu, B., Biofunctionalization of Polyelectrolyte Microcapsules with Biotinylated Polyethylene Glycol-Grafted Liposomes. *Macromol Biosci* **2011,** *11* (8), 1079-87.

21. Hu, Q.; Wang, X. Y.; Kang, L. K.; Wei, H. M.; Xu, C. M.; Wang, T.; Wen, Z. H., Rgd-Targeted Ultrasound Contrast Agent for Longitudinal Assessment of Hep-2 Tumor Angiogenesis in Vivo. *PLoS One* **2016,** *11* (2), e0149075.

22. Ren, J.; Chen, Y. I.; Mackey, A. M.; Liu, P. K., Imaging Rhodopsin Degeneration in Vivo in a New Model of Ocular Ischemia in Living Mice. *Faseb j* **2016,** *30* (2), 612-23.

23. Omichi, M.; Asano, A.; Tsukuda, S.; Takano, K.; Sugimoto, M.; Saeki, A.; Sakamaki, D.; Onoda, A.; Hayashi, T.; Seki, S., Fabrication of Enzyme-Degradable and Size-Controlled Protein Nanowires Using Single Particle Nano-Fabrication Technique. *Nat Commun* **2014,** *5*, 3718.

24. Kim, M. C.; Hong, M. H.; Lee, B. H.; Choi, H. J.; Ko, Y. M.; Lee, Y. K., Bone Tissue Engineering by Using Calcium Phosphate Glass Scaffolds and the Avidin-Biotin Binding System. *Ann Biomed Eng* **2015,** *43* (12), 3004-14.

25. Yao, Z.; Zhang, M.; Sakahara, H.; Saga, T.; Arano, Y.; Konishi, J., Avidin Targeting of Intraperitoneal Tumor Xenografts. *J Natl Cancer Inst.* **1998,** *90* (1), 25-29.

26. Rosano, C.; Arosio, P.; Bolognesi, M., The X-Ray Three-Dimensional Structure of Avidin. *Biomol Eng* **1999,** *16* (1-4), 5-12.

27. Pazy, Y.; Eisenberg-Domovich, Y.; Laitinen, O. H.; Kulomaa, M. S.; Bayer, E. A.; Wilchek, M.; Livnah, O., Dimer-Tetramer Transition between Solution and Crystalline States of Streptavidin and Avidin Mutants. *Journal of Bacteriology* **2003,** *185* (14), 4050-4056.

28. Taskinen, B.; Airenne, T. T.; Janis, J.; Rahikainen, R.; Johnson, M. S.; Kulomaa, M. S.; Hytonen, V. P., A Novel Chimeric Avidin with Increased Thermal Stability Using DNA Shuffling. *PLoS One* **2014,** *9* (3), e92058.

29. Maatta, J. A.; Eisenberg-Domovich, Y.; Nordlund, H. R.; Hayouka, R.; Kulomaa, M. S.; Livnah, O.; Hytonen, V. P., Chimeric Avidin Shows Stability against Harsh Chemical Conditions--Biochemical Analysis and 3d Structure. *Biotechnol Bioeng* **2011,** *108* (3), 481-90.

30. Taskinen, B.; Airenne, T. T.; Jänis, J.; Rahikainen, R.; Johnson, M. S.; Kulomaa, M. S.; Hytönen, V. P., A Novel Chimeric Avidin with Increased Thermal Stability Using DNA Shuffling. *PLoS ONE* **2014,** *9* (3), e92058.

31. Hirsch, J. D.; Eslamizar, L.; Filanoski, B. J.; Malekzadeh, N.; Haugland, R. P.; Beechem, J. M.; Haugland, R. P., Easily Reversible Desthiobiotin Binding to Streptavidin, Avidin, and Other Biotin-Binding Proteins: Uses for Protein Labeling, Detection, and Isolation. *Anal Biochem* **2002,** *308* (2), 343-57.

32. Chivers, C. E.; Crozat, E.; Chu, C.; Moy, V. T.; Sherratt, D. J.; Howarth, M., A Streptavidin Variant with Slower Biotin Dissociation and Increased Mechanostability. *Nat Methods* **2010,** *7* (5), 391-3.

33. Tausig, F.; Wolf, F. J., Streptavidin--a Substance with Avidin-Like Properties Produced by Microorganisms. *Biochem Biophys Res Commun* **1964,** *14*, 205-9.

34. Dundas, C. M.; Demonte, D.; Park, S., Streptavidin-Biotin Technology: Improvements and Innovations in Chemical and Biological Applications. *Appl Microbiol Biotechnol* **2013,** *97* (21), 9343-53.

35. Huberman, T.; Eisenberg-Domovich, Y.; Gitlin, G.; Kulik, T.; Bayer, E. A.; Wilchek, M.; Livnah, O., Chicken Avidin Exhibits Pseudo-Catalytic Properties. Biochemical, Structural, and Electrostatic Consequences. *J Biol Chem* **2001,** *276* (34), 32031-9.

36. Hendrickson, W. A.; Pahler, A.; Smith, J. L.; Satow, Y.; Merritt, E. A.; Phizackerley, R. P., Crystal Structure of Core Streptavidin Determined from Multiwavelength Anomalous Diffraction of Synchrotron Radiation. *Proc Natl Acad Sci U S A* **1989,** *86* (7), 2190-4.

37. Nguyen, T. T.; Sly, K. L.; Conboy, J. C., Comparison of the Energetics of Avidin, Streptavidin, Neutravidin, and Anti-Biotin Antibody Binding to Biotinylated Lipid Bilayer Examined by Second-Harmonic Generation. *Anal Chem* **2012,** *84* (1), 201-8.

38. Schechter, B.; Silberman, R.; Arnon, R.; Wilchek, M., Tissue Distribution of Avidin and Streptavidin Injected to Mice. Effect of Avidin Carbohydrate, Streptavidin Truncation and Exogenous Biotin. *Eur J Biochem* **1990,** *189* (2), 327-31.

39. Baumann, F.; Bauer, M. S.; Milles, L. F.; Alexandrovich, A.; Gaub, H. E.; Pippig, D. A., Monovalent Strep-Tactin for Strong and Site-Specific Tethering in Nanospectroscopy. *Nat Nanotechnol.* **2016,** *11* (1), 89-94.

40. Schmidt, T. G.; Skerra, A., The Strep-Tag System for One-Step Purification and High-Affinity Detection or Capturing of Proteins. *Nat Protoc* **2007,** *2* (6), 1528-35.

41. Moosmeier, M. A.; Bulkescher, J.; Reed, J.; Schnolzer, M.; Heid, H.; Hoppe-Seyler, K.; Hoppe-Seyler, F., Transtactin: A Universal Transmembrane Delivery System for Strep-Tag Ii-Fused Cargos. *J Cell Mol Med* **2010,** *14* (7), 1935-45.

42. Knabel, M.; Franz, T. J.; Schiemann, M.; Wulf, A.; Villmow, B.; Schmidt, B.; Bernhard, H.; Wagner, H.; Busch, D. H., Reversible Mhc Multimer Staining for Functional Isolation of T-Cell Populations and Effective Adoptive Transfer. *Nat Med* **2002,** *8* (6), 631-7.

43. Nampally, M.; Moerschbacher, B. M.; Kolkenbrock, S., Fusion of a Novel Genetically Engineered Chitosan Affinity Protein and Green Fluorescent Protein for Specific Detection of Chitosan in Vitro and in Situ. *Appl Environ Microbiol* **2012,** *78* (9), 3114-9.

44. Vermette, P.; Gengenbach, T.; Divisekera, U.; Kambouris, P. A.; Griesser, H. J.; Meagher, L., Immobilization and Surface Characterization of Neutravidin Biotin-Binding Protein on Different Hydrogel Interlayers. *J Colloid Interface Sci.* **2003,** *259* (1), 13-26.

45. De Cuyper, M.; Hodenius, M.; Lacava, Z. G. M.; Azevedo, R. B.; da Silva, M. d. F.; Morais, P. C.; Santana, M. H. A., Attachment of Water-Soluble Proteins to the Surface of (Magnetizable) Phospholipid Colloids Via Neutravidin-Derivatized Phospholipids. *J Colloid Interface Sci.* **2002,** *245* (2), 274-280.

46. Lippert, L. G.; Hallock, J. T.; Dadosh, T.; Diroll, B. T.; Murray, C. B.; Goldman, Y. E., Neutravidin Functionalization of Cdse/Cds Quantum Nanorods and Quantification of Biotin Binding Sites Using Biotin-4-Fluorescein Fluorescence Quenching. *Bioconjug Chem* **2016,** *27* (3), 562-8.

47. Zhang, J.; Lang, H. P.; Battiston, F.; Backmann, N.; Huber, F.; Gerber, C., Development of Robust and Standardized Cantilever Sensors Based on Biotin/Neutravidin Coupling for Antibody Detection. *Sensors (Basel)* **2013,** *13* (4), 5273-85.

48. Helppolainen, S. H.; Maatta, J. A.; Halling, K. K.; Slotte, J. P.; Hytonen, V. P.; Janis, J.; Vainiotalo, P.; Kulomaa, M. S.; Nordlund, H. R., Bradavidin Ii from Bradyrhizobium Japonicum: A New Avidin-Like Biotin-Binding Protein. *Biochim Biophys Acta* **2008,** *1784* (7-8), 1002-10.

49. Meir, A.; Helppolainen, S. H.; Podoly, E.; Nordlund, H. R.; Hytonen, V. P.; Maatta, J. A.; Wilchek, M.; Bayer, E. A.; Kulomaa, M. S.; Livnah, O., Crystal Structure

of Rhizavidin: Insights into the Enigmatic High-Affinity Interaction of an Innate Biotin-Binding Protein Dimer. *J Mol Biol* **2009,** *386* (2), 379-90.

50. Avraham, O.; Meir, A.; Fish, A.; Bayer, E. A.; Livnah, O., Hoefavidin: A Dimeric Bacterial Avidin with a C-Terminal Binding Tail. *J Struct Biol* **2015,** *191* (2), 139-48.

51. Takakura, Y.; Suzuki, J.; Oka, N.; Kakuta, Y., Tamavidin 2-Hot, a Highly Thermostable Biotin-Binding Protein. *J Biotechnol* **2014,** *169*, 1-8.

52. Meir, A.; Bayer, E. A.; Livnah, O., Structural Adaptation of a Thermostable Biotin-Binding Protein in a Psychrophilic Environment. *J Biol Chem* **2012,** *287* (22), 17951-62.

53. Taskinen, B.; Zauner, D.; Lehtonen, S. I.; Koskinen, M.; Thomson, C.; Kahkonen, N.; Kukkurainen, S.; Maatta, J. A.; Ihalainen, T. O.; Kulomaa, M. S.; Gruber, H. J.; Hytonen, V. P., Switchavidin: Reversible Biotin-Avidin-Biotin Bridges with High Affinity and Specificity. *Bioconjug Chem* **2014,** *25* (12), 2233-43.

54. Taskinen, B.; Zmurko, J.; Ojanen, M.; Kukkurainen, S.; Parthiban, M.; Maatta, J. A.; Leppiniemi, J.; Janis, J.; Parikka, M.; Turpeinen, H.; Ramet, M.; Pesu, M.; Johnson, M. S.; Kulomaa, M. S.; Airenne, T. T.; Hytonen, V. P., Zebavidin--an Avidin-Like Protein from Zebrafish. *PLoS One* **2013,** *8* (10), e77207.

55. Chen, S.; Zhao, X.; Chen, J.; Chen, J.; Kuznetsova, L.; Wong, S. S.; Ojima, I., Mechanism-Based Tumor-Targeting Drug Delivery System. Validation of Efficient Vitamin Receptor-Mediated Endocytosis and Drug Release. *Bioconjug Chem* **2010,** *21* (5), 979-87.

56. Ren, W. X.; Han, J.; Uhm, S.; Jang, Y. J.; Kang, C.; Kim, J. H.; Kim, J. S., Recent Development of Biotin Conjugation in Biological Imaging, Sensing, and Target Delivery. *Chem Commun (Camb)* **2015,** *51* (52), 10403-18.

57. Yamamoto, T.; Aoki, K.; Sugiyama, A.; Doi, H.; Kodama, T.; Shimizu, Y.; Kanai, M., Design and Synthesis of Biotin Analogues Reversibly Binding with Streptavidin. *Chem Asian J* **2015,** *10* (4), 1071-8.

58. Fudem-Goldin, B.; Orr, G. A., 2-Iminobiotin-Containing Reagent and Affinity Columns. *Methods Enzymol* **1990,** *184*, 167-73.

59. Schmidt, T. G.; Skerra, A., One-Step Affinity Purification of Bacterially Produced Proteins by Means of the "Strep Tag" and Immobilized Recombinant Core Streptavidin. *J Chromatogr A* **1994,** *676* (2), 337-45.

60. Liu, L.; Sommermeyer, D.; Cabanov, A.; Kosasih, P.; Hill, T.; Riddell, S. R., Inclusion of Strep-Tag Ii in Design of Antigen Receptors for T-Cell Immunotherapy. *Nat Biotechnol* **2016,** *34* (4), 430-4.

61. Baumann, F.; Bauer, M. S.; Milles, L. F.; Alexandrovich, A.; Gaub, H. E.; Pippig, D. A., Monovalent Strep-Tactin for Strong and Site-Specific Tethering in Nanospectroscopy. *Nat Nanotechnol* **2016,** *11* (1), 89-94.

62. Schmidt, T. G.; Koepke, J.; Frank, R.; Skerra, A., Molecular Interaction between the Strep-Tag Affinity Peptide and Its Cognate Target, Streptavidin. *J Mol Biol* **1996,** *255* (5), 753-66.

63. Whitehead, K. A.; Langer, R.; Anderson, D. G., Knocking Down Barriers: Advances in Sirna Delivery. *Nat Rev Drug Discov* **2009,** *8* (2), 129-138.

64. Takahashi, Y.; Nishikawa, M.; Takakura, Y., Nonviral Vector-Mediated Rna Interference: Its Gene Silencing Characteristics and Important Factors to Achieve Rnai-Based Gene Therapy. *Adv Drug Deliv Rev* **2009,** *61* (9), 760-6.

65. Grimm, D., Small Silencing Rnas: State-of-the-Art. *Adv Drug Deliv Rev* **2009,** *61* (9), 672-703.

66. Hauser, P. V.; Pippin, J. W.; Kaiser, C.; Krofft, R. D.; Brinkkoetter, P. T.; Hudkins, K. L.; Kerjaschki, D.; Reiser, J.; Alpers, C. E.; Shankland, S. J., Novel Sirna Delivery System to Target Podocytes in Vivo. *PLoS One* **2010,** *5* (3), e9463.

67. Leisi, R.; von Nordheim, M.; Kempf, C.; Ros, C., Specific Targeting of Proerythroblasts and Erythroleukemic Cells by the Vp1u Region of Parvovirus B19. *Bioconjug Chem* **2015,** *26* (9), 1923-30.

68. Shukla, R. S.; Tai, W.; Mahato, R.; Jin, W.; Cheng, K., Development of Streptavidin-Based Nanocomplex for Sirna Delivery. *Mol Pharm* **2013,** *10* (12), 4534-45.

69. Shukla, R. S.; Jain, A.; Zhao, Z.; Cheng, K., Intracellular Trafficking and Exocytosis of a Multi-Component Sirna Nanocomplex. *Nanomedicine* **2016,** *12* (5), 1323-34.

70. Hajdu, P.; Chimote, A. A.; Thompson, T. H.; Koo, Y.; Yun, Y.; Conforti, L., Functionalized Liposomes Loaded with Sirnas Targeting Ion Channels in Effector Memory T Cells as a Potential Therapy for Autoimmunity. *Biomaterials* **2013,** *34* (38), 10249-57.

71. Thomas, C. E.; Ehrhardt, A.; Kay, M. A., Progress and Problems with the Use of Viral Vectors for Gene Therapy. *Nat Rev Genet* **2003,** *4* (5), 346-58.

72. Pack, D. W.; Hoffman, A. S.; Pun, S.; Stayton, P. S., Design and Development of Polymers for Gene Delivery. *Nat Rev Drug Discov* **2005,** *4* (7), 581-93.

73. Huang, X.; Hu, Q.; Braun, G. B.; Pallaoro, A.; Morales, D. P.; Zasadzinski, J.; Clegg, D. O.; Reich, N. O., Light-Activated Rna Interference in Human Embryonic Stem Cells. *Biomaterials* **2015,** *63*, 70-79.

74. Buda, A.; Facchin, S.; Dassie, E.; Casarin, E.; Jepson, M. A.; Neumann, H.; Hatem, G.; Realdon, S.; D'Inca, R.; Sturniolo, G. C.; Morpurgo, M., Detection of a Fluorescent-Labeled Avidin-Nucleic Acid Nanoassembly by Confocal Laser Endomicroscopy in the Microvasculature of Chronically Inflamed Intestinal Mucosa. *Int J Nanomedicine* **2015,** *10*, 399-408.

75. Bigini, P.; Previdi, S.; Casarin, E.; Silvestri, D.; Violatto, M. B.; Facchin, S.; Sitia, L.; Rosato, A.; Zuccolotto, G.; Realdon, N.; Fiordaliso, F.; Salmona, M.; Morpurgo, M., In Vivo Fate of Avidin-Nucleic Acid Nanoassemblies as Multifunctional Diagnostic Tools. *ACS Nano* **2014,** *8* (1), 175-87.

76. Palanca-Wessels, M. C.; Convertine, A. J.; Cutler-Strom, R.; Booth, G. C.; Lee, F.; Berguig, G. Y.; Stayton, P. S.; Press, O. W., Anti-Cd22 Antibody Targeting of Ph-Responsive Micelles Enhances Small Interfering Rna Delivery and Gene Silencing in Lymphoma Cells. *Mol Ther* **2011,** *19* (8), 1529-37.

77. Mitragotri, S.; Burke, P. A.; Langer, R., Overcoming the Challenges in Administering Biopharmaceuticals: Formulation and Delivery Strategies. *Nat Rev Drug Discov* **2014,** *13* (9), 655-72.

78. Albarran, B.; Hoffman, A. S.; Stayton, P. S., Efficient Intracellular Delivery of a Pro-Apoptotic Peptide with a Ph-Responsive Carrier. *React Funct Polym.* **2011,** *71* (3), 261-265.

79. Putney, S. D.; Burke, P. A., Improving Protein Therapeutics with Sustained-Release Formulations. *Nat Biotech* **1998,** *16* (2), 153-157.

80. Saalik, P.; Padari, K.; Niinep, A.; Lorents, A.; Hansen, M.; Jokitalo, E.; Langel, U.; Pooga, M., Protein Delivery with Transportans Is Mediated by Caveolae Rather Than Flotillin-Dependent Pathways. *Bioconjug Chem* **2009,** *20* (5), 877-87.

81. Saalik, P.; Elmquist, A.; Hansen, M.; Padari, K.; Saar, K.; Viht, K.; Langel, U.; Pooga, M., Protein Cargo Delivery Properties of Cell-Penetrating Peptides. A Comparative Study. *Bioconjug Chem* **2004,** *15* (6), 1246-53.

82. Howl, J.; Jones, S., Cell Penetrating Peptide-Mediated Transport Enables the Regulated Secretion of Accumulated Cargoes from Mast Cells. *J Control Release* **2015,** *202*, 108-117.

83. Qu, W.; Chen, W.-H.; Kuang, Y.; Zeng, X.; Cheng, S.-X.; Zhou, X.; Zhuo, R.-X.; Zhang, X.-Z., Avidin–Biotin Interaction Mediated Peptide Assemblies as Efficient Gene Delivery Vectors for Cancer Therapy. *Mol Pharm* **2013,** *10* (1), 261-269.

84. Martin, S. E.; Peterson, B. R., Non-Natural Cell Surface Receptors: Synthetic Peptides Capped with N-Cholesterylglycine Efficiently Deliver Proteins into Mammalian Cells. *Bioconjug Chem* **2003,** *14* (1), 67-74.

85. Cu, Y.; Booth, C. J.; Saltzman, W. M., In Vivo Distribution of Surface-Modified Plga Nanoparticles Following Intravaginal Delivery. *J Control Release* **2011,** *156* (2), 258-264.

86. Steinbach, J. M.; Seo, Y. E.; Saltzman, W. M., Cell Penetrating Peptide-Modified Poly(Lactic-Co-Glycolic Acid) Nanoparticles with Enhanced Cell Internalization. *Acta Biomater* **2016,** *30*, 49-61.

87. Wierzbicki, P. M.; Kogut-Wierzbicka, M.; Ruczynski, J.; Siedlecka-Kroplewska, K.; Kaszubowska, L.; Rybarczyk, A.; Alenowicz, M.; Rekowski, P.; Kmiec, Z., Protein and Sirna Delivery by Transportan and Transportan 10 into Colorectal Cancer Cell Lines. *Folia Histochem Cytobiol* **2014,** *52* (4), 270-80.

88. Kaufmann, S. H. E.; Juliana McElrath, M.; Lewis, D. J. M.; Del Giudice, G., Challenges and Responses in Human Vaccine Development. *Curr Opin Immunol.* **2014,** *28*, 18-26.

89. Liao, T. Y.; Lau, A.; Joseph, S.; Hytonen, V.; Hmama, Z., Improving the Immunogenicity of the Mycobacterium Bovis Bcg Vaccine by Non-Genetic Bacterial Surface Decoration Using the Avidin-Biotin System. *PLoS One* **2015,** *10* (12), e0145833.

90. Liao, T.-Y. A.; Lau, A.; Joseph, S.; Hytönen, V.; Hmama, Z., Improving the Immunogenicity of the <Italic>Mycobacterium Bovis</Italic> Bcg Vaccine by Non-Genetic Bacterial Surface Decoration Using the Avidin-Biotin System. *PLoS ONE* **2016,** *10* (12), e0145833.

91. Leblanc, P.; Moise, L.; Luza, C.; Chantaralawan, K.; Lezeau, L.; Yuan, J.; Field, M.; Richer, D.; Boyle, C.; Martin, W. D.; Fishman, J. B.; Berg, E. A.; Baker, D.; Zeigler,

B.; Mais, D. E.; Taylor, W.; Coleman, R.; Warren, H. S.; Gelfand, J. A.; De Groot, A. S.; Brauns, T.; Poznansky, M. C., Vaxcelerate Ii: Rapid Development of a Self-Assembling Vaccine for Lassa Fever. *Hum Vaccin Immunother* **2014,** *10* (10), 3022-38.

92. Scibelli, A.; van der Most, R. G.; Turkstra, J. A.; Ariaans, M. P.; Arkesteijn, G.; Hensen, E. J.; Meloen, R. H., Fast Track Selection of Immunogens for Novel Vaccines through Visualisation of the Early Onset of the B-Cell Response. *Vaccine* **2005,** *23* (16), 1900-1909.

93. Alon, R.; Hershkoviz, R.; Bayer, E. A.; Wilchek, M.; Lider, O., Streptavidin Blocks Immune Reactions Mediated by Fibronectin-Vla-5 Recognition through an Arg-Gly-Asp Mimicking Site. *Eur J Immunol* **1993,** *23* (4), 893-8.

94. Bachmann, M. F.; Jennings, G. T., Vaccine Delivery: A Matter of Size, Geometry, Kinetics and Molecular Patterns. *Nat Rev Immunol* **2010,** *10* (11), 787-96.

95. Schiller, J.; Chackerian, B., Why Hiv Virions Have Low Numbers of Envelope Spikes: Implications for Vaccine Development. *PLoS Pathog* **2014,** *10* (8), e1004254.

96. Thrane, S.; Janitzek, C. M.; Agerbaek, M. O.; Ditlev, S. B.; Resende, M.; Nielsen, M. A.; Theander, T. G.; Salanti, A.; Sander, A. F., A Novel Virus-Like Particle Based Vaccine Platform Displaying the Placental Malaria Antigen Var2csa. *PLoS One* **2015,** *10* (11), e0143071.

97. Tacken, P. J.; de Vries, I. J. M.; Torensma, R.; Figdor, C. G., Dendritic-Cell Immunotherapy: From Ex Vivo Loading to in Vivo Targeting. *Nat Rev Immunol* **2007,** *7* (10), 790-802.

98. Shortman, K.; Lahoud, M. H.; Caminschi, I., Improving Vaccines by Targeting Antigens to Dendritic Cells. *Exp Mol Med* **2009,** *41*, 61-66.

99. Raghuwanshi, D.; Mishra, V.; Suresh, M. R.; Kaur, K., A Simple Approach for Enhanced Immune Response Using Engineered Dendritic Cell Targeted Nanoparticles. *Vaccine* **2012,** *30* (50), 7292-7299.

100. Wang, W. W.; Das, D.; Suresh, M. R., A Versatile Bifunctional Dendritic Cell Targeting Vaccine Vector. *Mol Pharm* **2009,** *6* (1), 158-172.

101. Pardridge, W. M., Blood–Brain Barrier Drug Delivery of Igg Fusion Proteins with a Transferrin Receptor Monoclonal Antibody. *Expert Opin Drug Deliv* **2015,** *12* (2), 207-222.

102. Yoshikawa, T.; Pardridge, W. M., Biotin Delivery to Brain with a Covalent Conjugate of Avidin and a Monoclonal Antibody to the Transferrin Receptor. *J Pharmacol Exp Ther* **1992,** *263* (2), 897-903.

103. Zhou, Q. H.; Lu, J. Z.; Hui, E. K.; Boado, R. J.; Pardridge, W. M., Delivery of a Peptide Radiopharmaceutical to Brain with an Igg-Avidin Fusion Protein. *Bioconjug Chem* **2011,** *22* (8), 1611-8.

104. Sumbria, R. K.; Boado, R. J.; Pardridge, W. M., Imaging Amyloid Plaque in Alzheimer's Disease Brain with a Biotinylated Abeta Peptide Radiopharmaceutical Conjugated to an Igg-Avidin Fusion Protein. *Bioconjug Chem* **2012,** *23* (6), 1318-21.

105. Sakahara, H.; Saga, T., Avidin-Biotin System for Delivery of Diagnostic Agents. *Adv Drug Deliv Rev* **1999,** *37* (1-3), 89-101.

106. Pagel, J. M.; Lin, Y.; Hedin, N.; Pantelias, A.; Axworthy, D.; Stone, D.; Hamlin, D. K.; Wilbur, D. S.; Press, O. W., Comparison of a Tetravalent Single-Chain Antibody-Streptavidin Fusion Protein and an Antibody-Streptavidin Chemical Conjugate for Pretargeted Anti-Cd20 Radioimmunotherapy of B-Cell Lymphomas. *Blood* **2006,** *108* (1), 328-36.

107. Frost, S. H.; Jensen, H.; Lindegren, S., In Vitro Evaluation of Avidin Antibody Pretargeting Using 211at-Labeled and Biotinylated Poly-L-Lysine as Effector Molecule. *Cancer* **2010,** *116* (4 Suppl), 1101-10.

108. Frost, S. H.; Back, T.; Chouin, N.; Jensen, H.; Hultborn, R.; Jacobsson, L.; Lindegren, S., In Vivo Distribution of Avidin-Conjugated Mx35 and (211)at-Labeled, Biotinylated Poly-L-Lysine for Pretargeted Intraperitoneal Alpha-Radioimmunotherapy. *Cancer Biother Radiopharm* **2011,** *26* (6), 727-36.

109. Ng, P. P.; Dela Cruz, J. S.; Sorour, D. N.; Stinebaugh, J. M.; Shin, S. U.; Shin, D. S.; Morrison, S. L.; Penichet, M. L., An Anti-Transferrin Receptor-Avidin Fusion Protein Exhibits Both Strong Proapoptotic Activity and the Ability to Deliver Various Molecules into Cancer Cells. *Proc Natl Acad Sci U S A* **2002,** *99* (16), 10706-11.

110. Boado, R. J.; Zhang, Y.; Zhang, Y.; Xia, C. F.; Wang, Y.; Pardridge, W. M., Genetic Engineering, Expression, and Activity of a Chimeric Monoclonal Antibody-Avidin Fusion Protein for Receptor-Mediated Delivery of Biotinylated Drugs in Humans. *Bioconjug Chem* **2008,** *19* (3), 731-9.

111. Xia, C. F.; Boado, R. J.; Pardridge, W. M., Antibody-Mediated Targeting of Sirna Via the Human Insulin Receptor Using Avidin-Biotin Technology. *Mol Pharm* **2009,** *6* (3), 747-51.

112. Barve, A.; Jain, A.; Liu, H.; Jin, W.; Cheng, K., An Enzyme-Responsive Conjugate Improves the Delivery of a Pi3k Inhibitor to Prostate Cancer. *Nanomedicine* **2016,** *12* (8), 2373-2381.

113. van Rijt, S. H.; Bolukbas, D. A.; Argyo, C.; Datz, S.; Lindner, M.; Eickelberg, O.; Konigshoff, M.; Bein, T.; Meiners, S., Protease-Mediated Release of Chemotherapeutics from Mesoporous Silica Nanoparticles to Ex Vivo Human and Mouse Lung Tumors. *ACS Nano* **2015,** *9* (3), 2377-89.

114. Li, H.; Yu, S. S.; Miteva, M.; Nelson, C. E.; Werfel, T.; Giorgio, T. D.; Duvall, C. L., Matrix Metalloproteinase Responsive, Proximity-Activated Polymeric Nanoparticles for Sirna Delivery. *Adv Funct Mater* **2013,** *23* (24), 3040-3052.

115. Urbanska, K.; Lanitis, E.; Poussin, M.; Lynn, R. C.; Gavin, B. P.; Kelderman, S.; Yu, J.; Scholler, N.; Powell, D. J., Jr., A Universal Strategy for Adoptive Immunotherapy of Cancer through Use of a Novel T-Cell Antigen Receptor. *Cancer Res* **2012,** *72* (7), 1844-52.

116. Martensson, L.; Nilsson, R.; Ohlsson, T.; Sjogren, H. O.; Strand, S. E.; Tennvall, J., Improved Tumor Targeting and Decreased Normal Tissue Accumulation through Extracorporeal Affinity Adsorption in a Two-Step Pretargeting Strategy. *Clin Cancer Res* **2007,** *13* (18 Pt 2), 5572s-5576s.

117. Li, M.; Lam, J. W. Y.; Mahtab, F.; Chen, S.; Zhang, W.; Hong, Y.; Xiong, J.; Zheng, Q.; Tang, B. Z., Biotin-Decorated Fluorescent Silica Nanoparticles with Aggregation-Induced Emission Characteristics: Fabrication, Cytotoxicity and Biological Applications. *J. Mater. Chem. B* **2013,** *1* (5), 676-684.

118. Patel, M.; Vadlapatla, R. K.; Shah, S.; Mitra, A. K., Molecular Expression and Functional Activity of Sodium Dependent Multivitamin Transporter in Human Prostate Cancer Cells. *Int J Pharm* **2012,** *436* (1-2), 324-31.

119. Ogawa, M.; Kosaka, N.; Longmire, M. R.; Urano, Y.; Choyke, P. L.; Kobayashi, H., Fluorophore-Quencher Based Activatable Targeted Optical Probes for Detecting in Vivo Cancer Metastases. *Mol Pharm* **2009,** *6* (2), 386-95.

120. Hama, Y.; Urano, Y.; Koyama, Y.; Kamiya, M.; Bernardo, M.; Paik, R. S.; Shin, I. S.; Paik, C. H.; Choyke, P. L.; Kobayashi, H., A Target Cell-Specific Activatable Fluorescence Probe for in Vivo Molecular Imaging of Cancer Based on a Self-Quenched Avidin-Rhodamine Conjugate. *Cancer Res* **2007,** *67* (6), 2791-9.

121. Doane, T.; Burda, C., Nanoparticle Mediated Non-Covalent Drug Delivery. *Adv Drug Deliv Rev* **2013,** *65* (5), 607-21.

122. Yan, F.; Li, L.; Deng, Z.; Jin, Q.; Chen, J.; Yang, W.; Yeh, C. K.; Wu, J.; Shandas, R.; Liu, X.; Zheng, H., Paclitaxel-Liposome-Microbubble Complexes as Ultrasound-Triggered Therapeutic Drug Delivery Carriers. *J Control Release* **2013,** *166* (3), 246-55.

123. Xiong, M. P.; Forrest, M. L.; Karls, A. L.; Kwon, G. S., Biotin-Triggered Release of Poly(Ethylene Glycol)−Avidin from Biotinylated Polyethylenimine Enhances in Vitro Gene Expression. *Bioconjug Chem* **2007,** *18* (3), 746-753.

124. Xiong, M. P.; Forrest, M. L.; Karls, A. L.; Kwon, G. S., Biotin-Triggered Release of Poly(Ethylene Glycol)-Avidin from Biotinylated Polyethylenimine Enhances in Vitro Gene Expression. *Bioconjug Chem* **2007,** *18* (3), 746-53.

125. Cui, Y.; Li, Y.; Duan, Q.; Kakuchi, T., Preparation of Hyaluronic Acid Micro-Hydrogel by Biotin-Avidin-Specific Bonding for Doxorubicin-Targeted Delivery. *Appl Biochem Biotechnol* **2013,** *169* (1), 239-49.

126. Palekar, R. U.; Jallouk, A. P.; Goette, M. J.; Chen, J.; Myerson, J. W.; Allen, J. S.; Akk, A.; Yang, L.; Tu, Y.; Miller, M. J.; Pham, C. T. N.; Wickline, S. A.; Pan, H., Quantifying Progression and Regression of Thrombotic Risk in Experimental Atherosclerosis. *FASEB J* **2015,** *29* (7), 3100-3109.

127. Ana Rute, N.; Joana Fontes, Q.; Babette, W.; Ignacio, A. R.; Pierre-Olivier, C.; Salette, R., Solid Lipid Nanoparticles as a Vehicle for Brain-Targeted Drug Delivery: Two New Strategies of Functionalization with Apolipoprotein E. *Nanotechnology* **2015,** *26* (49), 495103.

128. Orr, G. A., The Use of the 2-Iminobiotin-Avidin Interaction for the Selective Retrieval of Labeled Plasma Membrane Components. *J Biol Chem* **1981,** *256* (2), 761-6.

129. Zhu, K.; Dietrich, R.; Didier, A.; Doyscher, D.; Martlbauer, E., Recent Developments in Antibody-Based Assays for the Detection of Bacterial Toxins. *Toxins (Basel)* **2014,** *6* (4), 1325-48.

130. Montoro Bustos, A. R.; Garcia-Cortes, M.; Gonzalez-Iglesias, H.; Ruiz Encinar, J.; Costa-Fernandez, J. M.; Coca-Prados, M.; Sanz-Medel, A., Sensitive Targeted Multiple Protein Quantification Based on Elemental Detection of Quantum Dots. *Anal Chim Acta* **2015,** *879*, 77-84.

131. Park, J. W.; Park, A.-Y.; Lee, S.; Yu, N.-K.; Lee, S.-H.; Kaang, B.-K., Detection of Trkb Receptors Distributed in Cultured Hippocampal Neurons through Bioconjugation between Highly Luminescent (Quantum Dot-Neutravidin) and (Biotinylated Anti-Trkb Antibody) on Neurons by Combined Atomic Force Microscope and Confocal Laser Scanning Microscope. *Bioconjug Chem* **2010,** *21* (4), 597-603.

132. Iyer, A.; Chandra, A.; Swaminathan, R., Hydrolytic Enzymes Conjugated to Quantum Dots Mostly Retain Whole Catalytic Activity. *Biochim Biophys Acta* **2014,** *1840* (9), 2935-2943.

133. Kristian Raty, J.; Liimatainen, T.; Unelma Kaikkonen, M.; Grohn, O.; Jumani Airenne, K.; Yla-Herttuala, S., Non-Invasive Imaging in Gene Therapy. *Mol Ther* **2007,** *15* (9), 1579-1586.

134. Xu, C.; Xu, K.; Gu, H.; Zheng, R.; Liu, H.; Zhang, X.; Guo, Z.; Xu, B., Dopamine as a Robust Anchor to Immobilize Functional Molecules on the Iron Oxide Shell of Magnetic Nanoparticles. *J Am Chem Soc* **2004,** *126* (32), 9938-9939.

135. Kelly, K. A.; Allport, J. R.; Tsourkas, A.; Shinde-Patil, V. R.; Josephson, L.; Weissleder, R., Detection of Vascular Adhesion Molecule-1 Expression Using a Novel Multimodal Nanoparticle. *Circ Res* **2005,** *96* (3), 327-336.

136. Amstad, E.; Zurcher, S.; Mashaghi, A.; Wong, J. Y.; Textor, M.; Reimhult, E., Surface Functionalization of Single Superparamagnetic Iron Oxide Nanoparticles for Targeted Magnetic Resonance Imaging. *Small* **2009,** *5* (11), 1334-42.

137. Roper, M. G.; Guillo, C., New Technologies in Affinity Assays to Explore Biological Communication. *Anal Bioanal Chem* **2009,** *393* (2), 459-65.

138. Brody, E. N.; Gold, L.; Lawn, R. M.; Walker, J. J.; Zichi, D., High-Content Affinity-Based Proteomics: Unlocking Protein Biomarker Discovery. *Expert Rev Mol Diagn* **2010,** *10* (8), 1013-22.

139. He, J.; Evers, D. L.; O'Leary, T. J.; Mason, J. T., Immunoliposome-Pcr: A Generic Ultrasensitive Quantitative Antigen Detection System. *J Nanobiotechnology* **2012,** *10* (1), 26.

140. Gould, E. A.; Buckley, A.; Cammack, N., Use of the Biotin-Streptavidin Interaction to Improve Flavivirus Detection by Immunofluorescence and Elisa Tests. *J Virol Methods* **1985,** *11* (1), 41-8.

141. Zhu, M.; Gong, X.; Hu, Y.; Ou, W.; Wan, Y., Streptavidin-Biotin-Based Directional Double Nanobody Sandwich Elisa for Clinical Rapid and Sensitive Detection of Influenza H5n1. *J Transl Med* **2014,** *12*, 352.

142. Fan, P.; Li, X.; Su, W.; Kong, W.; Kong, X.; Wang, Z.; Wang, Y.; Jiang, C.; Gao, F., Enhanced Sensitivity for Detection of Hiv-1 P24 Antigen by a Novel Nuclease-Linked Fluorescence Oligonucleotide Assay. *PLoS ONE* **2015,** *10* (4), e0125701.

143. Galli, F.; Rapisarda, A. S.; Stabile, H.; Malviya, G.; Manni, I.; Bonanno, E.; Piaggio, G.; Gismondi, A.; Santoni, A.; Signore, A., In Vivo Imaging of Natural Killer Cell Trafficking in Tumors. *J Nucl Med* **2015,** *56* (10), 1575-80.

144. Barbet, J.; Bardies, M.; Bourgeois, M.; Chatal, J. F.; Cherel, M.; Davodeau, F.; Faivre-Chauvet, A.; Gestin, J. F.; Kraeber-Bodere, F., Radiolabeled Antibodies for Cancer Imaging and Therapy. *Methods Mol Biol* **2012,** *907*, 681-97.

145. Liu, Y.; Cheng, D.; Liu, X.; Liu, G.; Dou, S.; Xiao, N.; Chen, L.; Rusckowski, M.; Hnatowich, D. J., Comparing the Intracellular Fate of Components within a Noncovalent Streptavidin Nanoparticle with Covalent Conjugation. *Nucl Med Biol* **2012,** *39* (1), 101-7.

146. Hnatowich, D. J.; Fritz, B.; Virzi, F.; Mardirossian, G.; Rusckowski, M., Improved Tumor Localization with (Strept)Avidin and Labeled Biotin as a Substitute for Antibody. *Nucl Med Biol* **1993,** *20* (2), 189-95.

147. Petronzelli, F.; Pelliccia, A.; Anastasi, A. M.; D'Alessio, V.; Albertoni, C.; Rosi, A.; Leoni, B.; De Angelis, C.; Paganelli, G.; Palombo, G.; Dani, M.; Carminati, P.; De Santis, R., Improved Tumor Targeting by Combined Use of Two Antitenascin Antibodies. *Clin Cancer Res* **2005,** *11* (19), 7137s-7145s.

148. Hoffman, R. M.; Yang, M., Dual-Color, Whole-Body Imaging in Mice. *Nat Biotech* **2005,** *23* (7), 790-790.

149. Ntziachristos, V.; Ripoll, J.; Wang, L. V.; Weissleder, R., Looking and Listening to Light: The Evolution of Whole-Body Photonic Imaging. *Nat Biotech* **2005,** *23* (3), 313-320.

150. Wu, C.; Mino, K.; Akimoto, H.; Kawabata, M.; Nakamura, K.; Ozaki, M.; Ohmiya, Y., In Vivo Far-Red Luminescence Imaging of a Biomarker Based on Bret from Cypridina Bioluminescence to an Organic Dye. *Proc Natl Acad Sci U S A* **2009,** *106* (37), 15599-603.

151. Barth, B. M.; Sharma, R.; Altinoglu, E. I.; Morgan, T. T.; Shanmugavelandy, S. S.; Kaiser, J. M.; McGovern, C.; Matters, G. L.; Smith, J. P.; Kester, M.; Adair, J. H., Bioconjugation of Calcium Phosphosilicate Composite Nanoparticles for Selective Targeting of Human Breast and Pancreatic Cancers in Vivo. *ACS Nano* **2010,** *4* (3), 1279-87.

152. Nademanee, A.; Forman, S.; Molina, A.; Fung, H.; Smith, D.; Dagis, A.; Kwok, C.; Yamauchi, D.; Anderson, A.-L.; Falk, P.; Krishnan, A.; Kirschbaum, M.; Kogut, N.; Nakamura, R.; O'Donnell, M.; Parker, P.; Popplewell, L.; Pullarkat, V.; Rodriguez, R.; Sahebi, F.; Smith, E.; Snyder, D.; Stein, A.; Spielberger, R.; Zain, J.; White, C.; Raubitschek, A., A Phase 1/2 Trial of High-Dose Yttrium-90-Ibritumomab Tiuxetan in Combination with High-Dose Etoposide and Cyclophosphamide Followed by Autologous Stem Cell Transplantation in Patients with Poor-Risk or Relapsed Non-Hodgkin Lymphoma. *Blood* **2005,** *106* (8), 2896-2902.

153. Green, D. J.; Orgun, N. N.; Jones, J. C.; Hylarides, M. D.; Pagel, J. M.; Hamlin, D. K.; Wilbur, D. S.; Lin, Y.; Fisher, D. R.; Kenoyer, A. L.; Frayo, S. L.; Gopal, A. K.; Orozco, J. J.; Gooley, T. A.; Wood, B. L.; Bensinger, W. I.; Press, O. W., A Preclinical Model of Cd38-Pretargeted Radioimmunotherapy for Plasma Cell Malignancies. *Cancer Res* **2014,** *74* (4), 1179-89.

154. Ryu, Y.; Jin, Z.; Lee, J. J.; Noh, S. H.; Shin, T. H.; Jo, S. M.; Choi, J.; Park, H.; Cheon, J.; Kim, H. S., Size-Controlled Construction of Magnetic Nanoparticle Clusters Using DNA-Binding Zinc Finger Protein. *Angew Chem Int Ed Engl* **2015,** *54* (3), 923-6.

155. Yeom, C. J.; Zeng, L.; Zhu, Y.; Hiraoka, M.; Harada, H., Strategies to Assess Hypoxic/Hif-1-Active Cancer Cells for the Development of Innovative Radiation Therapy. *Cancers* **2011,** *3* (3), 3610-3631.

156. Kudo, T.; Ueda, M.; Kuge, Y.; Mukai, T.; Tanaka, S.; Masutani, M.; Kiyono, Y.; Kizaka-Kondoh, S.; Hiraoka, M.; Saji, H., Imaging of Hif-1-Active Tumor Hypoxia Using a Protein Effectively Delivered to and Specifically Stabilized in Hif-1-Active Tumor Cells. *J Nucl Med* **2009,** *50* (6), 942-9.

157. Kudo, T.; Ueda, M.; Konishi, H.; Kawashima, H.; Kuge, Y.; Mukai, T.; Miyano, A.; Tanaka, S.; Kizaka-Kondoh, S.; Hiraoka, M.; Saji, H., Pet Imaging of Hypoxia-Inducible Factor-1-Active Tumor Cells with Pretargeted Oxygen-Dependent Degradable Streptavidin and a Novel 18f-Labeled Biotin Derivative. *Mol Imaging Biol* **2011,** *13* (5), 1003-10.

158. Liang, M.; Liu, X.; Cheng, D.; Liu, G.; Dou, S.; Wang, Y.; Rusckowski, M.; Hnatowich, D. J., Multimodality Nuclear and Fluorescence Tumor Imaging in Mice Using a Streptavidin Nanoparticle. *Bioconjug Chem* **2010,** *21* (7), 1385-1388.

159. Henderson, J.; Arya, R.; Gillespie, P., Skin Graft Meshing, over-Meshing and Cross-Meshing. *Int J Surg* **2012,** *10* (9), 547-50.

160. MacNeil, S., Progress and Opportunities for Tissue-Engineered Skin. *Nature* **2007,** *445* (7130), 874-80.

161. Hynes, R. O., Integrins: Versatility, Modulation, and Signaling in Cell Adhesion. *Cell* **1992,** *69* (1), 11-25.

162. Kuo, S. C.; Lauffenburger, D. A., Relationship between Receptor/Ligand Binding Affinity and Adhesion Strength. *Biophys J* **1993,** *65* (5), 2191-200.

163. Pan, J. F.; Liu, N. H.; Shu, L. Y.; Sun, H., Application of Avidin-Biotin Technology to Improve Cell Adhesion on Nanofibrous Matrices. *J Nanobiotechnology* **2015,** *13*, 37.

164. Wang, X.; Kaplan, D. L., Functionalization of Silk Fibroin with Neutravidin and Biotin. *Macromol Biosci* **2011,** *11* (1), 100-10.

165. Anamelechi, C. C.; Truskey, G. A.; Reichert, W. M., Mylar and Teflon-Af as Cell Culture Substrates for Studying Endothelial Cell Adhesion. *Biomaterials* **2005,** *26* (34), 6887-96.

166. Mistry, A. S.; Mikos, A. G., Tissue Engineering Strategies for Bone Regeneration. *Adv Biochem Eng Biotechnol* **2005,** *94*, 1-22.

167. Hench, L. L.; Polak, J. M., Third-Generation Biomedical Materials. *Science* **2002,** *295* (5557), 1014-7.

168. Baeza, A.; Izquierdo-Barba, I.; Vallet-Regi, M., Biotinylation of Silicon-Doped Hydroxyapatite: A New Approach to Protein Fixation for Bone Tissue Regeneration. *Acta Biomater* **2010,** *6* (3), 743-9.

169. Dou, X. Q.; Zhang, J.; Feng, C., Biotin-Avidin Based Universal Cell-Matrix Interaction for Promoting Three-Dimensional Cell Adhesion. *ACS Appl Mater Interfaces* **2015,** *7* (37), 20786-92.

170. Jiang, T.; Nukavarapu, S. P.; Deng, M.; Jabbarzadeh, E.; Kofron, M. D.; Doty, S. B.; Abdel-Fattah, W. I.; Laurencin, C. T., Chitosan–Poly(Lactide-Co-Glycolide) Microsphere-Based Scaffolds for Bone Tissue Engineering: In Vitro Degradation and in Vivo Bone Regeneration Studies. *Acta Biomater* **2010,** *6* (9), 3457-3470.

171. Kweon, H.; Yoo, M. K.; Park, I. K.; Kim, T. H.; Lee, H. C.; Lee, H.-S.; Oh, J.-S.; Akaike, T.; Cho, C.-S., A Novel Degradable Polycaprolactone Networks for Tissue Engineering. *Biomaterials* **2003,** *24* (5), 801-808.

172. Chen, F.; Yu, S.; Liu, B.; Ni, Y.; Yu, C.; Su, Y.; Zhu, X.; Yu, X.; Zhou, Y.; Yan, D., An Injectable Enzymatically Crosslinked Carboxymethylated Pullulan/Chondroitin Sulfate Hydrogel for Cartilage Tissue Engineering. *Sci Rep* **2016,** *6*, 20014.

173. Jo, J. Y.; Jeong, S. I.; Shin, Y. M.; Kang, S. S.; Kim, S. E.; Jeong, C. M.; Huh, J. B., Sequential Delivery of Bmp-2 and Bmp-7 for Bone Regeneration Using a Heparinized Collagen Membrane. *Int J Oral Maxillofac Surg* **2015,** *44* (7), 921-8.

174. Li, X.; Yi, W.; Jin, A.; Duan, Y.; Min, S., Effects of Sequentially Released Bmp-2 and Bmp-7 from Pela Microcapsule-Based Scaffolds on the Bone Regeneration. *Am J Transl Res* **2015,** *7* (8), 1417-28.

175. Yonezawa, T.; Lee, J.-W.; Hibino, A.; Asai, M.; Hojo, H.; Cha, B.-Y.; Teruya, T.; Nagai, K.; Chung, U.-I.; Yagasaki, K.; Woo, J.-T., Harmine Promotes Osteoblast

Differentiation through Bone Morphogenetic Protein Signaling. *Biochem Biophys Res Commun* **2011,** *409* (2), 260-265.

176. Igwe, J. C.; Mikael, P. E.; Nukavarapu, S. P., Design, Fabrication and in Vitro Evaluation of a Novel Polymer-Hydrogel Hybrid Scaffold for Bone Tissue Engineering. *J Tissue Eng Regen Med* **2014,** *8* (2), 131-42.

177. Metzger, S.; Lienemann, P. S.; Ghayor, C.; Weber, W.; Martin, I.; Weber, F. E.; Ehrbar, M., Modular Poly(Ethylene Glycol) Matrices for the Controlled 3d-Localized Osteogenic Differentiation of Mesenchymal Stem Cells. *Adv Healthc Mater* **2015,** *4* (4), 550-8.

178. Chivers, C. E.; Koner, A. L.; Lowe, E. D.; Howarth, M., How the Biotin-Streptavidin Interaction Was Made Even Stronger: Investigation Via Crystallography and a Chimaeric Tetramer. *Biochem J* **2011,** *435* (1), 55-63.

179. Ke, X.; Ng, V. W.; Ono, R. J.; Chan, J. M.; Krishnamurthy, S.; Wang, Y.; Hedrick, J. L.; Yang, Y. Y., Role of Non-Covalent and Covalent Interactions in Cargo Loading Capacity and Stability of Polymeric Micelles. *J Control Release* **2014,** *193*, 9-26.

180. Helmlinger, G.; Yuan, F.; Dellian, M.; Jain, R. K., Interstitial Ph and Po2 Gradients in Solid Tumors in Vivo: High-Resolution Measurements Reveal a Lack of Correlation. *Nat Med* **1997,** *3* (2), 177-82.

181. Cheng, Y.; A, C. S.; Meyers, J. D.; Panagopoulos, I.; Fei, B.; Burda, C., Highly Efficient Drug Delivery with Gold Nanoparticle Vectors for in Vivo Photodynamic Therapy of Cancer. *J Am Chem Soc* **2008,** *130* (32), 10643-7.

182. Choi, H. S.; Liu, W.; Liu, F.; Nasr, K.; Misra, P.; Bawendi, M. G.; Frangioni, J. V., Design Considerations for Tumour-Targeted Nanoparticles. *Nat Nanotechnol* **2010,** *5* (1), 42-7.

183. Tessmer, I.; Kaur, P.; Lin, J.; Wang, H., Investigating Bioconjugation by Atomic Force Microscopy. *J Nanobiotechnology* **2013,** *11*, 25.

184. Kotterman, M. A.; Schaffer, D. V., Engineering Adeno-Associated Viruses for Clinical Gene Therapy. *Nat Rev Genet* **2014,** *15* (7), 445-51.

185. Tatiparti, K.; Sau, S.; Kashaw, S. K.; Iyer, A. K., Sirna Delivery Strategies: A Comprehensive Review of Recent Developments. *Nanomaterials (Basel)* **2017,** *7* (4).

186. Schroeder, A.; Levins, C. G.; Cortez, C.; Langer, R.; Anderson, D. G., Lipid-Based Nanotherapeutics for Sirna Delivery. *J Intern Med* **2010,** *267* (1), 9-21.

187. Terp, M. C.; Bauer, F.; Sugimoto, Y.; Yu, B.; Brueggemeier, R. W.; Lee, L. J.; Lee, R. J., Differential Efficacy of Dotap Enantiomers for Sirna Delivery in Vitro. *Int J Pharm* **2012,** *430* (1-2), 328-34.

188. Arima, H.; Motoyama, K.; Higashi, T., Polyamidoamine Dendrimer Conjugates with Cyclodextrins as Novel Carriers for DNA, Shrna and Sirna. *Pharmaceutics* **2012,** *4* (1), 130-148.

189. Boussif, O.; Lezoualc'h, F.; Zanta, M. A.; Mergny, M. D.; Scherman, D.; Demeneix, B.; Behr, J. P., A Versatile Vector for Gene and Oligonucleotide Transfer into Cells in Culture and in Vivo: Polyethylenimine. *Proc Natl Acad Sci U S A* **1995,** *92* (16), 7297-301.

190. Guo, J.; Cheng, W. P.; Gu, J.; Ding, C.; Qu, X.; Yang, Z.; O'Driscoll, C., Systemic Delivery of Therapeutic Small Interfering Rna Using a Ph-Triggered Amphiphilic Poly-L-Lysine Nanocarrier to Suppress Prostate Cancer Growth in Mice. *Eur J Pharm Sci* **2012,** *45* (5), 521-32.

191. Lynn, D. M.; Langer, R., Degradable Poly(B-Amino Esters): Synthesis, Characterization, and Self-Assembly with Plasmid DNA. *J. Am. Chem. Soc.* **2000,** *122* (44), 10761-10768.

192. Xue, H. Y.; Guo, P.; Wen, W.-C.; Wong, H. L., Lipid-Based Nanocarriers for Rna Delivery. *Curr Pharm Des.* **2015,** *21* (22), 3140-3147.

193. Geary, R. S.; Norris, D.; Yu, R.; Bennett, C. F., Pharmacokinetics, Biodistribution and Cell Uptake of Antisense Oligonucleotides. *Adv Drug Deliv Rev* **2015,** *87*, 46-51.

194. Juliano, R. L., The Delivery of Therapeutic Oligonucleotides. *Nucleic Acids Res* **2016,** *44* (14), 6518-6548.

195. Dominska, M.; Dykxhoorn, D. M., Breaking Down the Barriers: Sirna Delivery and Endosome Escape. *J Cell Sci* **2010,** *123* (Pt 8), 1183-9.

196. Liu, L.; Hitchens, T. K.; Ye, Q.; Wu, Y.; Barbe, B.; Prior, D. E.; Li, W. F.; Yeh, F. C.; Foley, L. M.; Bain, D. J.; Ho, C., Decreased Reticuloendothelial System Clearance and Increased Blood Half-Life and Immune Cell Labeling for Nano- and Micron-Sized Superparamagnetic Iron-Oxide Particles Upon Pre-Treatment with Intralipid. *Biochim Biophys Acta* **2013,** *1830* (6), 3447-53.

197. Dahlman, J. E.; Barnes, C.; Khan, O.; Thiriot, A.; Jhunjunwala, S.; Shaw, T. E.; Xing, Y.; Sager, H. B.; Sahay, G.; Speciner, L.; Bader, A.; Bogorad, R. L.; Yin, H.;

Racie, T.; Dong, Y.; Jiang, S.; Seedorf, D.; Dave, A.; Sandu, K. S.; Webber, M. J.; Novobrantseva, T.; Ruda, V. M.; Lytton-Jean, A. K. R.; Levins, C. G.; Kalish, B.; Mudge, D. K.; Perez, M.; Abezgauz, L.; Dutta, P.; Smith, L.; Charisse, K.; Kieran, M. W.; Fitzgerald, K.; Nahrendorf, M.; Danino, D.; Tuder, R. M.; von Andrian, U. H.; Akinc, A.; Schroeder, A.; Panigrahy, D.; Kotelianski, V.; Langer, R.; Anderson, D. G., In Vivo Endothelial Sirna Delivery Using Polymeric Nanoparticles with Low Molecular Weight. *Nat Nanotechnol* **2014,** *9* (8), 648-655.

198. White, P. J.; Anastasopoulos, F.; Pouton, C. W.; Boyd, B. J., Overcoming Biological Barriers to in Vivo Efficacy of Antisense Oligonucleotides. *Expert Rev Mol Med* **2009,** *11*, e10.

199. Takakura, Y.; Mahato, R. I.; Hashida, M., Extravasation of Macromolecules. *Adv Drug Deliv Rev* **1998,** *34* (1), 93-108.

200. Lorenzer, C.; Dirin, M.; Winkler, A.-M.; Baumann, V.; Winkler, J., Going Beyond the Liver: Progress and Challenges of Targeted Delivery of Sirna Therapeutics. *J Control Release* **2015,** *203*, 1-15.

201. Doherty, G. J.; McMahon, H. T., Mechanisms of Endocytosis. *Annu Rev Biochem* **2009,** *78*, 857-902.

202. Sandvig, K.; Pust, S.; Skotland, T.; van Deurs, B., Clathrin-Independent Endocytosis: Mechanisms and Function. *Curr Opin Cell Biol* **2011,** *23* (4), 413-20.

203. Lorenzer, C.; Dirin, M.; Winkler, A. M.; Baumann, V.; Winkler, J., Going Beyond the Liver: Progress and Challenges of Targeted Delivery of Sirna Therapeutics. *J Control Release* **2015,** *203*, 1-15.

204. Huotari, J.; Helenius, A., Endosome Maturation. *EMBO J* **2011,** *30* (17), 3481-500.

205. Tai, W.; Qin, B.; Cheng, K., Inhibition of Breast Cancer Cell Growth and Invasiveness by Dual Silencing of Her-2 and Vegf. *Mol Pharm* **2010,** *7* (2), 543-56.

206. Qin, B.; Cheng, K., Silencing of the Ikkepsilon Gene by Sirna Inhibits Invasiveness and Growth of Breast Cancer Cells. *Breast Cancer Res* **2010,** *12* (5), R74.

207. Mahato, R.; Qin, B.; Cheng, K., Blocking Ikkalpha Expression Inhibits Prostate Cancer Invasiveness. *Pharm Res* **2011,** *28* (6), 1357-69.

208. Vaishnaw, A. K.; Gollob, J.; Gamba-Vitalo, C.; Hutabarat, R.; Sah, D.; Meyers, R.; de Fougerolles, T.; Maraganore, J., A Status Report on Rnai Therapeutics. *Silence* **2010,** *1* (1), 14.

209. Cheng, K.; Mahato, R. I., Biological and Therapeutic Applications of Small Rnas. *Pharm Res* **2011,** *28* (12), 2961-5.

210. Cheng, K.; Qin, B., Rna Interference for Cancer Therapy. In *Pharmaceutical Perspectives of Cancer Therapeutics*, Lu, Y.; Mahato, R. I., Eds. Springer US: 2009; pp 399-440.

211. Cheng, K.; Mahato, R. I., Sirna Delivery and Targeting. *Mol Pharm* **2009,** *6* (3), 649-50.

212. Whitehead, K. A.; Dorkin, J. R.; Vegas, A. J.; Chang, P. H.; Veiseh, O.; Matthews, J.; Fenton, O. S.; Zhang, Y.; Olejnik, K. T.; Yesilyurt, V.; Chen, D.; Barros, S.; Klebanov, B.; Novobrantseva, T.; Langer, R.; Anderson, D. G., Degradable Lipid

Nanoparticles with Predictable in Vivo Sirna Delivery Activity. *Nat Commun* **2014,** *5*, 4277.

213. Qin, B.; Chen, Z.; Jin, W.; Cheng, K., Development of Cholesteryl Peptide Micelles for Sirna Delivery. *J Control Release* **2013,** *172* (1), 159-68.

214. Kim, D. C.; Cho, Y. A.; Li, H.; Yung, B. C.; Lee, R. J., Proteinase K-Containing Lipid Nanoparticles for Therapeutic Delivery of Sirna Lor-1284. *Anticancer Res* **2014,** *34* (7), 3531-5.

215. Alabi, C. A.; Love, K. T.; Sahay, G.; Stutzman, T.; Young, W. T.; Langer, R.; Anderson, D. G., Fret-Labeled Sirna Probes for Tracking Assembly and Disassembly of Sirna Nanocomplexes. *ACS Nano* **2012,** *6* (7), 6133-41.

216. Sakhtianchi, R.; Minchin, R. F.; Lee, K.-B.; Alkilany, A. M.; Serpooshan, V.; Mahmoudi, M., Exocytosis of Nanoparticles from Cells: Role in Cellular Retention and Toxicity. *Adv Colloid Interface Sci.* **2013,** *201–202* (0), 18-29.

217. Chithrani, B. D.; Chan, W. C. W., Elucidating the Mechanism of Cellular Uptake and Removal of Protein-Coated Gold Nanoparticles of Different Sizes and Shapes. *Nano Lett.* **2007,** *7* (6), 1542-1550.

218. Stayton, I.; Winiarz, J.; Shannon, K.; Ma, Y., Study of Uptake and Loss of Silica Nanoparticles in Living Human Lung Epithelial Cells at Single Cell Level. *Anal Bioanal Chem* **2009,** *394* (6), 1595-1608.

219. Qin, B.; Tai, W.; Shukla, R. S.; Cheng, K., Identification of a Lncap-Specific Binding Peptide Using Phage Display. *Pharm Res* **2011,** *28* (10), 2422-34.

220. Sahay, G.; Querbes, W.; Alabi, C.; Eltoukhy, A.; Sarkar, S.; Zurenko, C.; Karagiannis, E.; Love, K.; Chen, D.; Zoncu, R.; Buganim, Y.; Schroeder, A.; Langer, R.; Anderson, D. G., Efficiency of Sirna Delivery by Lipid Nanoparticles Is Limited by Endocytic Recycling. *Nat Biotechnol* **2013,** *31* (7), 653-8.

221. El-Sayed, A.; Futaki, S.; Harashima, H., Delivery of Macromolecules Using Arginine-Rich Cell-Penetrating Peptides: Ways to Overcome Endosomal Entrapment. *Aaps j* **2009,** *11* (1), 13-22.

222. Perez, A. P.; Cosaka, M. L.; Romero, E. L.; Morilla, M. J., Uptake and Intracellular Traffic of Sirna Dendriplexes in Glioblastoma Cells and Macrophages. *Int J Nanomedicine* **2011,** *6*, 2715-28.

223. Cheng, K.; Yang, N.; Mahato, R. I., Tgf-Beta1 Gene Silencing for Treating Liver Fibrosis. *Mol Pharm* **2009,** *6* (3), 772-9.

224. Lu, J. J.; Langer, R.; Chen, J., A Novel Mechanism Is Involved in Cationic Lipid-Mediated Functional Sirna Delivery. *Mol Pharm* **2009,** *6* (3), 763-71.

225. Wang, S.; Qin, B.; Cheng, K., Delivery of Nucleic Acids. In *Advanced Drug Delivery*, Mitra, A. K.; Lee, C. H.; Cheng, K., Eds. John Wiley & Sons: 2013; pp 257-274.

226. Gilleron, J.; Querbes, W.; Zeigerer, A.; Borodovsky, A.; Marsico, G.; Schubert, U.; Manygoats, K.; Seifert, S.; Andree, C.; Stoter, M.; Epstein-Barash, H.; Zhang, L.; Koteliansky, V.; Fitzgerald, K.; Fava, E.; Bickle, M.; Kalaidzidis, Y.; Akinc, A.; Maier, M.; Zerial, M., Image-Based Analysis of Lipid Nanoparticle-Mediated Sirna Delivery, Intracellular Trafficking and Endosomal Escape. *Nat Biotechnol* **2013,** *31* (7), 638-46.

227. Park, K., Extravascular Transport of Nanoparticles in Solid Tumors. *J Control Release* **2012,** *161* (3), 967.

228. Hirsch, M.; Helm, M., Live Cell Imaging of Duplex Sirna Intracellular Trafficking. *Nucleic Acids Res* **2015,** *43* (9), 4650-4660.

229. Ge, X.; Zhang, Q.; Cai, Y.; Duan, S.; Chen, S.; Lv, N.; Jin, T.; Chen, Y.; Yuan, W., Peg-Pcl-Dex Polymersome-Protamine Vector as an Efficient Gene Delivery System Via Peg-Guided Self-Assembly. *Nanomedicine (Lond)* **2014,** *9* (8), 1193-207.

230. Wang, Y.; Xu, Z.; Guo, S.; Zhang, L.; Sharma, A.; Robertson, G. P.; Huang, L., Intravenous Delivery of Sirna Targeting Cd47 Effectively Inhibits Melanoma Tumor Growth and Lung Metastasis. *Mol Ther* **2013,** *21* (10), 1919-29.

231. Kim, Y. M.; Park, M. R.; Song, S. C., An Injectable Cell Penetrable Nano-Polyplex Hydrogel for Localized Sirna Delivery. *Biomaterials* **2013,** *34* (18), 4493-500.

232. Chang, L. C.; Lee, H. F.; Yang, Z.; Yang, V. C., Low Molecular Weight Protamine (Lmwp) as Nontoxic Heparin/Low Molecular Weight Heparin Antidote (I): Preparation and Characterization. *AAPS pharmSci* **2001,** *3* (3), E17.

233. Delgado, D.; del Pozo-Rodriguez, A.; Solinis, M. A.; Rodriguez-Gascon, A., Understanding the Mechanism of Protamine in Solid Lipid Nanoparticle-Based Lipofection: The Importance of the Entry Pathway. *Eur J Pharm Biopharm* **2011,** *79* (3), 495-502.

234. Futaki, S.; Suzuki, T.; Ohashi, W.; Yagami, T.; Tanaka, S.; Ueda, K.; Sugiura, Y., Arginine-Rich Peptides. An Abundant Source of Membrane-Permeable Peptides Having

Potential as Carriers for Intracellular Protein Delivery. *J Biol Chem* **2001,** *276* (8), 5836-40.

235. Ohrt, T.; Merkle, D.; Birkenfeld, K.; Echeverri, C. J.; Schwille, P., In Situ Fluorescence Analysis Demonstrates Active Sirna Exclusion from the Nucleus by Exportin 5. *Nucleic Acids Res.* **2006,** *34* (5), 1369-1380.

236. Zhang, Z.; Zhou, L.; Zhou, Y.; Liu, J.; Xing, X.; Zhong, J.; Xu, G.; Kang, Z.; Liu, J., Mitophagy Induced by Nanoparticle-Peptide Conjugates Enabling an Alternative Intracellular Trafficking Route. *Biomaterials* **2015,** *65*, 56-65.

237. Erazo-Oliveras, A.; Muthukrishnan, N.; Baker, R.; Wang, T.-Y.; Pellois, J.-P., Improving the Endosomal Escape of Cell-Penetrating Peptides and Their Cargos: Strategies and Challenges. *Pharmaceuticals (Basel)* **2012,** *5* (11), 10.3390/ph5111177.

238. Takano, M.; Kawami, M.; Aoki, A.; Yumoto, R., Receptor-Mediated Endocytosis of Macromolecules and Strategy to Enhance Their Transport in Alveolar Epithelial Cells. *Expert Opin Drug Deliv* **2014,** *12* (5), 813-825.

239. Nieto, N.; Friedman, S. L.; Greenwel, P.; Cederbaum, A. I., Cyp2e1-Mediated Oxidative Stress Induces Collagen Type I Expression in Rat Hepatic Stellate Cells. *Hepatology* **1999,** *30* (4), 987-96.

240. Rozema, D. B.; Blokhin, A. V.; Wakefield, D. H.; Benson, J. D.; Carlson, J. C.; Klein, J. J.; Almeida, L. J.; Nicholas, A. L.; Hamilton, H. L.; Chu, Q.; Hegge, J. O.; Wong, S. C.; Trubetskoy, V. S.; Hagen, C. M.; Kitas, E.; Wolff, J. A.; Lewis, D. L., Protease-Triggered Sirna Delivery Vehicles. *J Control Release* **2015,** *209* (0), 57-66.

241. Doronina, S. O.; Toki, B. E.; Torgov, M. Y.; Mendelsohn, B. A.; Cerveny, C. G.; Chace, D. F.; DeBlanc, R. L.; Gearing, R. P.; Bovee, T. D.; Siegall, C. B.; Francisco, J. A.; Wahl, A. F.; Meyer, D. L.; Senter, P. D., Development of Potent Monoclonal Antibody Auristatin Conjugates for Cancer Therapy. *Nat Biotech* **2003,** *21* (7), 778-784.

242. Li, J.; Zhou, Y.; Li, C.; Wang, D.; Gao, Y.; Zhang, C.; Zhao, L.; Li, Y.; Liu, Y.; Li, X., Poly(2-Ethyl-2-Oxazoline)-Doxorubicin Conjugate-Based Dual Endosomal Ph-Sensitive Micelles with Enhanced Antitumor Efficacy. *Bioconjug Chem* **2015,** *26* (1), 110-9.

243. Ruan, S.; Yuan, M.; Zhang, L.; Hu, G.; Chen, J.; Cun, X.; Zhang, Q.; Yang, Y.; He, Q.; Gao, H., Tumor Microenvironment Sensitive Doxorubicin Delivery and Release to Glioma Using Angiopep-2 Decorated Gold Nanoparticles. *Biomaterials* **2015,** *37*, 425-35.

244. Oh, N.; Park, J. H., Endocytosis and Exocytosis of Nanoparticles in Mammalian Cells. *Int J Nanomedicine* **2014,** *9 Suppl 1*, 51-63.

245. Alabi, C. A.; Sahay, G.; Langer, R.; Anderson, D. G., Development of Sirna-Probes for Studying Intracellular Trafficking of Sirna Nanoparticles. *Integr Biol (Camb)* **2013,** *5* (1), 224-30.

246. Yu, X. H.; Jiang, N.; Yao, P. B.; Zheng, X. L.; Cayabyab, F. S.; Tang, C. K., Npc1, Intracellular Cholesterol Trafficking and Atherosclerosis. *Clin Chim Acta* **2014,** *429*, 69-75.

247. Lam, J. K. W.; Liang, W.; Lan, Y.; Chaudhuri, P.; Chow, M. Y. T.; Witt, K.; Kudsiova, L.; Mason, A. J., Effective Endogenous Gene Silencing Mediated by Ph

Responsive Peptides Proceeds Via Multiple Pathways. *J control release* **2012,** *158* (2), 293-303.

248. Bartlett, D. W.; Davis, M. E., Insights into the Kinetics of Sirna-Mediated Gene Silencing from Live-Cell and Live-Animal Bioluminescent Imaging. *Nucleic Acids Res* **2006,** *34* (1), 322-333.

249. Shi, J.; Xu, Y.; Xu, X.; Zhu, X.; Pridgen, E.; Wu, J.; Votruba, A. R.; Swami, A.; Zetter, B. R.; Farokhzad, O. C., Hybrid Lipid-Polymer Nanoparticles for Sustained Sirna Delivery and Gene Silencing. *Nanomedicine* **2014,** *10* (5), 897-900.

250. Mudhakir, D.; Akita, H.; Tan, E.; Harashima, H., A Novel Irq Ligand-Modified Nano-Carrier Targeted to a Unique Pathway of Caveolar Endocytic Pathway. *J Control Release* **2008,** *125* (2), 164-73.

251. Takano, M.; Kawami, M.; Aoki, A.; Yumoto, R., Receptor-Mediated Endocytosis of Macromolecules and Strategy to Enhance Their Transport in Alveolar Epithelial Cells. *Expert Opin Drug Deliv* **2015,** *12* (5), 813-25.

252. Schnitzer, J. E.; Oh, P., Albondin-Mediated Capillary Permeability to Albumin. Differential Role of Receptors in Endothelial Transcytosis and Endocytosis of Native and Modified Albumins. *J Biol Chem* **1994,** *269* (8), 6072-82.

253. Kafa, H.; Wang, J. T.; Rubio, N.; Venner, K.; Anderson, G.; Pach, E.; Ballesteros, B.; Preston, J. E.; Abbott, N. J.; Al-Jamal, K. T., The Interaction of Carbon Nanotubes with an in Vitro Blood-Brain Barrier Model and Mouse Brain in Vivo. *Biomaterials* **2015,** *53*, 437-52.

254. Kreuter, J., Drug Delivery to the Central Nervous System by Polymeric Nanoparticles: What Do We Know? *Adv Drug Deliv Rev* **2014,** *71*, 2-14.

255. Akinc, A.; Goldberg, M.; Qin, J.; Dorkin, J. R.; Gamba-Vitalo, C.; Maier, M.; Jayaprakash, K. N.; Jayaraman, M.; Rajeev, K. G.; Manoharan, M.; Koteliansky, V.; Rohl, I.; Leshchiner, E. S.; Langer, R.; Anderson, D. G., Development of Lipidoid-Sirna Formulations for Systemic Delivery to the Liver. *Mol Ther* **2009,** *17* (5), 872-879.

256. Eguchi, A.; Meade, B. R.; Chang, Y.-C.; Fredrickson, C. T.; Willert, K.; Puri, N.; Dowdy, S. F., Efficient Sirna Delivery into Primary Cells by a Peptide Transduction Domain-Dsrna Binding Domain Fusion Protein. *Nat Biotech* **2009,** *27* (6), 567-571.

257. Hou, K. K.; Pan, H.; Ratner, L.; Schlesinger, P. H.; Wickline, S. A., Mechanisms of Nanoparticle-Mediated Sirna Transfection by Melittin-Derived Peptides. *ACS Nano* **2013,** *7* (10), 8605-8615.

258. Chen, M.; Gao, S.; Dong, M.; Song, J.; Yang, C.; Howard, K. A.; Kjems, J.; Besenbacher, F., Chitosan/Sirna Nanoparticles Encapsulated in Plga Nanofibers for Sirna Delivery. *ACS Nano* **2012,** *6* (6), 4835-4844.

259. Choi, K.-m.; Choi, S.-H.; Jeon, H.; Kim, I.-S.; Ahn, H. J., Chimeric Capsid Protein as a Nanocarrier for Sirna Delivery: Stability and Cellular Uptake of Encapsulated Sirna. *ACS Nano* **2011,** *5* (11), 8690-8699.

260. Liu, H. Y.; Yu, X.; Liu, H.; Wu, D.; She, J. X., Co-Targeting Egfr and Survivin with a Bivalent Aptamer-Dual Sirna Chimera Effectively Suppresses Prostate Cancer. *Sci Rep* **2016,** *6*, 30346.

261. Binzel, D. W.; Shu, Y.; Li, H.; Sun, M.; Zhang, Q.; Shu, D.; Guo, B.; Guo, P., Specific Delivery of Mirna for High Efficient Inhibition of Prostate Cancer by Rna Nanotechnology. *Mol Ther* **2016**.

262. Khatri, N.; Baradia, D.; Vhora, I.; Rathi, M.; Misra, A., Crgd Grafted Liposomes Containing Inorganic Nano-Precipitate Complexed Sirna for Intracellular Delivery in Cancer Cells. *J Control Release* **2014,** *182*, 45-57.

263. Park, D. H.; Cho, J.; Kwon, O. J.; Yun, C. O.; Choy, J. H., Biodegradable Inorganic Nanovector: Passive Versus Active Tumor Targeting in Sirna Transportation. *Angew Chem Int Ed Engl* **2016,** *55* (14), 4582-6.

264. Piradashvili, K.; Fichter, M.; Mohr, K.; Gehring, S.; Wurm, F. R.; Landfester, K., Biodegradable Protein Nanocontainers. *Biomacromolecules* **2015**.

265. Shukla, R. S.; Jain, A.; Zhao, Z.; Cheng, K., Intracellular Trafficking and Exocytosis of a Multi-Component Sirna Nanocomplex. *Nanomedicine* **2016**.

266. Yumura, K.; Ui, M.; Doi, H.; Hamakubo, T.; Kodama, T.; Tsumoto, K.; Sugiyama, A., Mutations for Decreasing the Immunogenicity and Maintaining the Function of Core Streptavidin. *Protein Sci* **2013,** *22* (2), 213-21.

267. Lesch, H. P.; Kaikkonen, M. U.; Pikkarainen, J. T.; Yla-Herttuala, S., Avidin-Biotin Technology in Targeted Therapy. *Expert Opin Drug Deliv* **2010,** *7* (5), 551-64.

268. Jain, A.; Cheng, K., The Principles and Applications of Avidin-Based Nanoparticles in Drug Delivery and Diagnosis. *J Control Release* **2017,** *245*, 27-40.

269. Zhao, S.; Walker, D. S.; Reichert, W. M., Cooperativity in the Binding of Avidin to Biotin-Lipid-Doped Langmuir-Blodgett Films. *Langmuir* **1993,** *9* (11), 3166-3173.

270. Kuriakose, A.; Chirmule, N.; Nair, P., Immunogenicity of Biotherapeutics: Causes and Association with Posttranslational Modifications. *J Immunol Res* **2016,** *2016*, 1298473.

271. Wang, W., Advanced Protein Formulations. *Protein Sci* **2015,** *24* (7), 1031-1039.

272. Ratanji, K. D.; Derrick, J. P.; Dearman, R. J.; Kimber, I., Immunogenicity of Therapeutic Proteins: Influence of Aggregation. *J Immunotoxicol* **2014,** *11* (2), 99-109.

273. Huang, H.; Quan, Y. Y.; Wang, X. P.; Chen, T. S., Gold Nanoparticles of Diameter 13 Nm Induce Apoptosis in Rabbit Articular Chondrocytes. *Nanoscale Res Lett* **2016,** *11* (1), 249.

274. Kim, J. S.; Song, K. S.; Lee, J. H.; Yu, I. J., Evaluation of Biocompatible Dispersants for Carbon Nanotube Toxicity Tests. *Arch Toxicol* **2011,** *85* (12), 1499-508.

275. Wolf, B.; Morgan, H.; Krieg, J.; Gani, Z.; Milicov, A.; Warncke, M.; Brennan, F.; Jones, S.; Sims, J.; Kiessling, A., A Whole Blood in Vitro Cytokine Release Assay with Aqueous Monoclonal Antibody Presentation for the Prediction of Therapeutic Protein Induced Cytokine Release Syndrome in Humans. *Cytokine* **2012,** *60* (3), 828-37.

276. Coch, C.; Lück, C.; Schwickart, A.; Putschli, B.; Renn, M.; Höller, T.; Barchet, W.; Hartmann, G.; Schlee, M., A Human <Italic>in Vitro</Italic> Whole Blood Assay to Predict the Systemic Cytokine Response to Therapeutic Oligonucleotides Including Sirna. *PLoS ONE* **2013,** *8* (8), e71057.

277. Martinez, V.; Mitjans, M.; Vinardell, M. P., Tnf Alpha Measurement in Rat and Human Whole Blood as an in Vitro Method to Assay Pyrogens and Its Inhibition by Dexamethasone and Erythromycin. *J Pharm Sci* **2004,** *93* (11), 2718-23.

278. Marttila, A. T.; Laitinen, O. H.; Airenne, K. J.; Kulik, T.; Bayer, E. A.; Wilchek, M.; Kulomaa, M. S., Recombinant Neutralite Avidin: A Non-Glycosylated, Acidic Mutant of Chicken Avidin That Exhibits High Affinity for Biotin and Low Non-Specific Binding Properties. *FEBS Lett* **2000,** *467* (1), 31-36.

279. Cherng, J. Y.; van de Wetering, P.; Talsma, H.; Crommelin, D. J.; Hennink, W. E., Effect of Size and Serum Proteins on Transfection Efficiency of Poly ((2-Dimethylamino)Ethyl Methacrylate)-Plasmid Nanoparticles. *Pharm Res* **1996,** *13* (7), 1038-42.

280. Dobrovolskaia, M. A.; Germolec, D. R.; Weaver, J. L., Evaluation of Nanoparticle Immunotoxicity. *Nat Nanotechnol* **2009,** *4* (7), 411-4.

281. Bienvenu, J.; Monneret, G.; Fabien, N.; Revillard, J. P., The Clinical Usefulness of the Measurement of Cytokines. *Clin Chem Lab Med* **2000,** *38* (4), 267-85.

282. Liu, C.; Zhang, W.; Yang, H.; Sun, W.; Gong, X.; Zhao, J.; Sun, Y.; Diao, G., A Water-Soluble Inclusion Complex of Pedunculoside with the Polymer Beta-Cyclodextrin: A Novel Anti-Inflammation Agent with Low Toxicity. *PLoS One* **2014,** *9* (7), e101761.

283. Deenadayalan, A.; Maddineni, P.; Raja, A., Comparison of Whole Blood and Pbmc Assays for T-Cell Functional Analysis. *BMC Res Notes* **2013,** *6* (1), 1-5.

284. Scheller, J.; Chalaris, A.; Schmidt-Arras, D.; Rose-John, S., The Pro- and Anti-Inflammatory Properties of the Cytokine Interleukin-6. *Biochim Biophys Acta* **2011,** *1813* (5), 878-888.

285. Liu, C.; Zhao, J.; Liu, Y.; Huang, Y.; Shen, Y.; Wang, J.; Sun, W.; Sun, Y., A Novel Pentacyclic Triterpenoid, Ilexgenin a, Shows Reduction of Atherosclerosis in Apolipoprotein E Deficient Mice. *Int Immunopharmacol* **2016,** *40*, 115-124.

286. Medarova, Z.; Pham, W.; Farrar, C.; Petkova, V.; Moore, A., In Vivo Imaging of Sirna Delivery and Silencing in Tumors. *Nat Med* **2007,** *13* (3), 372-7.

287. Cheng, K.; Ye, Z.; Guntaka, R. V.; Mahato, R. I., Biodistribution and Hepatic Uptake of Triplex-Forming Oligonucleotides against Type Alpha1(I) Collagen Gene Promoter in Normal and Fibrotic Rats. *Mol Pharm* **2005,** *2* (3), 206-17.

288. Zhu, L.; Ye, Z.; Cheng, K.; Miller, D. D.; Mahato, R. I., Site-Specific Delivery of Oligonucleotides to Hepatocytes after Systemic Administration. *Bioconjug Chem* **2008,** *19* (1), 290-8.

289. Cheng, K.; Ye, Z.; Guntaka, R. V.; Mahato, R. I., Enhanced Hepatic Uptake and Bioactivity of Type Alpha1(I) Collagen Gene Promoter-Specific Triplex-Forming Oligonucleotides after Conjugation with Cholesterol. *J Pharmacol Exp Ther* **2006,** *317* (2), 797-805.

290. Liu, D. V.; Yang, N. J.; Wittrup, K. D., A Nonpolycationic Fully Proteinaceous Multiagent System for Potent Targeted Delivery of Sirna. *Mol Ther Nucleic Acids* **2014,** *3* (5), e162.

291. Ciechanover, A., Intracellular Protein Degradation: From a Vague Idea, through the Lysosome and the Ubiquitin-Proteasome System, and onto Human Diseases and Drug Targeting (Nobel Lecture). *Angew Chem Int Ed Engl* **2005,** *44* (37), 5944-67.

292. Vugmeyster, Y.; Xu, X.; Theil, F.-P.; Khawli, L. A.; Leach, M. W., Pharmacokinetics and Toxicology of Therapeutic Proteins: Advances and Challenges. *World J Biol Chem* **2012,** *3* (4), 73-92.

293. Elsabahy, M.; Wooley, K. L., Cytokines as Biomarkers of Nanoparticle Immunotoxicity. *Chem Soc Rev* **2013,** *42* (12), 5552-76.

294. Wolfram, J.; Zhu, M.; Yang, Y.; Shen, J.; Gentile, E.; Paolino, D.; Fresta, M.; Nie, G.; Chen, C.; Shen, H.; Ferrari, M.; Zhao, Y., Safety of Nanoparticles in Medicine. *Curr Drug Targets* **2014**.

295. Park, J.; Park, J.; Pei, Y.; Xu, J.; Yeo, Y., Pharmacokinetics and Biodistribution of Recently-Developed Sirna Nanomedicines. *Adv Drug Deliv Rev* **2016,** *104*, 93-109.

296. Muriel, P.; Rivera-Espinoza, Y., Beneficial Drugs for Liver Diseases. *J Appl Toxicol* **2008,** *28* (2), 93-103.

297. Gonzalez, S. A.; Fiel, M. I.; Sauk, J.; Canchis, P. W.; Liu, R. C.; Chiriboga, L.; Yee, H. T.; Jacobson, I. M.; Talal, A. H., Inverse Association between Hepatic Stellate Cell Apoptosis and Fibrosis in Chronic Hepatitis C Virus Infection. *J Viral Hepat* **2009,** *16* (2), 141-8.

298. Friedman, S. L., Targeting Sirna to Arrest Fibrosis. *Nat Biotechnol* **2008,** *26*, 399.

299. Sato, Y.; Murase, K.; Kato, J.; Kobune, M.; Sato, T.; Kawano, Y.; Takimoto, R.; Takada, K.; Miyanishi, K.; Matsunaga, T.; Takayama, T.; Niitsu, Y., Resolution of Liver Cirrhosis Using Vitamin a–Coupled Liposomes to Deliver Sirna against a Collagen-Specific Chaperone. *Nature Biotechnology* **2008,** *26*, 431.

300. Jain, A.; Barve, A.; Zhao, Z.; Jin, W.; Cheng, K., Comparison of Avidin, Neutravidin, and Streptavidin as Nanocarriers for Efficient Sirna Delivery. *Mol Pharm* **2017,** *14* (5), 1517-1527.

301. Zhao, Z.; Li, Y.; Jain, A.; Chen, Z.; Liu, H.; Jin, W.; Cheng, K., Development of a Peptide-Modified Sirna Nanocomplex for Hepatic Stellate Cells. *Nanomedicine* **2018,** *14* (1), 51-61.

302. Zhao, Z.; Li, Y.; Jain, A.; Chen, Z.; Liu, H.; Jin, W.; Cheng, K., Development of a Peptide-Modified Sirna Nanocomplex for Hepatic Stellate Cells. *Nanomedicine* **2017**.

303. Chen, Z.; Liu, H.; Jain, A.; Zhang, L.; Liu, C.; Cheng, K., Discovery of Aptamer Ligands for Hepatic Stellate Cells Using Selex. *Theranostics* **2017,** *7* (12), 2982-2995.

304. Goodman, Z. D., Grading and Staging Systems for Inflammation and Fibrosis in Chronic Liver Diseases. *J Hepatol* **2007,** *47* (4), 598-607.

305. Wang, K., Molecular Mechanisms of Hepatic Apoptosis. *Cell Death Dis* **2014,** *5*, e996.

306. Guicciardi, M. E.; Gores, G. J., Apoptosis: A Mechanism of Acute and Chronic Liver Injury. *Gut* **2005,** *54* (7), 1024-33.

307. Renehan, A. G.; Bach, S. P.; Potten, C. S., The Relevance of Apoptosis for Cellular Homeostasis and Tumorigenesis in the Intestine. *Can J Gastroenterol* **2001,** *15* (3), 166-76.

308. Borthwick, L. A.; Wynn, T. A.; Fisher, A. J., Cytokine Mediated Tissue Fibrosis. *Biochim Biophys Acta* **2013,** *1832* (7), 1049-1060.

309. Fabregat, I.; Moreno-Caceres, J.; Sanchez, A.; Dooley, S.; Dewidar, B.; Giannelli, G.; Ten Dijke, P., Tgf-Beta Signalling and Liver Disease. *Febs j* **2016,** *283* (12), 2219-32.

310. Bonner, J. C., Regulation of Pdgf and Its Receptors in Fibrotic Diseases. *Cytokine Growth Factor Rev* **2004,** *15* (4), 255-73.

311. Tsukamoto, H., Cytokine Regulation of Hepatic Stellate Cells in Liver Fibrosis. *Alcohol Clin Exp Res* **1999,** *23* (5), 911-6.

312. Sadeghi, M.; Lahdou, I.; Oweira, H.; Daniel, V.; Terness, P.; Schmidt, J.; Weiss, K. H.; Longerich, T.; Schemmer, P.; Opelz, G.; Mehrabi, A., Serum Levels of Chemokines Ccl4 and Ccl5 in Cirrhotic Patients Indicate the Presence of Hepatocellular Carcinoma. *Br J Cancer* **2015,** *113* (5), 756-62.

313. Farci, P.; Wollenberg, K.; Diaz, G.; Engle, R. E.; Lai, M. E.; Klenerman, P.; Purcell, R. H.; Pybus, O. G.; Alter, H. J., Profibrogenic Chemokines and Viral Evolution Predict Rapid Progression of Hepatitis C to Cirrhosis. *Proc Natl Acad Sci U S A* **2012,** *109* (36), 14562-7.

314. Berres, M. L.; Koenen, R. R.; Rueland, A.; Zaldivar, M. M.; Heinrichs, D.; Sahin, H.; Schmitz, P.; Streetz, K. L.; Berg, T.; Gassler, N.; Weiskirchen, R.; Proudfoot, A.;

Weber, C.; Trautwein, C.; Wasmuth, H. E., Antagonism of the Chemokine Ccl5 Ameliorates Experimental Liver Fibrosis in Mice. *J Clin Invest* **2010,** *120* (11), 4129-40.

315. Braet, F.; Wisse, E., Structural and Functional Aspects of Liver Sinusoidal Endothelial Cell Fenestrae: A Review. *Comp Hepatol* **2002,** *1* (1), 1.

316. Longmire, M.; Choyke, P. L.; Kobayashi, H., Clearance Properties of Nano-Sized Particles and Molecules as Imaging Agents: Considerations and Caveats. *Nanomedicine (Lond)* **2008,** *3* (5), 703-17.

317. Lytle, K. A.; Depner, C. M.; Wong, C. P.; Jump, D. B., Docosahexaenoic Acid Attenuates Western Diet-Induced Hepatic Fibrosis in Ldlr-/- Mice by Targeting the Tgfbeta-Smad3 Pathway. *J Lipid Res* **2015,** *56* (10), 1936-46.

318. Lee, H.; Jeong, H.; Park, S.; Yoo, W.; Choi, S.; Choi, K.; Lee, M. G.; Lee, M.; Cha, D.; Kim, Y. S.; Han, J.; Kim, W.; Park, S. H.; Oh, J., Fusion Protein of Retinol-Binding Protein and Albumin Domain Iii Reduces Liver Fibrosis. *EMBO Mol Med* **2015,** *7* (6), 819-30.

319. Furuhashi, H.; Tomita, K.; Teratani, T.; Shimizu, M.; Nishikawa, M.; Higashiyama, M.; Takajo, T.; Shirakabe, K.; Maruta, K.; Okada, Y.; Kurihara, C.; Watanabe, C.; Komoto, S.; Aosasa, S.; Nagao, S.; Yamamoto, J.; Miura, S.; Hokari, R., Vitamin a-Coupled Liposome System Targeting Free Cholesterol Accumulation in Hepatic Stellate Cells Offers a Beneficial Therapeutic Strategy for Liver Fibrosis. *Hepatol Res* **2018,** *48* (5), 397-407.

320. Yang, N.; Singh, S.; Mahato, R. I., Targeted Tfo Delivery to Hepatic Stellate Cells. *J Control Release* **2011,** *155* (2), 326-30.

321. Adrian, J. E.; Poelstra, K.; Scherphof, G. L.; Molema, G.; Meijer, D. K.; Reker-Smit, C.; Morselt, H. W.; Kamps, J. A., Interaction of Targeted Liposomes with Primary Cultured Hepatic Stellate Cells: Involvement of Multiple Receptor Systems. *J Hepatol* **2006,** *44* (3), 560-7.

322. Brigger, I.; Dubernet, C.; Couvreur, P., Nanoparticles in Cancer Therapy and Diagnosis. *Adv Drug Deliv Rev* **2002,** *54* (5), 631-51.

323. Zimmermann, T. S.; Lee, A. C.; Akinc, A.; Bramlage, B.; Bumcrot, D.; Fedoruk, M. N.; Harborth, J.; Heyes, J. A.; Jeffs, L. B.; John, M.; Judge, A. D.; Lam, K.; McClintock, K.; Nechev, L. V.; Palmer, L. R.; Racie, T.; Rohl, I.; Seiffert, S.; Shanmugam, S.; Sood, V.; Soutschek, J.; Toudjarska, I.; Wheat, A. J.; Yaworski, E.; Zedalis, W.; Koteliansky, V.; Manoharan, M.; Vornlocher, H. P.; MacLachlan, I., Rnai-Mediated Gene Silencing in Non-Human Primates. *Nature* **2006,** *441* (7089), 111-4.

324. Walsh, T. J.; Finberg, R. W.; Arndt, C.; Hiemenz, J.; Schwartz, C.; Bodensteiner, D.; Pappas, P.; Seibel, N.; Greenberg, R. N.; Dummer, S.; Schuster, M.; Holcenberg, J. S., Liposomal Amphotericin B for Empirical Therapy in Patients with Persistent Fever and Neutropenia. National Institute of Allergy and Infectious Diseases Mycoses Study Group. *N Engl J Med* **1999,** *340* (10), 764-71.

325. Yano, J.; Hirabayashi, K.; Nakagawa, S.; Yamaguchi, T.; Nogawa, M.; Kashimori, I.; Naito, H.; Kitagawa, H.; Ishiyama, K.; Ohgi, T.; Irimura, T., Antitumor Activity of Small Interfering Rna/Cationic Liposome Complex in Mouse Models of Cancer. *Clin Cancer Res* **2004,** *10* (22), 7721-6.

326. Takahashi, N.; Tamagawa, K.; Shimizu, K.; Fukui, T.; Maitani, Y., Effects on M5076-Hepatic Metastasis of Retinoic Acid and N-(4-Hydroxyphenyl) Retinamide, Fenretinide Entrapped in Sg-Liposomes. *Biol Pharm Bull* **2003,** *26* (7), 1060-3.

327. Behlke, M. A., Progress Towards in Vivo Use of Sirnas. *Mol Ther* **2006,** *13* (4), 644-70.

328. Sato, Y.; Murase, K.; Kato, J.; Kobune, M.; Sato, T.; Kawano, Y.; Takimoto, R.; Takada, K.; Miyanishi, K.; Matsunaga, T.; Takayama, T.; Niitsu, Y., Resolution of Liver Cirrhosis Using Vitamin a-Coupled Liposomes to Deliver Sirna against a Collagen-Specific Chaperone. *Nat Biotechnol* **2008,** *26* (4), 431-42.

329. Mederacke, I.; Hsu, C. C.; Troeger, J. S.; Huebener, P.; Mu, X.; Dapito, D. H.; Pradere, J. P.; Schwabe, R. F., Fate Tracing Reveals Hepatic Stellate Cells as Dominant Contributors to Liver Fibrosis Independent of Its Aetiology. *Nat Commun* **2013,** *4*, 2823.

330. Pradere, J. P.; Kluwe, J.; De Minicis, S.; Jiao, J. J.; Gwak, G. Y.; Dapito, D. H.; Jang, M. K.; Guenther, N. D.; Mederacke, I.; Friedman, R.; Dragomir, A. C.; Aloman, C.; Schwabe, R. F., Hepatic Macrophages but Not Dendritic Cells Contribute to Liver Fibrosis by Promoting the Survival of Activated Hepatic Stellate Cells in Mice. *Hepatology* **2013,** *58* (4), 1461-73.

331. Ding, B. S.; Cao, Z.; Lis, R.; Nolan, D. J.; Guo, P.; Simons, M.; Penfold, M. E.; Shido, K.; Rabbany, S. Y.; Rafii, S., Divergent Angiocrine Signals from Vascular Niche Balance Liver Regeneration and Fibrosis. *Nature* **2014,** *505* (7481), 97-102.

332. Radaeva, S.; Sun, R.; Jaruga, B.; Nguyen, V. T.; Tian, Z.; Gao, B., Natural Killer Cells Ameliorate Liver Fibrosis by Killing Activated Stellate Cells in Nkg2d-Dependent

and Tumor Necrosis Factor-Related Apoptosis-Inducing Ligand-Dependent Manners. *Gastroenterology* **2006,** *130* (2), 435-52.

333. Yang, H.; Lee, P. J.; Jeong, E. J.; Kim, H. P.; Kim, Y. C., Selective Apoptosis in Hepatic Stellate Cells Mediates the Antifibrotic Effect of Phenanthrenes from Dendrobium Nobile. *Phytother Res* **2012,** *26* (7), 974-80.

334. Mehal, W.; Imaeda, A., Cell Death and Fibrogenesis. *Semin Liver Dis* **2010,** *30* (3), 226-231.

335. Friedman, S. L., Hepatic Stellate Cells: Protean, Multifunctional, and Enigmatic Cells of the Liver. *Physiol Rev* **2008,** *88* (1), 125-72.

336. Seki, E.; Schwabe, R. F., Hepatic Inflammation and Fibrosis: Functional Links and Key Pathways. *Hepatology* **2015,** *61* (3), 1066-79.

337. Cheng, K.; Yang, N.; Mahato, R. I., Tgf-B1 Gene Silencing for Treating Liver Fibrosis. *Mol pharm* **2009,** *6* (3), 772-779.

338. Czochra, P.; Klopcic, B.; Meyer, E.; Herkel, J.; Garcia-Lazaro, J. F.; Thieringer, F.; Schirmacher, P.; Biesterfeld, S.; Galle, P. R.; Lohse, A. W.; Kanzler, S., Liver Fibrosis Induced by Hepatic Overexpression of Pdgf-B in Transgenic Mice. *J Hepatol* **2006,** *45* (3), 419-28.

339. Dooley, S.; ten Dijke, P., Tgf-B in Progression of Liver Disease. *Cell Tissue Res* **2012,** *347* (1), 245-256.

340. Son, G.; Iimuro, Y.; Seki, E.; Hirano, T.; Kaneda, Y.; Fujimoto, J., Selective Inactivation of Nf-Kappab in the Liver Using Nf-Kappab Decoy Suppresses Ccl4-

Induced Liver Injury and Fibrosis. *Am J Physiol Gastrointest Liver Physiol* **2007,** *293* (3), G631-9.

341. Gandhi, C. R., Hepatic Stellate Cell Activation and Pro-Fibrogenic Signals. *J Hepatol* **2017,** *67* (5), 1104-1105.

VITA

Akshay Jain received his Bachelor of Pharmacy degree (B.Pharm.) from Devi Ahilya University (India) in July 2009. In 2011, Akshay joined university of Toledo to pursue graduate research in Pharmaceutical Science and Industrial Pharmacy. His research was focused on the oral dosage formulation development and characterization. In 2013, he obtained his Master of Science (M.S.) degree from university of Toledo.

In August 2013, Akshay joined Dr. Kun Cheng's laboratory and worked as Graduate Research and Teaching Assistant in Division of Pharmaceutical Sciences in University of Missouri-Kansas City. In Dr. Cheng's lab, Akshay's research was focused on 1) Identification of intracellular trafficking pathway for the protein based siRNA delivery systems; 2) Development of novel protein based nanocomplexes for the delivery of PCBP2 siRNA in vitro and in vivo for liver fibrosis therapy. Akshay published 6 research articles and 1 review paper as an author. During his tenure as graduate research and teaching assistant at UMKC, Akshay received several prestigious national awards for his academic excellence, including 2017 AAPS Foundation Graduate Student Fellowship Award, 2017 Excellence in Graduate Research Award - AAPS DDDI section, 2017 Best Manuscript Contest winner - AAPS-PPB Section, Best Abstract Award - AAPS 2018, 2015 AAPS PPB Section Travelship Award. Akshay also received several prestigious recognitions in UMKC such as Preparing Future Faculty Fellowship Award, Graduate Faculty Fellowship Award, Richard and Paula Johnson Graduate Student Award, UMKC Health Science Research Summit Best poster award 2018, Spring 2017-Best Seminar Speaker Award. Akshay has been served actively in graduate student organizations in capacity of Vice Chair, Chair Elect and Chair of AAPS-UMKC student chapter. Akshay

also co-chaired the scientific committee and fund raiser committee for the PGSRM 2016 conference at UMKC where they hosted approximately 200 participants from pharmaceutical sciences graduate students and post docs. Akshay is also affiliated to the Rho Chi Honor Society. Akshay is also a member of American Association of Pharmaceutical Scientists (AAPS).

PUBLICATIONS

1. **Jain A**, Barve A, Zhao Z, Liu H, Cheng K; Targeted Delivery of an siRNA Nanocomplex Reverses Carbon Tetrachloride-induced Liver Fibrosis. **(under preparation)**
2. Jin W, **Jain A**, Liu H, Zhao Z, Cheng K; Noncovalent Attachment of Chemical Moieties to siRNA Using Peptide Nucleic Acid As a Complementary Linker. ACS Appl. Bio Mater. 2018 Aug. Just accepted manuscript.
3. Zhao Z, Li Y, **Jain A**, Chen Z, Liu H, Jin W, Cheng K; Development of a Peptide-Modified siRNA Nanocomplex for Hepatic Stellate Cells; Nanomedicine. 2018 Jan;14(1):51-61
4. Chen Z, Liu H, **Jain A**, Zhang L, Liu C, Cheng K; Discovery of Aptamer Ligands for Hepatic Stellate Cells Using SELEX; Theranostics 2017; 7(12):2982-2995
5. **Jain A**, Barve A, Zhao Z, Jin W, Cheng K; Comparison of Avidin, Neutravidin and Streptavidin as Nanocarrier for Efficient siRNA Delivery; Mol Pharm. 2017 May 1;14(5):1517
6. **Jain A**, Cheng K; The Principles and Applications of Avidin-based Nanoparticles in Drug Delivery and Diagnosis; J Control Release. 2017 Jan 10;245:27-40
7. Barve A, **Jain A**, Liu H, Jin W, Cheng K; An Enzyme-Responsive Conjugate Improves the Delivery of a PI3K Inhibitor to Prostate Cancer. Nanomedicine, 2016 Nov;12(8):2373-2381.
8. Shukla RS*, **Jain A***, Zhao Z, Cheng K.; Intracellular Trafficking and Exocytosis of a Multi-Component siRNA Nanocomplex; Nanomedicine. 2016 Jul;12(5):1323-34 **(*Co-first Author)**

COPYRIGHT CLEARANCE

Title: The principles and applications of avidin-based nanoparticles in drug delivery and diagnosis

Author: Akshay Jain,Kun Cheng

Publication: Journal of Controlled Release

Publisher: Elsevier

Date: 10 January 2017

Title: Intracellular trafficking and exocytosis of a multi-component siRNA nanocomplex

Author: Ravi S. Shukla,Akshay Jain,Zhen Zhao,Kun Cheng

Publication: Nanomedicine: Nanotechnology, Biology and Medicine

Publisher: Elsevier

Date: July 2016

Title: Comparison of Avidin, Neutravidin, and Streptavidin as Nanocarriers for Efficient siRNA Delivery

Author: Akshay Jain, Ashutosh Barve, Zhen Zhao, et al

Publication: Molecular Pharmaceutics

Publisher: American Chemical Society

Date: May 1, 2017

LOGIN

If you're a copyright.com user, you can login to RightsLink using your copyright.com credentials.

Already a RightsLink user or want to learn more?

PERMISSION/LICENSE IS GRANTED FOR YOUR ORDER AT NO CHARGE

This type of permission/license, instead of the standard Terms & Conditions, is sent to you because no fee is being charged for your order. Please note the following:

- Permission is granted for your request in both print and electronic formats, and translations.
- If figures and/or tables were requested, they may be adapted or used in part.
- Please print this page for your records and send a copy of it to your publisher/graduate school.
- Appropriate credit for the requested material should be given as follows: "Reprinted (adapted) with permission from (COMPLETE REFERENCE CITATION). Copyright (YEAR) American Chemical Society." Insert appropriate information in place of the capitalized words.
- One-time permission is granted only for the use specified in your request. No additional uses are granted (such as derivative works or other editions). For any other uses, please submit a new request.

BACK CLOSE WINDOW